

THE TRANSITIONAL PROTOPLANETARY DISK FREQUENCY AS A FUNCTION OF AGE: DISK EVOLUTION IN THE CORONET CLUSTER, TAURUS, AND OTHER 1–8 MYR-OLD REGIONS

THAYNE CURRIE¹ AND AURORA SICILIA-AGUILAR²

Draft version August 18, 2018

ABSTRACT

We present Spitzer 3.6–24 μm photometry and spectroscopy for stars in the 1–3 Myr-old Coronet Cluster, expanding upon the survey of Sicilia-Aguilar et al. (2008). Using sophisticated radiative transfer models, we analyze these new data and those from Sicilia-Aguilar et al. (2008) to identify disks with evidence for substantial dust evolution consistent with disk clearing: transitional disks. We then analyze data in Taurus and other young clusters – IC 348, NGC 2362, and η Cha – to constrain the transitional disk frequency as a function of time. Our analysis confirms previous results finding evidence for two types of transitional disks – those with inner holes and those that are homologously depleted. The percentage of disks in the transitional phase increases from ~ 15 –20% at 1–2 Myr to $\geq 50\%$ at 5–8 Myr; the mean transitional disk lifetime is closer to ~ 1 Myr than 0.1–0.5 Myr, consistent with previous studies by Currie et al. (2009) and Sicilia-Aguilar et al. (2009). In the Coronet Cluster and IC 348, transitional disks are more numerous for very low-mass M3–M6 stars than for more massive K5–M2 stars, while Taurus lacks a strong spectral type-dependent frequency. Assuming standard values for the gas-to-dust ratio and other disk properties, the lower limit for the masses of optically-thick primordial disks is $M_{\text{disk}} \approx 0.001$ – $0.003 M_{\star}$. We find that single color-color diagrams do not by themselves uniquely identify transitional disks or primordial disks. Full SED modeling is required to accurately assess disk evolution for individual sources and inform statistical estimates of the transitional disk population in large samples using mid-IR colors.

Subject headings:

1. INTRODUCTION

Transitional protoplanetary disks identify important stages in planet formation, linking epochs when disks are optically-thick *primordial* protoplanetary disks, rich in gas and containing massive amounts of small dust, and when they are gas-poor/free, optically-thin *debris* disks and thus are in the post gas planet-building stage (Currie et al. 2009; Strom et al. 1989). Compared to primordial disks, transitional disks have weaker near-to-mid IR emission indicating that they are depleted in warm, micron-sized dust within several AU of the host star (e.g. Strom et al. 1989; Calvet et al. 2002). If this dust traces the bulk mass of solids, transitional disks then show evidence for the removal of planet-building material.

Though transitional disks are not primarily identified by their levels of gas, they typically have a lower rate/frequency of stellar accretion (Sicilia-Aguilar et al. 2006a; Muzerolle et al. 2010; Cieza et al. 2010). Transitional disks may also be losing much of their gas from a photoevaporative wind driven by stellar EUV photons (Pascucci and Sterzik 2009), may lack gas-rich inner disks (Salyk et al. 2009), or may have a low density of cold outer disk gas (Hughes et al. 2010). Thus, transitional disks are also plausibly depleted of circumstellar gas responsible for the envelopes of gas/ice giant planets and may be signposts for the last phases of protoplanetary disk evolution and gas giant planet formation.

Spitzer studies have better constrained the morphologies and lifetimes of transitional disks around solar to slightly subsolar-mass stars ($M_{\star} \sim 0.5$ – $1.4 M_{\odot}$, see

Currie 2010 and Muzerolle 2010 for reviews). Transitional disks exhibit one of two general morphologies: 1) disks with weak or negligible levels of near-to-mid IR emission indicative of inner dust holes but more strongly emitting, typically optically-thick outer disks consistent with an inside-out clearing of dust or 2) disks lacking evidence for inner holes but having weaker emission at all IR wavelengths consistent with a more homologous depletion of dust (Currie et al. 2009). Transitional disks comprise $\lesssim 10$ –20% of the disk population in ≈ 1 Myr-old clusters (e.g. Muzerolle et al. 2010; Currie and Kenyon 2009) but are relatively more frequent by ~ 5 Myr, consistent with a transitional disk phase comprising a substantial fraction of the total protoplanetary disk lifetime (e.g. ~ 1 Myr out of 3–5 Myr, Currie et al. 2009; Sicilia-Aguilar et al. 2009).

The 1–3 Myr-old Coronet Cluster (Meyer and Wilking 2009, and references therein) may provide a particularly useful probe of transitional disk properties in the youngest clusters and as a function of stellar mass. Sicilia-Aguilar et al. (2008) find that transitional disks comprise nearly half of the disk population, much larger than frequencies derived for other clusters of comparable age (e.g. Currie and Kenyon 2009; Muzerolle et al. 2010). At first glance, these results appear to be in conflict, but Sicilia-Aguilar et al. (2008) note that the members in their sample have systematically low masses (see also López-Martí et al. 2010). Compared to solar and slightly subsolar-mass stars, disks around very low-mass stars and brown dwarfs may have very different structures and different dispersal timescales (e.g. Lada et al. 2006; Hartmann et al. 2006). Thus, it is unclear whether the high reported transitional disk frequency in the Coro-

¹ NASA-Goddard Space Flight Center, Greenbelt, MD

² Max-Planck-Institute for Astronomy, Königstuhl 17, 69117 Heidelberg, Germany

net Cluster is anomalous or identifies a stellar mass-dependent transitional disk frequency. Addressing this issue requires analyzing disks around higher-mass Coronet stars and assessing the transitional disk frequency as a function of stellar mass for many clusters.

In this paper, we investigate the transitional disk population in the Coronet Cluster as a function of spectral type/stellar mass by presenting Spitzer photometry and spectroscopy for additional, predominantly solar-mass members. By comparing results for solar mass and subsolar-mass members, we determine whether the Coronet Cluster disk population shows evidence for a stellar mass-dependent frequency of transitional disks. §2 describes our new observations, data reduction, and photometry/spectroscopy. In §3, we model the SEDs of disk-bearing stars to determine plausible disk evolutionary states following previous methods (e.g. Currie et al. 2009). Finally, in §4 we compare these results to those for other clusters to investigate the duration of the transitional disk phase.

2. DATA

2.1. Spitzer IRAC and MIPS Photometry

To the sample of stars analyzed by Sicilia-Aguilar et al. (2008), we add IRAC and MIPS photometry of other Coronet Cluster members located on the processed IRAC and MIPS mosaics obtained from Program IDs 6 (AORs 3650816 and 3664640), 248 (AOR 13469696), and 30784 (AOR 17672960). Image processing and photometry for these stars was performed following methods described in Sicilia-Aguilar et al. (2008). Briefly, the basic calibration data (BCD) frames were mosaiced together using MOPEX using standard input parameters for the overlap correction, pixel interpolation, and outlier rejection. Aperture photometry was performed with APEX using a 3 pixel aperture, a 12–20 pixel background radius, and aperture corrections listed in the IRAC data handbook (1.112, 1.113, 1.125, and 1.218 for the four channels, respectively). For MIPS, we used a 5 pixel aperture with a 8–13 pixel background annulus, and the aperture correction listed in the MIPS data handbook (1.167).

We select cluster stars from the catalog of Forbrich and Preibisch (2007), which identifies x-ray bright sources with near-IR/optical counterparts as Coronet Cluster members. We add 32 cluster members from Forbrich and Preibisch (2007) to the list of stars analyzed in Sicilia-Aguilar et al. (2008). The IRAC and MIPS coverage areas do not completely overlap, and many cluster members lack photometry in two of the four IRAC channels ([3.6] and [5.8] or [4.5] and [8]) or lack MIPS data. Other sources, particularly Class I protostars and bright, higher-mass stars (e.g. R CrA) saturate the IRAC and/or MIPS detector. Table 1 lists the names and coordinates for these targets. Table 2 lists their photometry. Sources with an "FP" prefix for their names were classified as members only by Forbrich and Preibisch (2007): the numbers following this prefix correspond to the row number in Table 2 of Forbrich and Preibisch (2007).

To further assess photometric quality, we inspected the processed IRAC and MIPS mosaics and compared the known target positions to the computed target centroids. Most sources lie in regions of low background and are thus uncontaminated by nebulosity. Most sources lo-

cated in high-background regions are much brighter than the background, which is typically uniform. However, two sources – TY CrA and HD 176386B – are located in regions of high and highly-variable background. In the longer wavelength 5.8 μm and 8 μm channels, the computed centroid positions are well offset from the apparent star positions, especially for HD 176386B. Figure 1 illustrates this offset for the 5.8 μm channel.

To investigate how the mid-IR fluxes from TY CrA and HD 176386B are affected by nebular emission, we recomputed the flux for these sources using much smaller apertures and background annuli, ranging from our default assumptions to a small 2 pixel aperture radius and 2–6 pixel background annulus. Depending on the choice of aperture radii and background annuli, their fluxes at 5.8 μm and 8 μm vary by $\sim 50\%$ –200%. Therefore, we consider the 5.8 μm and 8 μm photometry for these sources to be unreliable. Since the nebular background emission increases with wavelength, it also renders fluxes for these sources uncertain at 24–100 μm .

2.2. Spitzer IRS Spectroscopy

To supplement our photometric data, we add spectroscopic data from the Infrared Spectrograph (Houck et al. 2004) spectroscopy for several intermediate-mass members: S CrA, V709, T CrA, IRS7w, and IRS5. The spectra were processed starting from the BCD data and using the spectral extraction tools developed for the FEPS Spitzer science legacy team (Bouwman et al. 2008), based on the SMART software package (Higdon et al. 2004). The spectra were extracted using 6 and 5 pixel wide apertures in the spatial dimension for short- (7.5 - 14 μm) and the long-wavelength (14 - 35 μm) modules, respectively. The background was subtracted using associated pairs of imaged spectra from the two nodded positions along the slit, also eliminating stray light contamination and anomalous dark currents. The long-wavelength modules were not available for S CrA, and in the cases of IRS7w, IRS5, and T CrA, strong background contamination and/or extended emission makes the spectral extraction uncertain at $\lambda > 14\mu\text{m}$. Therefore, we only include in the analysis the short-wavelength region for these sources.

2.3. Ancillary Data

To compare the stellar and circumstellar properties of all Coronet Cluster members, we add IRAC/MIPS photometry and IRS spectroscopy presented in Sicilia-Aguilar et al. (2008); optical photometry from López-Martí et al. (2005), Torres et al. (2006) and from the SIMBAD Astronomical Database (various sources); near-IR photometry from 2MASS Skrutskie et al. (2006) and Meyer and Wilking (2009). Spectral types for most cluster stars with new Spitzer data derive from Meyer and Wilking (2009) or Nisini et al. (2005). Most stars studied in Sicilia-Aguilar et al. (2008), have spectral types derived from VLT/FLAMES.

We also consider new, higher signal-to-noise VLT/FLAMES spectra of Coronet Cluster members, which yield new spectral types for several low-mass cluster stars – G-1, CrA-4107, CrA-4109, CrA-432, CrA-468, CrA-452, G-85, and G-87. These data will be discussed and analyzed in detail in a later contribution

(Sicilia-Aguilar et al., 2011, in preparation). Briefly, the medium resolution ($R \sim 6000$) spectra were centered on three bands covering 0.6–0.9 μm ($\lambda_c = 0.682, 0.773,$ and $0.881 \mu m$). For spectral classification, we first determined whether the stars were likely earlier or later than M3 using standard spectral indices. For later stars, we derived spectral types using spectral indices of TiO bands following Sicilia-Aguilar et al. (2008). Earlier stars were classified by comparing their spectra to Cep OB2 spectra described in Sicilia-Aguilar et al. (2005).

We estimate the spectral types of stars without spectra by deriving the best-fit effective temperature from model the optical to near-IR SED using the Robitaille et al. (2006) radiative transfer grid and then using the Currie et al. (2010) effective temperature scale for stars M2 or earlier and Luhman et al. (2003) for later stars. For some sources, we cannot derive a spectral type because the source lacks optical data or is a protostar. Tables 3 and 4 list the spectral types for each star.

To probe the mid-IR fluxes of bright stars that saturate the IRAC and MIPS detectors, we combined our source list with IRAS data for R CrA, TY CrA, and S CrA from Wilking et al. (1985, 1992). Our IRAC and MIPS mosaics indicate that the emission from R CrA and S CrA clearly dominates over the background nebular emission and thus are only weakly contaminated. As mentioned previously, TY CrA is heavily contaminated by background emission. Given the large beam size of IRAS compared to Spitzer, the IRAS flux quoted for TY CrA is also likely unreliable.

2.4. IRAC and MIPS Colors and Observed SEDs of Coronet Cluster Stars

To provide a first-order investigation of the Coronet Cluster disk population, we analyze the distribution of near-to-mid IR colors and optical/IR spectral energy distributions (SEDs). The left panel of Figure 2 displays the observed IRAC colors of cluster stars with new photometry (black dots) and stars analyzed by Sicilia-Aguilar et al. (2008, grey dots). The distributions appear similar. Many stars concentrate near zero color (as expected for bare stellar photospheres) and around $[3.6] - [4.5] = 0.3 - 0.6$ and $[5.8] - [8] = 0.5 - 0.7$. Compared to the typical IRAC colors of primordial disks in 1–2 Myr-old clusters (solid box, Hartmann et al. 2005), colors for Coronet Cluster stars may be slightly bluer by ~ 0.2 mag.

The longer wavelength colors for cluster stars exhibit a wider diversity (Figure 2, right panel). At least three sources, all from the Sicilia-Aguilar et al. (2008) sample, show evidence for weak/negligible $5.8 \mu m$ excess but a $\gtrsim 4$ magnitude excess at $24 \mu m$ characteristic of transitional disks with inner holes. Others have $24 \mu m$ and/or $5.8 \mu m$ excess emission characteristic of more homogeneously depleted transitional disks, such as those found in NGC 2362 (dotted enclosed region, Currie et al. 2009), which is weaker than emission for the lower-quartile median Taurus SED from Furlan et al. (2006, lower-left triangle). The cluster also includes many stars with strong IRAC and MIPS excesses comparable to the median Taurus and upper-quartile Taurus SED. Because only six stars in the new sample have K_s , $[5.8]$ and $[24]$ detections, it is less clear from the $K_s - [5.8] / K_s - [24]$ diagram whether the distribution of colors from the new cluster

sample displays the same diversity.

Examining the SEDs of new sources clearly shows that they have a wide range of morphologies (Figure 3). Many sources (e.g. IRS2, IRS5ab, IRS7w) have rising near-to-mid IR SEDs indicative of Class I protostars. Well-known sources with optically-thick disks, such as the intermediate-mass stars S CrA and R CrA, have nearly flat SEDs from $1 \mu m$ to $8 \mu m$.

IRS spectra strengthens our identification of sources whose photometric data alone make them difficult to classify. In particular, V709 shows evidence for a weak excess based on its MIPS-24 μm flux and IRS spectra. Its SED gradually peels away from the stellar photosphere from $\sim 8 \mu m$ to $30 - 35 \mu m$. Based on their $10 \mu m$ absorption features, IRS-5 and IRS-7w are likely protostars with cool envelopes (e.g. Willner et al. 1982; Andre and Montmerle 1994), consistent with previous classifications (Henning et al. 1994; Chini et al. 2003; Groppi et al. 2007).

3. ANALYSIS

To assess the evolutionary states of Coronet Cluster disks, we analyze source SEDs from the new sample and the Sicilia-Aguilar et al. (2008) sample using both simple theoretical comparisons and sophisticated radiative transfer modeling. We follow a slightly modified version of the analysis methods used in Currie et al. (2009) to distinguish disks in different states. These classifications are based solely on 1–24 μm data: since far-IR/submm data provides crucial constraints on disk properties, in particular the inferred disk mass, we consider these classifications to be provisional. We will revisit these classifications later after analyzing stars in other clusters with longer wavelength data (§4).

In our classification, we consider protostars and disks with three main evolutionary states: primordial disks, transitional disks, and debris disk candidates. We identify protostars as sources with rising SEDs from the near-IR to mid-IR consistent with emission predominantly from a cold dusty envelope ($T \leq 200 - 300$ K). *Primordial* disks are disks that are optically thick ($\tau_{IR} \gg 1$) and thus lack evidence for dust evolution consistent with active disk clearing.

Transitional disks are disks that show substantial dust evolution consistent with active disk clearing. They can have one of two morphologies. First, they can exhibit a drop in the optical depth ($\tau \approx 1$ or less) of emitting dust either at all IR wavelengths consistent with a reduced disk mass (a homogeneously depleted transitional disk). Second, they can also have photospheric or weak, optically-thin emission at shorter wavelengths (e.g. $3.6 - 5.8 \mu m$) and more optically thick emission at longer wavelengths consistent with inside-out disk clearing (a transitional disk with an inner hole). In this latter group, we include so-called 'pre-transitional disks' (Espaillat et al. 2007). These disks have a small amount of high optical depth material very close to the star but otherwise have large, dust-poor inner regions (e.g. large gaps) and optically-thick outer regions and thus also identify an inside-out disk clearing.

Debris disk candidates lack evidence for accretion and have very optically-thin emission ($\tau_{IR} \ll 1$) from a low mass ($\lesssim 0.01 M_{Jup}$, Chen et al. 2005) of second-generation dust (Backman and Paresce 1993;

Currie et al. 2008; Kenyon and Bromley 2008). Many of the Coronet Cluster stars are M dwarfs with very low masses. Even if these stars have tenuous emission and lack evidence for accretion, they also have grain removal timescales comparable to the host star’s age. Thus, their dust need not be second generation (Currie and Kenyon 2009), they could be very late-stage transitional disks, and at best can only be considered debris disk *candidates*. Our basis for identifying sources with tenuous $24\ \mu\text{m}$ excess emission as debris disk candidates follows Carpenter et al. (2009) and is purely empirical. They identify debris disk candidates around late-type stars as those with 0.25–0.5 $24\ \mu\text{m}$ excesses. In our analysis, we consider the evolutionary state of these tenuous disks around Coronet Cluster stars as indeterminable and simply label them as transitional disks/debris disk candidates³.

For most sources, only photometric data is available. For sources with IRS data from Sicilia-Aguilar et al. (2008), we add the IRS flux densities, which when combined with our photometry yields flux densities at equally spaced wavelengths (Table 5). The inclusion of the IRS data provides better sampling of the SED from 5 to $24\ \mu\text{m}$ and extends the wavelength coverage.

3.1. Method for Disk Identification

3.1.1. Fiducial SEDs

We first compare source SEDs to geometrically flat, optically-thick models to identify disks with evidence for a reduced optical depth of emitting material ($\tau_{IR} \lesssim 1$). Figure 4 shows two flattened reprocessing disk models appropriate for a $T_e = 3850\ \text{K}$ primary (M0 spectral type), though SEDs for earlier and later stars (e.g. K5 to M6) yield similar mid-IR fluxes relative to the stellar photosphere. The first model (dash-three dots/diamonds) is the standard, razor-thin flat reprocessing disk model from Kenyon and Hartmann (1987, see also Adams et al. 1987), truncating the inner disk at a dust sublimation temperature of $T = 1500\ \text{K}$. The second model (thick grey dashed line) is produced from the Whitney Monte Carlo radiative transfer code (Whitney et al. 2003a,b; Robitaille et al. 2006). The model assumes a disk mass of $0.05\ M_\odot$, no flaring ($H/r = \text{constant}$), no accretion, and no protostellar envelope emission. The disk is optically-thick to its own radiation over spatial scales relevant for our study ($\lesssim 10\ \text{AU}$).

The Whitney disk model consistently has weaker disk emission than the simple Kenyon and Hartmann flat disk model, because stellar photons in the Whitney model are partially attenuated before they reach the $\tau = 1$ surface, due to the disk’s finite thickness. Thus, the disk is colder at a given location and reradiates less energy. To provide an empirical comparison for source SEDs, we overplot the lower-quartile Taurus SED (Figure 4, left panel) from Furlan et al. (2006), which has been used in other work

³ While some debris disks have much stronger emission, nearly all of them surround what are (or will be) main sequence A stars or early F stars (e.g. Rieke et al. 2005; Currie et al. 2008) that have masses $\gtrsim 1.5\ M_\odot$. Debris disks detected around lower-mass stars (the focus of this paper) are far more infrequent and typically have $24\ \mu\text{m}$ excesses of only a few tenths of magnitudes (e.g. Plavchan 2009). Our results are insensitive as to whether or not stars with tenuous excesses are considered to have debris disks or transitional disks.

to help distinguish disks in different states (Cieza et al. 2008; Currie et al. 2009; Currie and Kenyon 2009). The lower-quartile Taurus SED almost perfectly tracks the Kenyon and Hartmann flat disk model.

In the right panel of Figure 4, we compare our fiducial SEDs to a flared optically-thick disk model (thick grey long-dashed line) with $H/r = r^{2/7}$ (e.g. Chiang and Goldreich 1997) using the Whitney code and a disk that has undergone significant dust settling (thick black long-dashed line). Following Lada et al. (2006), we quantify dust settling by reducing the disk scale height by a factor of 3 compared to the thermal equilibrium value adopted in the flared disk model⁴. The Whitney settled disk model predicts emission roughly equal to the Whitney flat disk model through $\sim 7\ \mu\text{m}$ and greater emission at longer wavelengths in spite of being flared: this probably happens because the puffed up inner wall effectively attenuates flux from disk regions slightly exterior (e.g. the disk only comes out of shadow at regions that effectively emit at $\lambda > 7\ \mu\text{m}$).

In Figure 5, we plot the $K_s-[5.8,8]$ vs. $K_s-[24]$ colors for the flattened and settled disk models as a function of disk inclination, produced by convolving the model output with 2MASS and Spitzer filter functions provided as a part of the Whitney code. There is little variation in color, especially for the flat model, except when the disk is viewed nearly edge on. In this case, the disk heavily extinguishes the star, causing its observed colors to be far redder than in face-on cases. The loci of colors indicate that flattened optically-thick disks should typically have $K_s-[5.8,8,24] > 1.1, 1.5, 3.5$. Settled disks have slightly bluer $K_s-[5.8]$ colors ($\sim 0.85-1$) but redder $K_s-[8,24]$ colors (1.6–1.9). For the models where the disk is not viewed edge on, the disks have K-band excess emission of $\sim 0.1-0.2$ magnitudes, consistent with a visual inspection of Figure 4. Thus, optically-thick, flattened disks lacking K band excess (e.g. because of submicron-sized grain growth), should then typically have $K_s-[5.8] \gtrsim 1.2$ and $K_s-[8] \gtrsim 1.6-1.7$. The colors for an optically-thick flared disk lie off the plot range (e.g. $K_s-[8] = 2.75$, $K_s-[24] = 6.75$). The disk emission at $24\ \mu\text{m}$ varies wildly with disk flaring, so MIPS- $24\ \mu\text{m}$ does not effectively probe the disk optical depth. The colors from disk models for K5–M6 stars agree to within $\sim 0.05-0.1\ \text{mag}$.

Since the Whitney flat disk model produces weaker emission through $8\ \mu\text{m}$ than the other fiducial models, it defines a conservative limit for disks with optically-thick emission. Because we identify primordial disks as those with optically-thick IR emission, disks with 2–8 μm emission greater than this flat disk model are consistent with being primordial disks. Conversely, disks with weaker emission correspond to later evolutionary stages: transitional disks and debris disk candidates.

We emphasize that our adopted optically-thick disk

⁴ Technically, we assume less “settling” than in other “settled disk” models, like those presented in D’Alessio et al. (2006). However, their treatment of settling assumes that some small, strongly emitting grains remain at larger heights above the disk midplane, whereas the Whitney code lacks this superheated grain population and thus may underpredict near-to-mid IR disk emission. Furthermore, some of the D’Alessio et al. (2006) “settling” models likely produce weak emission because they assume low disk masses, in addition to being “settled”.

limit is conservative. Emission in excess of this limit at $\lambda \sim 5\text{--}8 \mu\text{m}$ may be explained by disk flaring. While the model used to produce this limit lacks flaring, real disks almost assuredly have some flaring. Furthermore, the IRAC 8 μm channel overlaps with the 10 μm silicate feature, complicating comparisons with the flat disk limit (see Muzerolle et al. 2010). The model also lacks accretion luminosity, which contributes some IR flux, but many disks we model show unambiguous accretion signatures.

3.1.2. SED Modeling

After comparing source SEDs to our flat reprocessing disk SED, we model optical-to-mid IR fluxes with the grid of radiative transfer disk models from Robitaille et al. (2006), which yields estimates for disk properties (e.g. mass, inner radius) consistent with other independent work (see Robitaille et al. 2007). By identifying the best-fitting models ($\min(\chi^2)$), we determine whether the disk plausibly has an inner region cleared of dust and is thus consistent with being a transitional disk with an inner hole. The computed inner disk radius distinguishes disks that lack inner holes (primordial, homologously depleted transitional disk) and transitional disk with inner holes. To be conservative, we set the division at ten times the dust sublimation radius: disks with $R_{in} \geq 10 R_{sub}$ are identified as transitional disks with inner holes. To account for flux calibration uncertainties, photometric errors, and variability, we assume a minimum 10% flux uncertainty in each photometric filter and IRS monochromatic flux density.

We restrict ourselves to disk models which provide a good fit, which we define as $\chi^2 - \chi^2_{best} < 3$, where χ^2_{best} corresponds to the minimum χ^2 per datapoint. This criteria is very similar to that used in previous studies (e.g. Robitaille et al. 2007; Currie et al. 2009; Ercolano et al. 2009). Finally, we incorporate systematic uncertainties in the extinction A_V and distance. For the extinction, we nominally assume a 20% systematic uncertainty with a "floor" of ± 0.5 mags. For the distance, we assume 150 pc with an uncertainty of ± 20 pc.

3.2. Results

Tables 3 and 4 describe our provisional disk modeling results. The combined sample from both tables consists of 5 protostars, 16 stars with primordial disks, 6 with homologously depleted transitional disks, 4 that have transitional disks with inner holes, and 6 bare stellar photospheres. Sources not analyzed here lack sufficient photometric data to model their SEDs and/or determine their plausible range of spectral types (e.g. FP-8, FP-33, FP-37, and FP-38), making it impossible to identify their disk evolutionary states. Below we discuss modeling of several sources illustrating how we determine disk states.

3.2.1. Disks in Different Evolutionary States

Figure 6 compares the SED for CrA-159 from the new sample to the Kenyon and Hartmann razor-thin flat disk model and the flat disk model produced from the Whitney radiative transfer code. The observed SED is dereddened from $A_V = 3$. CrA-159 has an infrared excess detectable from 1.6–2 μm to 24 μm , which consistently lies well above the Whitney flat disk model, indicating that

its emission is optically thick. According to our criteria, this source then has a primordial disk. With the exception of one star (V709), all disks in the new Coronet sample, predominately comprised of higher-mass stars, yield emission lying above the flat, optically-thick disk limit.

The disk population for the Sicilia-Aguilar et al. (2008) sample is far more diverse, including many transitional disks. We show comparisons between three homologously depleted transitional disk SEDs and flat disk models in Figure 7. Each source has a reduced level of disk emission compared flat disk models. Likewise, all transitional disks with inner holes have weak/negligible 3.6–5.8 μm emission but optically-thick 24 μm emission.

The top panel of Figure 8 shows model fits for CrA-205, which has a transitional disk with an inner hole. CrA-205 exhibits no excess emission shortwards of $\sim 10 \mu\text{m}$ but has a rising SED clearly departing from the stellar photosphere by $\sim 15 \mu\text{m}$. All of the best-fitting Robitaille models have inner disk radii ($R_{in} > 1000 R_{sub}$) much larger than our threshold identifying transitional disks with inner holes ($10 R_{sub}$). Moreover, the grid sampling of inner disk radii (grey shaded region) is heavily peaked at $1 R_{sub}$ (e.g. no inner hole). In spite of this intrinsic bias against selecting disk models with holes, all disk models lacking inner holes fail our χ^2 threshold.

Our results for the Sicilia-Aguilar et al. sample are intermediate between those of Sicilia-Aguilar et al. (2008) and Ercolano et al. (2009) who disagreed over the fraction of transitional disks with inner holes. CrA-466 and G-65 have best-fit models that do not require an inner hole (Figure 8, middle and bottom panels). Like Ercolano et al. (2009), we identify them as primordial disks. However, our modeling supports the claim by Sicilia-Aguilar et al. (2008, 2009) that CrA-205 has an inner hole, in fact the largest one in our sample. Ercolano et al. (2009) did not identify CrA-205's inner hole probably because they do not include the IRAC 8 μm data nor any IRS data in their fitting.

While we also agree with Ercolano et al. (2009) that G-14 and G-87 lack evidence for an inner hole, our modeling suggests that both have weaker emission than a perfectly flat, optically-thick reprocessing disk. Thus, like Sicilia-Aguilar et al. (2008) we identify these as transitional disks, albeit ones that are homologously depleted. The Ercolano et al. (2009) study focused on identifying transitional disks with inner holes. Therefore, we identify more transitional disks because we adopt a more expansive definition for what constitutes a transitional disk.

Two of the sources labeled as homologously depleted transitional disks may be debris disk candidates, while one of the transitional disks with inner holes may be a debris disk candidate. The identity of V709 is particularly questionable: while we identify it as a disk-bearing star, it is possible that its weak excess could be due to nebular contamination or an offset between the near-IR data and the MIPS data/IRS spectra caused by variability such as that produced by an undetected eclipsing companion. More importantly, if it has a disk, it is unclear whether it is a debris disk or transitional disk.

Cluster members with new Spitzer photometry are mostly protostars or stars with primordial disks (5 and 8, respectively, Table 3). The disk population for M stars sample studied in Sicilia-Aguilar et al. (2008) is more

evenly divided between primordial disks (8) and transitional disks (3–4 with inner holes, 4–6 homologously depleted). Unlike the new sample, many stars in the Sicilia-Aguilar et al. (2008) sample have homologously depleted transitional disks. Thus, based on modeling 1–24/70 μm data, the percentage of protoplanetary (primordial + transitional) disks in our combined sample that are transitional disks is $\sim 30\%$ (7/23). The percentage rises to 41% if debris disk candidates are classified as transitional disks, including V709 (11/27).

3.2.2. Disk Properties As a Function of Stellar Mass

To examine the spectral type/stellar mass dependence of disk properties, we bin our sample into three spectral type groups: earlier than K5, K5–M2, and later than M2. Assuming the Baraffe et al. (1998) isochrones (mixing length = $1.9 H_p$) and the T_e vs. spectral type scale from Currie et al. (2010), the corresponding stellar mass division is $M_\star > 1 M_\odot$, $M_\star = 0.5\text{--}1 M_\odot$, and $M_\star < 0.5 M_\odot$ ⁵.

The transitional disk frequency for Coronet Cluster members may be spectral type dependent. At most one and probably none of the disks around stars earlier than K5 appear to be transitional disks (0–1/5). Stars between K5 and M2 also mostly have primordial disks (7/10) with 2–3 stars harboring transitional disks and 0–1 with debris disks. Accounting for the uncertain status of debris disk candidates, the relative fraction of transitional disks to all protoplanetary disks for stars M2 or earlier with plausible masses equal to $0.5 M_\odot$ or greater is then $f(\text{TD})/(f(\text{TD})+f(\text{PD})) \approx 0.15\text{--}0.27$ (2/13, 4/15). For K5–M2 stars only, 22–30% of the protoplanetary disks are transitional disks. Transitional disks are more prevalent around stars later than M2, comprising 50–58% of the protoplanetary disk population (5/10 or 7/12). This high frequency is consistent with previous results from Sicilia-Aguilar et al. (2008).

However, given the small population of Coronet Cluster stars studied here it is unclear whether our analysis truly identifies a *statistically significant* stellar-mass dependent frequency of transitional disks characteristic of most young clusters. Furthermore, it is possible that some transitional disks provisionally identified from modeling optical-to-mid IR data may instead be primordial disks whose weak emission is due to the growth and settling of submicron-sized grains (e.g. Furlan et al. 2006). Analyzing data from clusters where far-IR and submm data is available is required to more conclusively break these degeneracies. To explore these issues further, and provide a context for our results, we now analyze disks in other clusters.

4. TRANSITIONAL DISK FREQUENCIES AND LIFETIMES AS A FUNCTION OF STELLAR MASS: A COMPARISON WITH TAURUS, IC 348, NGC 2362, AND η CHA

4.1. Sample and Wavelength Ranges Used For Analysis

⁵ In making these divisions, we are grouping together intermediate-mass ($M_\star \sim 2\text{--}4 M_\odot$) and solar-mass T Tauri stars. Grouping together these stars as the first spectral type bin may hide additional evolutionary trends since disk evolution for intermediate mass stars ($\gtrsim 2\text{--}3 M_\odot$) and solar-mass stars may proceed at different rates even by 1–3 Myr (e.g. Currie and Kenyon 2009). Any differences between 1–4 M_\odot stars and lower-mass stars then applies only to the *ensemble average* of 1–4 M_\odot stars.

To investigate the evolution of the transitional disk frequency with time, we analyze data in other clusters spanning an age range of 1–8 Myr. Comparing our results for the Coronet Cluster with 1–2 Myr-old Taurus and 2–3 Myr-old IC 348 addresses whether a stellar mass-dependent transitional disk frequency is a general feature of 1–3 Myr-old clusters. By comparing these results with those for 5 Myr-old NGC 2362 and 6–8 Myr-old η Cha, we investigate how the frequency of transitional disks evolves with time and estimate the typical transitional disk lifetime.

Taurus – Members of the Taurus-Auriga star-forming region are listed in catalogs from Kenyon et al. (2008), Rebull et al. (2010), and Luhman et al. (2009), which are updates of the classic Kenyon and Hartmann (1995) catalog. We reanalyze Taurus members studied in Luhman et al. (2010) to provide direct comparisons with their disk analysis. For Spitzer photometry, we use the IRAC and MIPS 24 μm data from Luhman et al. (2010) and MIPS 70 μm and 160 μm data from Rebull et al. (2010). We adopt optical photometry from Kenyon and Hartmann (1995), White and Ghez (2001), and Audard et al. (2007) and submillimeter measurements from Andrews and Williams (2005), Jewitt et al. (1994), Jensen et al. (1994), and Beckwith and Sargent (1991). To deredden stars, we determine optical extinctions for Taurus members, using estimates from Furlan et al. (2006), Rebull et al. (2010), Kenyon and Hartmann (1995), and Luhman et al. (2010) as starting points and then fit the optical/near-IR portion of the SED to a synthetic SED produced using the Currie et al. (2010) intrinsic colors and the Currie et al. (2010) and Luhman et al. (2003) effective temperature scales.

A large number of Taurus sources have complete SEDs from optical to far-IR/submillimeter wavelengths. We model the SEDs of 25 K5–M6 stars whose IR colors plausibly identify both primordial disks and transitional disks based on various color-color selection criteria in the literature (e.g. Lada et al. 2006; Currie and Kenyon 2009; Luhman et al. 2010; Muzerolle et al. 2010)⁶. Quantitatively, our selection criteria includes K5–M6 sources with $K_s - [8] (\text{dereddened}) = 1.25\text{--}2$. We further restrict our sample to sources whose far-IR/submillimeter data can yield good constraints on the range of plausible disk masses (see Appendix). Specifically, we require that the source has published submillimeter data *or a detection* in the far-IR MIPS bandpasses (70 μm or 160 μm). While this criterion may bias our selection against including the most depleted disks, especially for the lowest mass stars, we include it to be conservative.

IC 348 – For IC 348, we compile optical, near-IR and Spitzer/IRAC photometry, spectral types and extinctions presented in Lada et al. (2006, and references therein) and MIPS photometry and upper limits presented in Currie and Kenyon (2009) for 307 members listed in both studies as well as data for 41 additional spectroscopically confirmed members from Muench et al. (2007). We restrict our analysis to sources with MIPS 24 μm detections. Currie and Kenyon (2009) identified mid-IR colors for disks in different evolutionary states

⁶ We do not present modeling results for sources such as DM Tau, whose classification as a transitional disk has broad agreement

by modeling the SEDs of newly-detected disks in IC 348, but their sample is comprised mainly of stars later than M3–M4. Here, we model the SEDs of 25 IC 348 stars previously detected by Lada et al. (2006) and Muench et al. (2007) with full SEDs through $24 \mu\text{m}$ focusing on those with the same range of mid-IR colors analyzed in Taurus. Most of these 25 stars are earlier than M3–M4.

As with the Taurus sample, we use the published extinction estimates as a starting point and fit the optical/near-IR portion of the SED to arrive at a final value. In most cases, the best-fit optical extinction (A_V) matches that listed by Lada et al. (2006). Exceptions include IDs 26, 58, 97, 110, and 9024: their new extinction estimates are generally larger.

NGC 2362 – For NGC 2362, we analyze the Spitzer IRAC and MIPS photometry presented by Currie et al. (2009). Currie et al. (2009) present data for two membership lists for NGC 2362: members/probable members identified by Dahm (2005) and candidate members identified by Irwin et al. (2008). Here we analyze Spitzer data only for members/probable members identified by Dahm (2005) to be conservative. We include the two sources – IDs 41 and 63 – not considered in analysis by Luhman et al. (2010), because both have $\approx 5\sigma$ detections and thus should be included in our analysis (Figure 9).

Currie et al. (2009) already model the SEDs for NGC 2362 stars with the Robitaille et al. (2006) radiative transfer grid to identify disks with inner holes. Therefore, we only compare NGC 2362 SEDs through $24 \mu\text{m}$ to the appropriate flat reprocessing disk models. As starting points for our flat disk comparisons, we use extinction estimates listed in Currie et al. (2009) that were based off of comparisons with the Kenyon and Hartmann (1995) colors and off of output from fits with the Robitaille et al. models treating the extinction as a free parameter.

η Cha – For η Cha, we use the IRAC and MIPS $24 \mu\text{m}$ and $70 \mu\text{m}$ photometry and spectral types from Sicilia-Aguilar et al. (2009), MIPS $70 \mu\text{m}$ upper limits and MIPS-160 μm photometry/upper limits from Gautier et al. (2008), and IRS data presented in Bouwman et al. (2006) and Sicilia-Aguilar et al. (2009). To model η Cha sources, we compare source SEDs to appropriate flat disk models and fit their SEDs through $160 \mu\text{m}$ with the Robitaille model grid to identify inner holes and estimate disk masses.

4.2. Classification Method

Our disk classification method is an expanded, more thorough version of that used in §3. As in §3, we identify transitional disks with inner holes from fitting source SEDs with the Robitaille radiative transfer models. The difference between our method here and in §3 is in our differentiation between primordial disks and homologously depleted transitional disks. In §3, members of the latter group were identified as those having optically thin mid-IR emission (from comparing their emission to the flat disk limit) but lacking evidence for inner holes. As stated in §3, we considered the classification of these disks as provisional since weak mid-IR emission could be due to a low overall mass of submicron to submillimeter-sized dust *or* the growth and settling of just the smallest, submicron-sized grains to micron sizes or larger. Modeling based on 1– $24 \mu\text{m}$ data alone is unable to break this degeneracy.

However, SED modeling of sources with far-IR/submm data helps break this degeneracy (e.g. Wood et al. 2002). Taurus and η Cha include many sources with far-IR and/or submm data. Thus, SED modeling of Taurus and η Cha sources can identify which ones with optically-thin mid-IR emission but no inner hole have 1) a low inferred disk mass or 2) an inferred disk mass comparable to optically-thick primordial disks. The former group are classified as homologously depleted transitional disks (Currie et al. 2009); the latter group could be primordial disks undergoing extreme grain growth/dust settling/shadowing (Furlan et al. 2006).

To identify the range of disk masses for optically-thick primordial disks and thus most appropriate limit for dividing between primordial disks and homologously depleted transitional disks, we refer to SED modeling results for Taurus (Andrews and Williams 2005) which are discussed in detail in the Appendix. Briefly, typical primordial disk masses as a fraction of stellar mass are $M_{disk} \sim 0.01 M_\star$ for Taurus: the interquartile range covers $M_{disk} \sim 0.003\text{--}0.03 M_\star$ (Appendix, Figure 7 Andrews and Williams 2007)⁷. About 92–96% of the primordial disks in the Andrews and Williams Taurus sample have inferred masses greater than $0.001 M_\star$ (cf. Appendix). As discussed in the Appendix, far-IR data ($\lambda \gtrsim 70 \mu\text{m}$) is sufficient to estimate the disk mass at a precision useful for our study.

Thus, if we define the range of primordial disk masses by the interquartile range, the appropriate limit differentiating optically-thick primordial disks from homologously depleted transitional disks is $M_{disk} = 0.003 M_\star$. If we use the full range of primordial disk masses, the appropriate limit is $M_{disk} = 0.001 M_\star$. As discussed in the Appendix, these estimates for typical masses of optically-thick primordial disks, and thus our criteria for separating primordial and transitional disks, are not compromised by incompleteness. In our analysis, the disk mass is the median value of masses from the best-fit Robitaille et al. (2006) models; to determine the fractional disk mass, we use the Baraffe et al. (1998) isochrones and the effective temperature scales from Currie et al. (2010) for K5–M2 stars and Luhman et al. (2003) for later stars.

Combining our criteria from §3 with additional criteria presented in this section, we consider a disk in Taurus or η Cha to be a primordial disk if it meets the following two conditions:

- It lacks evidence for an inner hole/gap as inferred from SED modeling.
- Its mid-IR emission exceeds the optically-thick, flat disk limit *or* it has an inferred disk mass of $M_d > 0.003 M_\star$.

Disks with inferred masses of greater than $0.001 M_\star$ and up to $0.003 M_\star$ but no inner hole are considered to be borderline cases, as their classification depends on whether the interquartile range or full range of optically-thick primordial disk masses is used to separate primordial disks

⁷ Andrews and Williams (2005, 2007) use the term “Class II objects” to describe sources with optically-thick disk emission, though their sample includes some transitional disks with inner holes (e.g. UX Tau, CoKu Tau/4, GM Aur)

from homologously depleted transitional disks. Disks with masses $\leq 0.001 M_{\star}$, optically-thin mid-IR emission, and no inner hole are classified as homologously depleted transitional disks. We then determine the transitional disk frequency by dividing the number of transitional disks by the number of transitional + primordial disks.

To analyze disks in clusters lacking far-IR/submm data – IC 348 and NGC 2362 – we first assign provisional classifications based on §3 methods, which yield provisional frequencies for transitional disks. Since mid-IR data alone is unable to differentiate between disks with a low dust mass and those with substantial dust settling, some the disks identified as transitional based on mid-IR data could instead be primordial disks. Thus, we use the Taurus results to identify the mid-IR colors of transitional disks and determine the “contamination rate” of the transitional disk population selected by mid-IR data alone. Transitional disk frequencies for IC 348 and NGC 2362 are then revised after taking into account this contamination rate.

4.3. Transitional Disks in Taurus

Modeling results for 25 Taurus members are summarized in Tables 6 and 7. Several of these members have disks with inner holes - e.g. UX Tau, LkCa 15, and J04333905+2227207. Many others – e.g. VY Tau – lack clear evidence for an inner hole but have emission falling below the flat, optically thick disk limit (Figure 10). They also have weak submm emission (Table 7). The weak near-IR through submm emission from these disks identifies a substantial depletion of the entire dust grain population from hot inner disk regions to cold outer disk regions. Nearly all sources (94 %) with $K_s-[8] \leq 1.75$ have emission weaker than the optically-thick, flat disk limit.

4.3.1. Best-Estimated Masses of Disks in Taurus

Figure 11 displays the SEDs and histogram distribution of masses from best-fit models for several disks that lack inner holes but have weak near-to-mid IR emission – VY Tau, JH-223, ZZ Tau, and FP Tau – and indicates that they have low inferred masses ($M_{disk} \leq 0.001 M_{\star}$). Such sources fit our criteria for being a homologously depleted transitional disk. Several others (e.g. V807 Tau) lacking inner holes have optically-thin near-to-mid IR emission and $M_{disk} = 0.001-0.003 M_{\star}$: these are borderline cases. The intrinsic sampling of the Robitaille grid is heavily weighted towards disk models with masses $\sim 0.001-0.01 M_{\odot}$ (shaded region). In spite of this bias, the inferred disk masses for sources like those in Figure 11 are at least an order of magnitude lower.

Mass estimates based on submillimeter data alone (Andrews and Williams 2005) provide a simple but independent check on the estimates derived from radiative transfer modeling. All of the homologously depleted transitional disks with submillimeter data that are listed in Table 7 have non-detections at 350–850 μm , and thus their masses have a wide range of possible values. However, the submm-derived upper limits constrain the mass of optically thin emitting dust, which is useful since all of these sources have optically thin near-to-mid IR dust emission and optical depth decreases with increasing wavelength. For the homologously depleted disks, submm-derived upper limits range from $5.5 \times 10^{-4} M_{\star}$

to $10^{-3} M_{\star}$. In other words, submillimeter data alone provides evidence that these disks are less massive than primordial disks.

4.3.2. Frequency of Transitional Disks in Taurus

To compute the relative frequency of transitional disks around K5–M6 stars, we combine the transitional disk population identified by Luhman et al. (2010) and newly identified transitional disks from Table 7. For the primordial disk population, we consider all Taurus members with Spitzer photometry that are not Class I protostars. Based on mid-IR colors, Luhman et al. (2010) identified eighteen transitional disks around K5–M6 stars: nine around K5–M2 stars and nine around later stars. To these, we add 6–7 transitional disks around K5–M2 stars and 3–7 transitional disks around later stars identified from SED modeling.

Combining both transitional disk samples, the frequency of transitional disks is 0.19–0.22 (27–32/145) for the entire population, 0.20–0.21 (15–17/77) for K5–M2 stars, and 0.18–0.24 (12–16/68) for M3–M6 stars. Two transitional disks identified by Luhman et al. (2010) have extremely tenuous 24 μm excess emission ($K_s-[24] \sim 0.5-1$) and could be young debris disks (Carpenter et al. 2009). If we remove these sources, the transitional disk frequency for the entire population drops to 0.18 and 0.22, while the frequency for K5–M2 stars drops to $\sim 0.16-0.18$. Thus, we find a slightly higher percentage of transitional disks around K5–M6 stars than Luhman et al. (2010) find for K5–M5 stars ($\sim 20\%$ vs. their 13% (15/113)).

4.3.3. Mid-IR Colors of Primordial Disks and Transitional Disks

To guide our analysis of other clusters lacking far-IR/submm data (e.g. IC 348, NGC 2362), we determine the mid-IR colors ($K_s-[8]$) that identify primordial disks and transitional disks. Figure 12 plots the mid-IR colors of Taurus members separated by disk evolutionary state. Only members with primordial disks (black circles) have $K_s-[8] > 1.75$. Taurus members with $K_s-[8]$ bluer than the horizontal dashed line ($K_s-[8] = 1.25$) do not have primordial disks. Members with intermediate colors include primordial disks, transitional disks (grey circles enclosed by squares), and borderline cases (black circles enclosed by squares). Thus, there are two regions of mid-IR color-color space containing transitional disks: an “uncontaminated” region with blue colors consisting only of transitional disks and a “contaminated” region with redder colors which includes both transitional disks and primordial disks.

Comparing the number of transitional disks and primordial disks in the “contaminated” color region for Taurus members with far-IR/submm data provides an estimate for the level of contamination in other clusters lacking far-IR/submm data. As shown by Figure 12 and Table 6, there are 9 K5–M2 members with $K_s-[8] = 1.25-1.75$: 6 sources identified as transitional disks, two identified as primordial disks, and one borderline case (V807 Tau). Thus, 22–33% (2–3/9) of the sources with $K_s-[8]=1.25-1.75$ and provisionally identified as transitional disks from mid-IR data alone could in fact be primordial disks with substantial dust settling. For M3–M6 stars

with $K_s-[8]=1.25-1.75$, 3 sources listed in Table 7 plus two identified by Luhman et al. (2010) – J04330945 and J04213459 – are transitional disks, one is a primordial disk, and four are borderline cases. Thus, the contamination rate for M3–M6 stars with $K_s-[8] = 1.25-1.75$ is 10–50% (1–5/10).

4.3.4. Incorporating Uncertainties in Disk Mass Estimates

Here we quantitatively assess how the intrinsic uncertainty in disk mass estimates affects our conclusions about the frequency of transitional disks in Taurus and the contamination level from selecting transitional disks by mid-IR colors. First, we compare the interquartile range of disk masses from best-fit models for each star. Figure 13 shows that the range of disk masses for homologically depleted disks and primordial disks are distinct (see also Table 6). The upper quartile of disk masses for homologically depleted disks ranges from $\sim 9 \times 10^{-4} M_\star$ to $4 \times 10^{-3} M_\star$. The lower quartiles of masses for primordial disks is systematically larger and does not overlap, ranging from $4 \times 10^{-3} M_\star$ to $10^{-2} M_\star$. The masses of disks in borderline cases are also systematically low, though the upper quartiles for three of the five stars – J04231822+264116, J04153916+2818586, and ITG 15 – overlap slightly with the lower quartile masses for several primordial disks (e.g. GH Tau).

Second, we consider the full distribution of disk masses from best-fit models for each star to identify the fraction of models yielding $M_{disk}/M_\star \leq 0.001$ and 0.003 ($f < 1, 3 \times 10^{-3}$), our thresholds identifying homologically depleted transitional disks and borderline cases. Our goal here is to derive a purely probabilistic estimate of the transitional disk population from Table 6 to combine with the transitional disks listed by Luhman et al. (2010) and then to compare with previous estimates of the total population in this section. Here, the number of transitional disks around n stars listed in Table 6 each with $f(TD_i)$ of their disk models fulfilling our definition of a transitional disk is

$$n(TD) = \sum_{i=0}^n f(TD_i). \quad (1)$$

For disks with inner holes – e.g. LkCa 15 – determined by imaging and SED modeling $f(TD_i) = 1$, otherwise it equals $f(< 1, 3 \times 10^{-3})$ as listed in Table 6. This exercise yields $n(TD) = 10.6-13.8$ or $\sim 11-14$ ($n(TD) = 5.5-7.1$ for K5–M2 stars, 5.2–6.7 for M3–M6 stars).

Combining our probabilistic estimate for the transitional disks population drawn from Table 6 and the 18 transitional disks identified by Luhman et al. (2010) yields total population of 29–32 (18+ [11,14]), in agreement with estimates derived in §4.3.2. The estimates divided by spectral type range are likewise similar: 15–16 (9+[6,7]) for K5–M2 stars and 14–16 (9+[5,7]) for M3–M6 stars. Finally, the resulting contamination estimates agree well with previous ones: 22–33% (2–3/9) for K5–M2 stars and 10–30% (1–3/10) for M3–M6 stars⁸.

⁸ For K5–M2 stars, there are nine sources within our contamination region, our exercise predicts that $\sim 6-7$ are transitional disks, so the contamination rate is 2–3/9. For M3–M6 stars, there are 10 sources within the contamination region. Two of these are identi-

4.4. Frequency of Transitional Disks in IC 348

Table 9 summarizes our modeling results for selected IC 348 members; SEDs for members representing a range of mid-IR disk emission and provisional evolutionary states are shown in Figure 14. As with Taurus, we find that all but one of the members with $K_s-[8] \leq 1.75$ have optically-thin mid-IR disk emission. Since our Taurus analysis finds that most members with these colors have low disk masses or inner holes (29–32/35), we infer that most IC 348 members with these colors also have low disk masses or inner holes. Of the 25 IC 348 stars modeled, 17 are consistent with being transitional disks based on 1–24 μm data, while 8 are primordial disks.

To determine the frequency of transitional disks in IC 348, we use contamination estimates based on mid-IR colors from Taurus. Following the Taurus results, we adopt $K_s-[8] = 1.75$ as our fiducial division between primordial disks and transitional disks and derive a provisional frequency for transitional disks. Then we derive a revised frequency taking into account contamination by primordial disks with $K_s-[8] = 1.25-1.75$.

Based on this method, 8/33 K5–M2 stars and 43/81 M2.5–M6 stars have evidence for a disk with $K_s-[8] < 1.75$, and thus fit our nominal near-to-mid IR transitional disk criteria. Of the 8 (44) disks around K5–M2.5 (M2.5–M6) stars provisionally classified as transitional, 4 (19) have mid-IR colors within the “contaminated” region. Thus, corrected for contamination, about 32–40% of K5–M6 IC 348 disks are transitional disks. The transitional disk population is heavily weighted towards later-type stars: 18–24% of disks around K5–M2 stars have transitional disks (6/33 to 8/33), while $\sim 42-51\%$ of M2.5–M6 stars have transitional disks (34/81 to 41/81).

4.5. Frequency of Transitional Disks in NGC 2362

Table 10 summarizes our modeling results for NGC 2362. Near-to-mid IR emission from most cluster members lies well below the optically thick, flat reprocessing disk limit, indicating that the mid-IR emission is at least marginally optically thin ($\tau \lesssim 1$). Comparing this modeling to radiative transfer modeling performed for NGC 2362 in Currie et al. (2009) and for Taurus in this work shows that many sources with weak/negligible 1–8 μm emission and optically-thick 24 μm emission require inner holes while many with marginally optically-thin near-to-mid IR emission have low inferred disk masses. Figure 15 displays 4 representative SEDs comparing the observed emission to the optically thick, flat disk limit.

Our results are consistent with those from Currie et al. (2009) who argue that transitional disks are equal to or greater in number than primordial disks. Currie et al. (2009) find that 81% of disks around K0–M3 members are transitional disks (17/21). Here four disks are primordial disks (IDs 111, 139, 187, and 202), and one (ID 177) appears to be a borderline case (since it may have an inner hole) but is counted as a primordial disk in the analysis below to be conservative (since it has $K_s-[8] > 1.75$). The rest (16; 14 of which are K5–M3 stars) have near-to-mid IR emission consistent with being transitional disks. Of these, five K5–M3 stars either have

identified as transitional disks from Luhman et al. (2010), whereas our exercise predicts that 5–7 out of the eight others are transitional disks. Thus, the contamination rate is 1–3/10

K_s -[8] ≤ 1.25 (thus lying outside the range of colors contaminated by primordial disks) or show evidence for inner holes. The other 9 K5–M3 stars have mid-IR colors between K_s -[8] = 1.25 and 1.75, within the contaminated region. Based on our Taurus analysis, 2 K5–M2 stars and 0–1 M2.5–M3 stars provisionally identified as having transitional disks instead have primordial disks with dust settling. Therefore, we arrive at a final transitional disk frequency of 58%–63% (11/19–12/19) for K5–M3 stars. The frequency for K5–M2 stars (63%) and M2.5–M3 stars (33–66%) are statistically indistinguishable given the small number in the latter group (3).

4.6. Frequency of Transitional Disks in η Cha

Table 11 summarizes our modeling results for η Cha. Of the 15 late-type members with IRAC and MIPS photometry, 8 have evidence for a disk. Only three sources (RECX-11, J0843, and J0844) fulfill our definition of a primordial disk. Three members have transitional disks with inner holes (RECX-3, 4, and 5); two have homologically depleted transitional disks (RECX-9 and J0841). Thus, η Cha has a high transitional disk frequency (5/8 or 63%). Our results agree with those of Sicilia-Aguilar et al. (2009) who separately analyze Spitzer IRS data to find that transitional disks comprise 50–75% of the disk population. A “probabilistic” estimate of the transitional disk fraction (e.g. as in Section 4.3) yields the same answer: $n(\text{TD}) = 4.95$ or ~ 5 .

Gas diagnostics are consistent with our argument that most disks in η Cha are transitional disks. RECX-5 and 9 are accreting at extremely low rates ($4\text{--}5 \times 10^{-11} M_\odot \text{ yr}^{-1}$) (Lawson et al. 2004). RECX-3, RECX-4, and J0841 lack evidence for accretion circumstellar gas. RECX-3, 5, and 9 lack evidence for rovibrational H_2 emission from warm circumstellar gas (Ramsay-Howat and Greaves 2007). Only J0843, identified as a primordial disk from SED modeling, shows evidence for H_2 emission and for substantial accretion ($10^{-9} M_\odot \text{ yr}^{-1}$).

4.7. Revised Transitional Disk Frequency for the Coronet Cluster

Based on our analysis of Taurus data in §4, some fraction of Coronet Cluster stars determined to have transitional disks based on mid-IR data probably are primordial disks with dust settling. In particular, G-1 (M0), G-14 (M4.5), and G-87 (M1.5) have K_s -[8] colors placing them within the contaminated region: other transitional disks have inner holes or lie within the uncontaminated region. Accounting for contamination, the size of the transitional disk population drops to 11–22% for K5–M2 stars (1/9, 2/9) and 30–50% for M2.5–M6 stars (3/10, 6/12), where the ranges account both for contamination by primordial disks with substantial dust settling and for possible misclassification of debris disk candidates. Thus, our transitional disk frequencies for all five clusters now account for uncertainties in disk classification based on mid-IR data alone.

4.8. The Evolution of the Transitional Disk Population

Combining our results for the Coronet Cluster, Taurus, IC 348, NGC 2362, and η Cha, we now investigate the frequency of transitional disks as a function of

age and stellar properties. Table 12 lists the relative frequency of transitional disks as a function of time in three spectral type bins: mid-K to mid-M stars (K5–M6), K5–M2 stars, and M3–M6 stars. To compare with theoretical predictions, we overplot the approximate loci (Figure 17 top panel, solid and dotted lines) expected from the Alexander and Armitage (2009) disk evolution/planet formation models, which yield frequencies for transitional disks as a function of time and assume a disk clearing timescale of ~ 0.5 Myr.

The transitional disk frequency for K5–M6 stars increases as a function of time from $\sim 20\%$ at 1–2 Myr to $\sim 50\text{--}60\%$ by 5 Myr. The frequencies are consistently 1.5–3 times higher than those predicted by Alexander and Armitage (2009) for a 0.5 Myr transition timescale. Within the context of the Alexander and Armitage (2009) study, our results indicate that the transitional disk phase on average lasts longer than 0.5 Myr.

The bottom panel of Figure 17 compares our frequencies with those from Muzerolle et al. (2010) who use a more empirically-based approach to identify transitional disks based primarily on IRAC and MIPS flux slopes (bottom panel). Our transitional disks frequencies are substantially larger than those Muzerolle et al. derive based on their self-described *classical* definition for what constitutes a transitional disk (diamonds): a disk with an inner hole and optically-thick outer disk. However, Muzerolle et al. argues for an expanded definition for a transitional disk, including disks whose mid-IR emission plausibly identifies a more homologous depletion of emitting dust and disks with inner holes/cavities and more optically thin outer disks. Adopting this definition, their transitional disk frequencies (triangles) are in good agreement with those we derive for clusters older than 2 Myr. For the two clusters we both analyze, IC 348 and η Cha, our frequencies are nearly identical.

To derive a timescale for the transitional disk phase, we follow a parametric, Monte Carlo approach, similar to that from Muzerolle et al. (2010), evolving a population of 10^5 stars to simulate the frequency of disks in different states for clusters with ages less than 10 Myr. We adopt a 3 Myr e-folding timescale for the protoplanetary disk stage, consistent with Spitzer observations (Figure 18, top panel). Some fraction of the protoplanetary disk lifetime is spent in the transitional disk phase. To assess the duration of this phase, we vary the transitional disk e-folding timescale (t_{TD}); correspondingly, the e-folding timescale for the primordial disk phase is 3 Myr - t_{TD} . Through the first 0.54 Myr, we fix the disk fraction at 1 to account for the lifetime of Class I protostars (Evans 2009). Finally, we assume a 1 Myr age dispersion at each cluster age.

As shown by Figure 18 (bottom panel), transitional disk frequencies in all clusters are most consistent with a 1 Myr transition timescale, lying well above predictions for a 0.1–0.5 Myr timescale and below predictions for a 2 Myr timescale. Thus, our analysis confirms earlier results based on NGC 2362 and η Cha from Currie et al. (2009) and Sicilia-Aguilar et al. (2009) that the mean transitional disk lifetime must be an appreciable fraction of the total protoplanetary disk lifetime, estimated to be $\sim 3\text{--}5$ Myr (Hernandez et al. 2007a; Currie et al. 2009). Adopting Muzerolle et al. (2010)’s model for the

frequency of transitional disks with time yields the same qualitative result. They predict smaller transitional disk frequencies at 3–10 Myr than we do for a 1 Myr transition timescale. The identification of a long transition timescale based on our predictions is then conservative. On the other hand, our results are in conflict with other recent claims, particularly those of Luhman et al. (2010) who argue for a transitional disk lifetime less than 0.5 Myr. In §5, we compare our methodology with their’s and those from other recent studies.

We emphasize that our disk frequencies account for disks with *both* transitional disk morphologies: disks with inner holes and homologously depleted disks. Homologously depleted transitional disks generally appear to be more numerous than those with inner holes, up to a factor of 1.5–2 larger in number for the Coronet Cluster and NGC 2362. However, these differing frequencies do not constrain the relative lifetimes of disks following these evolutionary paths: we cannot tell between a morphology with a shorter lifetime and one that operates less frequently. We also note that these results are statistical. In other words, while there is some uncertainty in the state for individual objects, these uncertainties are averaged out at the end.

At least for the Coronet Cluster and IC 348, the transitional disk frequency is spectral type dependent (Figure 19). The transitional disk frequencies for M3–M6 stars in these clusters is marginally but consistently higher than those for K5–M2 stars by about a factor of ~ 1.5 . Formally, M3–M6 stars in Taurus also more frequently have transitional disks than do K5–M2 stars, though the difference is not statistically significant. Muzerolle et al. (2010) also find that the transitional disk population is dominated by later-type stars, though their correlation is stronger than what we find.

A spectral-type dependent transitional disk frequency may help explain the high transitional disk frequency found by Sicilia-Aguilar et al. (2008). Since the Sicilia-Aguilar et al. (2008) sample is drawn heavily from stars later than M2, their sample is predisposed towards having a high transitional disk fraction compared to cluster-averaged values and compared to those for brighter, more easily detectable K to M2 stars. The transitional disk frequency for the bulk cluster population (e.g. including members in Table 3) is similar to that for other 1–3 Myr-old clusters. At least one other cluster, IC 348, also has a very high transitional disk fraction for very low-mass stars.

5. DISCUSSION

5.1. *Summary of Results*

This paper expands upon previous Spitzer analysis of the Coronet Cluster disk population around very low-mass stars performed by Sicilia-Aguilar et al. (2008), presenting new photometry for other cluster members, including many with higher stellar masses. We use SED modeling and comparisons with simple disk models/empirical metrics to assess the Coronet Cluster disk population, focusing on identifying and characterizing candidate transitional disks. By analyzing the disk population for other 1–8 Myr-old clusters, we investigate the utility of using mid-IR data to probe disk evolutionary states, determine how the frequencies of transitional disks change with time, and investigate how this lifetime

may depend on stellar properties. Our study yields the following major results:

- The Coronet Cluster contains a high frequency of transitional disks: $\sim 30\%$ (formally, 21–36%) of the disk population around K5–M6 stars. Although the samples are small, our analysis hints at a spectral type-dependent frequency for transitional disks, confirming earlier suggestions by Sicilia-Aguilar et al. (2008, 2009): they appear more frequently around the very low-mass stars that were the focus of Sicilia-Aguilar et al. (2008). IC 348 exhibits the same spectral type/stellar-mass dependent transitional disk frequency.
- Based on optical to submm SED analysis of Taurus sources with high-quality photometry, we confirm that many disks lacking clear evidence for inner holes also have a low dust mass. Their mid-IR emission is due to a depletion of dust, not dust settling: these represent a more homologous depletion of disk material with time instead of an inside-out dispersal. Many transitional disks can only be identified from SED modeling as their mid-IR colors overlap with primordial disks. About 22–33% (10–50%) of disks around K5–M2 (M3–M6) stars identified as homologously depleted transitional disks based on optical to mid-IR data alone may in fact be primordial disks with a heavy depletion of submicron-sized dust but a large total dust mass. Disks with very different morphologies can occupy the same region of color-color space: SED modeling is required to avoid misclassifying disks.
- Combining analysis of the Coronet Cluster disk population with that for Taurus, IC 348, NGC 2362 and η Cha shows that the relative frequency of transitional disks around K5–M6 stars increases from $\sim 20\%$ at 1–2 Myr to $\sim 50\text{--}60\%$ by 5–8 Myr. Parametric modeling shows that this trend implies a mean transitional disk lifetime near 1 Myr, not $\sim 0.1\text{--}0.5$ Myr.

5.2. *Transitional Disk Identification in Other Recent Work: The Importance of SED Modeling*

Other recent studies of transitional disks provide evidence that the weak-IR-to-submm dust emission from homologously depleted transitional disks is likely due to disk clearing, consistent with our results. Cieza et al. (2008) selected transitional disks as those with mid-IR emission weaker than the lower-quartile Taurus SED and low levels of accretion, including many that lack any evidence for inner holes. They found that disks with weak mid-IR emission have low submm-inferred disk masses. Cieza et al. (2008) interpret this trend as evidence in favor of UV photoevaporation models for disk clearing: photoevaporation should begin to clear the inner disk once the total disk mass (probed by submm data) drops significantly. More generally, though, this trend implies that for some disks the mass of emitting dust drops simultaneously over a wide range of stellocentric distance, consistent with a homologous depletion of disk material.

Cieza et al. (2010) found that the disk mass and accretion rate for transitional disks, including those we would

identify as homologously depleted, appear to be correlated (Cieza et al. 2010): disks with lower accretion rates or small upper limits have lower inferred disk masses. There is no clear reason why the accretion rate should drop because submicron-sized grains had grown; however, disks undergoing a homologous depletion of their total mass in gas and dust should have low inferred masses *and* a lower frequency and rate of accretion.

Other studies, particularly the C2D survey of transitional disks presented in Merin et al. (2010), conclusively show that SED modeling is needed to properly characterize disks. By modeling optical through submm photometry and spectroscopy of a mid-IR selected sample of candidate transitional disks ("cold disks" in their terminology), they determine which disks have inner holes and which lack evidence for an inner hole and investigate typical mid-IR colors for both kinds of disks. Their analysis shows that the mid-IR colors of transitional disks overlap with primordial disks (e.g. their Figure 15). Computing the frequency of transitional disks using mid-IR colors is then error prone unless SED modeling of well characterized sources is used to identify uncontaminated regions of color-color space and quantitatively assess contamination where transitional disks and primordial disks have the same colors. This finding is qualitatively consistent with our Taurus modeling results.

Luhman et al. (2010) compile data for numerous 1–10 Myr-old clusters to uniformly identify transitional disks and quantify their population self consistently. Their modeling follows a different approach than that followed here and in some previous work (e.g. Currie et al. 2009; Merin et al. 2010), as they select synthetic K_s -[8] and K_s -[24] colors produced from the D'Alessio et al. (2006) 1+1D disk code as fiducial colors separating primordial disks from transitional disks. The model they use has two grain populations: where the "big" grain population extends from submicron to millimeter sizes and is confined to the disk midplane, while the "small" grains lie above the midplane and are $\lesssim 1 \mu\text{m}$ in size. It assumes a negligible accretion rate ($\dot{M} = 10^{-10} M_\odot \text{yr}^{-1}$) and a "depletion factor", $\epsilon=0.001$, which removes 99.9% of the small dust grains. They find lower transitional disk frequencies and thus derive a shorter lifetime for the transitional disk phase. They claim that previous work (e.g. Currie et al. 2009; Sicilia-Aguilar et al. 2009) arguing in favor of a longer transitional disk lifetime improperly identifies sources with emission weaker than the median Taurus SED as transitional disks or conflates a lack of near-IR emission with evidence for disk clearing⁹.

We agree with Luhman et al. (2010) that some primordial disks can have very blue colors due to dust settling. However, they did not quantitatively consider the possibility that some transitional disks may (in some color-color diagrams) have redder colors than the bluest primordial disks. Based on a more detailed, multiwavelength analysis, we derive higher transitional disk frequencies than they do for nearly all clusters, especially for those older than Taurus. Our disagreement primarily arises because many disks that Luhman et al. (2010)

⁹ As can be seen from a simple inspection of the Currie et al. (2009) analysis, their disk classification was instead based on comparing SEDs to the *lower-quartile* Taurus SED. This was clarified in later work (Currie and Kenyon 2009).

identifies as being optically-thick primordial disks from their color criteria are consistent with having optically thin/marginally optically-thin emitting dust in the mid-IR *and* low inferred disk masses. If their weak mid-IR emission were due only to the growth and settling of the smallest grains, their far-IR to submm emission (and thus inferred disk masses) should be comparable to known primordial disks, which is not observed. Therefore, these disks are more consistent with being transitional disks.

There are other aspects of Luhman et al.'s analysis that weaken or undermine their conclusions. First, while Luhman et al. (2010)'s adopted model results from a sophisticated code, their conclusions are prone to large uncertainties, mostly because they use color comparisons from a single model to identify transitional disks, not full SED modeling. Within the context of their model, the Luhman et al. conclusions are *extremely* sensitive to assumed values for their free parameters, ϵ and \dot{M} , and thus highly selective. Assuming either that disks remove 99% of their small dust instead of 99.9% or have a small accretion rate of $\dot{M} = 10^{-9} M_\odot \text{yr}^{-1}$ revises their fiducial mid-IR colors redwards by ~ 0.5 mags (e.g. K_s -[8] ~ 1.75 , K_s -[24] ~ 4.5 for K5–M2 stars). Using these colors to classify disks yields results similar to those presented here and in Currie et al. (2009) for 15 of the 16 model combinations of ϵ (0.001-1) and \dot{M} (10^{-10} – $10^{-7} M_\odot$) studied in D'Alessio et al. (2006, e.g. their Figure 13).

Second, while ϵ may be a true free parameter, measured accretion rates for many sources are much higher than that from the disk model used by Luhman et al. (2010), rendering their adopted model inapplicable. For example, ID-85 in NGC 2362, identified as a transitional disk by Currie et al. (2009), is a likely accretor based on its H_α emission. Using relations from Dahm (2008) and Herczeg and Hillenbrand (2008)¹⁰, its accretion rate is $\sim 4\text{--}7 \times 10^{-9} M_\odot \text{yr}^{-1}$, or *40 to 70 times greater* than what Luhman et al. assume. From comparing the SED of ID-85 to output from D'Alessio et al. disk models with realistic accretion rates, this source should be classified as a transitional disk, contrary to Luhman et al.'s results. Taurus-Auriga, Trumpler 37, and other clusters analyzed by Luhman et al. include many sources with weak mid-IR emission (transitional disks/borderline cases) whose measured accretion rates render Luhman et al.'s analysis inapplicable, such as ZZ Tau ($1.3 \times 10^{-9} M_\odot \text{yr}^{-1}$, White and Ghez 2001, see also Sicilia-Aguilar et al. 2010).

Third, the model that Luhman et al. (2010) adopt likely 1) has an extremely low disk mass which 2) is almost never optically thick and thus cannot distinguish *optically-thick* primordial disks from other disks. As shown in Tables 2.2 and 2.4 of Espaillat (2009), where the D'Alessio et al. input parameters are detailed, the disk mass for models with parameters adopted by Luhman is $\sim 1.38\text{--}1.45 \times 10^{-4} M_\odot$: an order-of-magnitude (or more) smaller than our primordial/transitional disk

¹⁰ Here we assume $E(B-V) = 0.01$ (1/10th the cluster average listed by Moitinho et al. 2001), an age of 5 Myr, a stellar radius for an M2 star of this age from Baraffe et al. (1998), and $R_{in} = 5 R_*$. The intrinsic uncertainty in the accretion rate is < 0.5 dex (see Dahm 2008). According to SED modeling presented here, the reddening is probably higher, meaning that the intrinsic H_α luminosity is higher and the resulting accretion rate is also higher.

division for all but the latest-type stars and the median primordial disk mass (Andrews and Williams 2005, and Appendix). Furthermore, Figure 2.6 of Espaillat (2009) shows that almost none of this disk is optically thick to its own radiation ($\tau_R \gg 1$), unlike our adopted model and other D’Alessio et al. models. Thus, a major reason why the Luhman’s adopted model yields weak mid-IR emission is because of its low dust mass, not just because of dust settling. To better parse disks into different states, Luhman et al. should have instead adopted a model yielding an optically-thick disk with a dust mass comparable to typical primordial disk masses (e.g. the fiducial model in D’Alessio et al. 2006 except with $\epsilon = 0.001$ and the accretion rate set to a negligible value).

Finally, SED modeling and imaging of individual sources shows that the Luhman et al. color criteria fails to uniquely identify primordial/transitional disks. For example, UX Tau and LkCa 15 are identified as primordial disks according to Luhman et al.’s color criteria as they are redder than the authors’ primordial disk limit. But SED modeling and/or high-contrast imaging show that both have large gaps with optically-thin dust/no dust extending from ≈ 0.1 AU to ≈ 50 AU from the star (Thalmann et al. 2010; Mulders et al. 2010; Espaillat et al. 2007). SED modeling also shows that sources in NGC 2362 (e.g. ID-3), IC 348 (e.g. ID-97), and Trumpler 37 (e.g. ID 14-11) classified by Luhman et al. as primordial disks probably have inner holes and thus are transitional disks (e.g. Currie et al. 2009; Sicilia-Aguilar et al. 2007, this work).

Even though we disagree with Luhman et al.’s conclusions for reasons described above, their study reinforces a major point made here – mid-IR colors of disks can be highly degenerate. The degeneracy highlighted from both of our studies shows that full SED modeling is needed to accurately assess the frequency of transitional disks and the duration of the transitional disk phase. While time intensive, this approach provides *de facto* more information about disk properties than can be provided by comparing source colors with synthetic colors resulting from a single disk model in a single color-color diagram.

5.3. *Transitional Disks In Young Clusters: Why the Paucity of Transitional Disks in Taurus Does Not Imply a Short Timescale for Disk Clearing*

Many pre-Spitzer studies have argued that the small number of transitional disks compared to optically-thick primordial disks and disk-less stars in young clusters like Taurus provides evidence in favor of a short ($\lesssim 0.1$ Myr) transition disk phase due to rapid disk clearing (e.g. Skrutskie et al. 1990; Simon and Prato 1995; Wolk and Walter 1996, and later work). Though transitional disks are infrequent compared to primordial disks and diskless stars in the youngest clusters (e.g. 20% for Taurus), it does *not* follow that the transitional phase must be very shortlived (e.g. $\lesssim 0.1$ Myr). Here, we review why this is the case, describe how our work and other recent studies support this position, and consider recent work that revives older claims.

As argued by Currie et al. (2009), stars in Taurus are typically too young compared to the mean protoplanetary disk lifetime (3–5 Myr) for the majority of them to begin clearing. Thus, it is unsurprising that relatively

few show evidence of active clearing. Our parametric modeling quantitatively supports this argument, showing that transitional disks do not comprise the majority of disks in the youngest clusters even for lengthy transitional disk phases (e.g. $t_{TD} = 1$ Myr). Thus, the size of the transitional disk population at ~ 1 –2 Myr does not, by itself, clarify how long protoplanetary disks show signs of active clearing over a typical lifetime of 3–5 Myr. To explain the large population of diskless stars in Taurus ($\sim 30\%$ of the total population), Currie et al. (2009) argue that stars with close binary companions lose their protoplanetary disks far more rapidly than stars without close binary companions (e.g. Ireland and Kraus 2008).

Luhman et al. disagree with both of these claims. They argue that age cannot explain Taurus’s paucity of transitional disks, since since diskless stars in Taurus are more dispersed and are thus older than stars with disks. We agree with Luhman et al. (2010) that an age spread may also explain the large number of diskless sources in Taurus. However, this fact would simply confirm that that older stars are less likely to have disks (e.g. Sicilia-Aguilar et al. 2006b; Hernandez et al. 2007a; Currie et al. 2007, 2009) and thus does not provide evidence in favor of rapid disk clearing.

Luhman et al. also argue that binarity cannot explain the large diskless population in Taurus. They note that the Taurus binary frequency declines with mass. They claim that if many Taurus disks are cleared by binaries then the disk fraction should be highest at low masses, which is not observed. However, the drop in binary frequency for low-mass stars is heavily weighted towards a drop in *wide binary companions* with separations of ~ 200 AU or greater, which are irrelevant here (Kraus et al. 2006, 2011). Moreover, many diskless stars in Taurus are tight binaries (Kraus et al. 2011, ApJ submitted). With tight binaries removed, the population of diskless stars shrinks significantly. Cieza et al. (2009) also find that disks in short-period binary systems are less frequent than those around wide-separation binaries or single stars (see also Bouwman et al. 2006).

In summary, either binarity or an age spread explain the smaller number of Taurus stars with transitional disks relative to primordial disks *and* diskless stars. Moreover, parametric modeling shows that the frequency of protoplanetary disks in the transitional disk phase is perfectly consistent with an extended transitional disk phase. Thus, Taurus data *provides no evidence* that the transitional disk phase must be rapid.

5.4. *Limitations and Uncertainties of Our Study and Future Work*

5.4.1. *Qualifications on Our Identification of Transitional Disks*

Our identification of some transitional disks (those labeled as homologously depleted) is predicated on 1) our assumptions about the range of primordial disk masses, 2) the reliability of the Robitaille models in estimating disk masses, and 3) the reliability of our assumed stellar masses. Current data shows that the lower quartile of masses for optically-thick primordial disks is $0.003 M_{\star}$ and nearly all primordial disks have masses greater than $0.001 M_{\star}$. Since not all Taurus members have been targeted by submillimeter observations, it is possible that

future surveys will uncover more disks with optically-thick near-to-mid IR emission but inferred masses that are systematically lower than the interquartile range/full range from current observations.

Additionally, as shown in Figure 11, the best-fit disk models for homologously depleted transitional disks have median values for absolute disk masses that yield fractional disk masses lying below our adopted primordial disk limit. However, some of the models for each disk (typically, 10–30%) yield masses lying above $0.001 M_{\star}$. Thus, it is possible, albeit unlikely, that some of these disks are not low mass.

However, submillimeter data constrain the mass of emitting, optically thin dust to be less than these limits. Moreover, the best-fit models for some primordial disks and all borderline cases include those with masses below $0.001 M_{\star}$. Thus, uncertainties in determining disk masses do not necessarily bias our results in favor of finding a high frequency of transitional disks. Similarly, the classification of some sources with optically-thin near-to-mid IR emission but large inferred disk masses (e.g. V836 Tau) as primordial disks is conservative. While these sources lack clear evidence for *cleaned* inner holes/gaps, their inner regions may be optically thin, and they may be undergoing the early stages of inner disk clearing.

More generally, the intrinsic sampling of the Robitaille et al. grid is non-uniform across all fitting parameters, which in principle could undermine our conclusions. As mentioned previously, disks without inner holes are more frequently represented than those without holes and massive disks ($M_{disk} \sim 0.01 M_{\odot}$) are also better represented than lower-mass disks. Figure 3 of Robitaille et al. indicates the presence of “coupled” non-uniform sampling between parameters: there are many more models with an envelope accretion rate greater than $10^{-6} M_{\odot} \text{ yr}^{-1}$ and that these models predominantly have disk masses greater than $10^{-3} M_{\odot}$.

However, our disk mass estimates are not undermined by non-uniform sampling. The lower two panels of Robitaille et al.’s Figure 3 and our Figure 20 indicate that simply including far-IR and submm data eliminates vast swaths of parameter space and overcomes these sampling biases. The intrinsic sampling of the Robitaille grid is weighted towards massive disks, yet we find numerous homologously depleted disks in spite of this bias because far-IR/submm non-detections rule out nearly all massive disks. Conversely, the submm detections for primordial disks provide strict limits on the inferred disk mass (see also Beckwith et al. 1990; Andrews and Williams 2005) and make the interquartile range of M_{disk}/M_{\star} for these objects nearly single valued in many cases (see Figure 13). On the other hand, uncertainties in deriving other disk parameters (e.g. flaring power) have not been fully explored here and may be seriously affected by non-uniform sampling.

Our analysis leverages not just on the precision with which we can estimate the mass of disks but also our accuracy. Estimating a mass of emitting dust from submm data alone requires assuming a value for the dust opacity, κ (e.g. Beckwith et al. 1990; Beckwith and Sargent 1991; Henning and Stognienko 1996, and later references). Since the dust opacity is not strictly known (and is affected by grain growth), what can be constrained from such data is the product of the dust mass and

the opacity, not simply the dust mass. On the other hand, grain growth/dust settling (which affect κ) have far stronger effects on the near-to-mid IR portion of disk SEDs than in the submm (e.g. Wood et al. 2002; D’Alessio et al. 2006). For instance, “settled disk” models from D’Alessio et al. (2006) have 250-1000 μm emission equal to or *larger* than that for disks without grain growth/settling (see Figure 13, top two sets of panels in D’Alessio et al. 2006).

The total disk mass is also uncertain. Since continuum IR to submm emission comes predominantly from dust, a gas-to-dust ratio must be assumed in converting a submm-inferred dust mass to a total disk mass. The models used here, in Currie et al. (2009), and other work (e.g. Cieza et al. 2010; Andrews and Williams 2005) assume standard values from κ and a solar gas-to-dust ratio (see Beckwith and Sargent 1991). However, comparisons with disk masses derived from accretion rates (assuming steady-state accretion) indicate that our methods may systematically underestimate true disk masses (e.g. Andrews and Williams 2007). This may be due either to an inaccurate assumed value for κ or a substantially non-solar gas-to-dust ratio, which may occur from grain growth and planetesimal formation. Our analysis provides evidence that masses for homologously depleted transitional disks are systematically lower by a factor of 10-1000 compared to primordial disks; other work provides evidence that gas and small dust deplete on similar timescales for disks in general and for homologously depleted transitional disks in particular (Fedele et al. 2010; Kennedy and Kenyon 2009; Cieza et al. 2010). However, given the uncertainties in determining κ and the gas-to-dust ratio, our analysis does not provide an absolute calibration for disk masses that can inform models for planet formation (e.g. Kenyon and Bromley 2009; Bromley and Kenyon 2011).

Accurately quantifying uncertainties in stellar mass for each star is another challenge. Between 1 Myr and 5 Myr, the Baraffe et al. (1998) isochrones with a mixing length parameter of $L_p = 1.9 H_p$ (“required to fit the Sun”) predict that $1.4 M_{\odot}$ stars increase in T_{eff} by ~ 125 K from 4663 K to 4786 K, thus changing in spectral type by ~ 1 subclass (cf. Currie et al. 2010). The variation is smaller (~ 100 K) for solar-mass stars and inconsequential for very low-mass stars ($M_{\star} \lesssim 0.7 M_{\odot}$). Adopting the conversion from spectral type to mass from Baraffe et al., our stellar masses are then intrinsically uncertain by $\approx 0.1 M_{\odot}$ or less due to the different mapping between spectral type and mass as a function of age. The uncertainties in measured spectral types are up to 1–2 subclasses, considering the range of spectral types reported in the literature for various Taurus members (e.g. White and Hillenbrand 2004). The age and spectral type uncertainties listed above indicate that our fractional disk masses could be uncertain by an additional 10–20%, and that considering these uncertainties could slightly broaden the interquartile range of fractional disk masses for some objects.

Finally, our analysis may miss some sources whose gaps cannot be inferred from photometric data alone. Among our sample, the SED for DH Tau shows evidence for a $\lambda F_{\lambda} \propto \lambda^{-3}$ decline from 3.6 μm to 8 μm , similar to that for transitional disks UX Tau and LkCa 15, which have large (tens of AU) gaps separating a small optically-thick,

~ 1500 K inner disk from an optically-thick outer disk. The SED fit to this source from the Robitaille et al grid is poor. Since the Robitaille et al grid provides good sampling for full disks with a range of masses (and thus mid-IR emission) *and* disks with cleaned inner holes, it is plausible that DH Tau's disk has a different morphology such as a disk with a developing gap. Since not all Taurus members have been targeted by mid-IR spectrographs, more disks with small holes/gaps may be identified by future observations. Indeed, Espaillat et al. (2011) argue that IP Tau, which we identify as having a primordial disk in spite of its weak mid-IR emission, has a ~ 2 AU gap. Thus, the true size of the transitional disk population in Taurus, especially the subset with small gaps/inner holes, is plausibly larger than what we find.

5.4.2. Limits on Our Study As a Probe of Transitional Disk Lifetimes/Disk Clearing

While our analysis provides strong evidence in favor of a long transitional disk phase, especially for very low-mass stars, several important caveats qualify this conclusion. First, many different mechanisms may be responsible for explaining the morphologies of transitional disks (Alexander and Armitage 2009; Cieza et al. 2010; Sicilia-Aguilar et al. 2010). Therefore, a "transition timescale/transitional disk lifetime" derived from the relative frequency of all transitional disks is only an averaged value of the timescales from a number of different mechanisms like gas giant planet formation and UV photoevaporation. Some of these mechanisms may operate on fast, $\lesssim 0.1$ – 0.5 Myr timescales but less frequently whereas others take $\gtrsim 1$ Myr to clear dust in disks and operate more frequently.

The disk clearing time for many candidate mechanisms (e.g. gas giant planet formation, UV photoevaporation) depends on properties such as disk viscosity, initial disk mass and initial angular momentum that are poorly con-

strained and likely have a large intrinsic dispersion. This dispersion in disk properties may produce a large dispersion in the duration of the transition phase similar to the observed dispersion in total protoplanetary disk lifetimes. While the mean transition timescale may be ~ 1 Myr as found here, in Currie et al. (2009), and Sicilia-Aguilar et al. (2009), the transitional disk phase for individual disks may last much shorter or longer.

Quantitatively assessing how transitional disks probe the clearing of both gas and dust requires diagnostics of circumstellar gas sensitive to the bulk gas content. The *Herschel Space Observatory* offers a sensitive probe of far-IR line emission to identify cool gas in planet-forming regions of the disk. *Herschel* programs such as GASPS will survey many 1–10 Myr-old stars for evidence of circumstellar gas and thus provide strong constraints on gas dissipation as a function of time. Comparing the gas properties of transitional disks with those for primordial disks will more definitively determine how transitional disks are clearing their gas, complementing studies of dust clearing investigated in our work.

The anonymous referee provided comments and suggestions that greatly improved the organization and content of this paper. We thank Cornelis Dullemond, Thomas Henning, Scott Kenyon, James Muzerolle, Carol Grady, Adam Kraus, and Meredith Hughes for useful conversations and suggestions. We also thank Richard Alexander for providing us with output from his disk evolution models presented in Alexander and Armitage (2009). Finally, we thank Jeroen Bouwman for assistance with our IRS data reduction. T.C. is supported by a NASA Postdoctoral Fellowship; A.S.A. acknowledges support from the Deutsche Forschungsgemeinschaft (DFG) grant SI-1486/1-1. This work made extensive use of the *Simbad Astronomical Database*.

REFERENCES

- Adams, F., Lada, C. J., Shu, F., 1987, ApJ, 312, 788
 Alexander, R., Armitage, P., 2009, ApJ, 704, 989
 Andre, P., Montmerle, T., 1994, ApJ, 420, 837
 Andrews, S., Williams, J., 2005, ApJ, 631, 1134
 Andrews, S., Williams, J., 2007, ApJ, 671, 1800
 Audard, M., et al., 2007, A&A, 468, 379
 Backman, D., Paresce, F., 1993, In Protostars and Planets III, p. 1253
 Baraffe, I., 1998, A&A, 337, 403
 Beckwith, S., et al., 1990, AJ, 99, 924
 Beckwith, S., Sargent, A., 1991, AJ, 381, 250
 Bouwman, J., et al., 2006, ApJ, 653, 57
 Bouwman, J., et al., 2008, ApJ, 683, 479
 Bromley, B., Kenyon, S. J., 2011, ApJ submitted, arXiv:1012.0574
 Calvet, N., et al., 2002, ApJ, 568, 1008
 Calvet, N., et al., 2005, ApJ, 630, 185L
 Carmona, A., et al., 2007, A&A, 464, 687
 Carpenter, J., et al., 2009, ApJ, 705, 1646
 Casey, B., et al., 1998, AJ, 115, 1617
 Chen, H., et al., 1997, ApJ, 478, 295
 Chen, C., et al., 2005, ApJ, 623, 493
 Chiang, E., Goldreich, P., 1997, ApJ, 490, 368
 Chiang, E., Goldreich, P., 1999, ApJ, 519, 279
 Chini, R., et al., 2003, A&A, 409, 235
 Cieza, L., et al., 2008, ApJ, 686, 115L
 Cieza, L., et al., 2009, ApJ, 696, 84L
 Cieza, L., et al., 2010, ApJ, 712, 925
 Currie, T., 2010, arXiv:1002.1715
 Currie, T., et al., 2007, ApJ, 659, 599
 Currie, T., et al., 2008, ApJ, 672, 558
 Currie, T., Kenyon, S. J., 2009, AJ, 138, 703
 Currie, T., Lada, C. J., et al., 2009, ApJ, 698, 1698, 1
 Currie, T., Rieke, G. H., Kenyon, S. J., et al., 2011, ApJ, in prep.
 Currie, T., Hernandez, J., et al., 2010, ApJS, 186, 131
 Dahm, S., 2005, AJ, 130, 1805
 Dahm, S., Hillenbrand, L., 2007, AJ, 133, 2072
 Dahm, S., 2008, AJ, 136, 521
 D'Alessio, P., et al., 2006, ApJ, 638, 314
 Dullemond, C., Dominik, C., 2005, A&A, 434, 971
 Ercolano, B., Clarke, C., Robitaille, T., 2009, MNRAS, 394, 141L
 Espaillat, C., et al., 2007, ApJ, 670, 135L
 Espaillat, C., et al., 2008, ApJ, 682, 125L
 Espaillat, C., 2009, PhD Thesis, University of Michigan
 Espaillat, C., et al., 2011, ApJ, 728, 49
 Evans, N., et al., 2009, ApJS, 181, 321
 Fedele, D., et al., 2010, A&A, 510, 72
 Flaherty, K., et al., 2007, AJ, 663, 1069
 Forbrich, J., Preibisch, T., 2007, A&A, 475, 959
 Furlan, E., et al., 2006, ApJS, 165, 568
 Gautier, T., et al., 2008, ApJ, 683, 813
 Groppi, C., et al., 2007, ApJ, 670, 489
 Gustafsson, B., et al., 2008, A&A, 486, 951
 Gutermuth, R., et al., 2008, ApJ, 674, 336
 Hartmann, L., et al., 1998, ApJ, 495, 385
 Hartmann, L., et al., 2005, ApJ, 629, 881
 Hartmann, L., et al., 2006, ApJ, 648, 484
 Hayashi, C., 1981, Progress of Theoretical Physics Supplement, 70, 35

- Henning, Th., et al., 1994, *A&A*, 291, 546
 Henning, Th., Stognienko, R., 1996, *A&A*, 311, 291
 Herczeg, G., Hillenbrand, L., 2008, *ApJ*, 681, 594
 Hernandez, J., et al., 2007a, *ApJ*, 662, 1067
 Hernandez, J., et al., 2007b, *ApJ*, 671, 1784
 Higdon, S., et al., 2004, *PASP*, 116, 975
 Houck, J. R., et al., 2004, *ApJS*, 154, 18
 Hughes, A. M., et al., 2008, *ApJ*, 698, 131
 Hughes, A. M., et al., 2010, *AJ*, 140, 887
 Indebetouw, R., et al., 2005, *ApJ*, 619, 931
 Ireland, M., Kraus, A., 2008, *ApJ*, 678, 59L
 Irwin, J., et al., 2008, *MNRAS*, 384, 675
 Jensen, E., et al., 1994, *ApJ*, 429, L29
 Jewitt, D., 1994, *AJ*, 108, 661
 Kennedy, G., Kenyon, S. J., 2009, *ApJ*, 695, 1210
 Kenyon, S. J., Hartmann, L., 1987, *ApJ*, 323, 714
 Kenyon, S. J., Hartmann, L., 1995, *ApJS*, 101, 117
 Kenyon, S. J., Bromley, B., 2008, *ApJS*, 179, 451
 Kenyon, S. J., Bromley, B., 2009, *ApJ*, 690, 140L
 Kenyon, S. J., et al., 2008, *The Star Formation Region Handbook*
 Kraus, A., et al., 2006, *ApJ*, 649, 306
 Kraus, A., et al., 2011, *ApJ* in press, arXiv:1101.4016
 Lada, C. J., et al., 2006, *AJ*, 131, 1574
 Lawson, W., Lyo, A.-R., Muzerolle, J., 2004, *MNRAS*, 351, L39
 Lopez-Marti, B., et al., 2005, *A&A*, 444, 175
 Lopez-Marti, B., et al., 2010, *A&A*, 515, 31
 Luhman, K., et al., 2003, *ApJ*, 593, 1093
 Luhman, K., Steeghs, D., 2004, *ApJ*, 609, 917
 Luhman, K., et al., 2009, *ApJ*, 703, 399
 Luhman, K., et al., 2010, *ApJS*, 186, 111
 Lyo, A.-R., et al., 2004, *MNRAS*, 355, 363
 Marraco, H., Rydgren, A., 1981, *AJ*, 86, 62
 Merin, B., Brown, J., Herczeg, G., et al., 2010, *ApJ*, 718, 1200
 Meyer, M., Wilking, B., 2009, *PASP*, 121, 350
 Moitinho, A., et al., 2001, *apj*, 563, 73
 Muench, A., Lada, C. J., et al., 2007, *ApJ*, 134, 411
 Mulders, G. D., Dominik, C., Min, M., 2010, *A&A*, 510, 11
 Muzerolle, J., et al., 2010, *ApJ*, 708, 1107
 Muzerolle, J., 2010, *HiA*, 15, 732
 Najita, J., Strom, S., Muzerolle, J., 2007, *MNRAS*, 378, 369
 Neuhauser, R., Forbrich, J., 2008, *The Star Formation Region Handbook*
 Nisini, B., et al., 2005, *A&A*, 429, 543
 Pascucci, I., Sterzik, M., 2009, *ApJ*, 702, 724
 Patten, B. M., 1998, *PASP*, 154, 1755
 Plavchan, P., et al., 2009, *ApJ*, 698, 1068
 Quillen, A., et al., 2004, *ApJ*, 612, 137
 Ramsay-Howat, S., Greaves, J., 2007, *MNRAS*, 379, 1658
 Rebull, L., et al., 2010, *ApJS*, 186, 259
 Rieke, G. H., et al., 2005, *ApJ*, 620, 1010
 Robitaille, T., et al., 2006, *ApJS*, 167, 256
 Robitaille, T., et al., 2007, *ApJS*, 169, 328
 Salyk, C., et al., 2009, *ApJ*, 699, 330
 Sicilia-Aguilar, A., et al., 2005, *AJ*, 130, 188
 Sicilia-Aguilar, A., et al., 2006a, *AJ*, 132, 2135
 Sicilia-Aguilar, A., et al., 2006b, *ApJ*, 638, 897
 Sicilia-Aguilar, A., et al., 2007, *ApJ*, 659, 1637
 Sicilia-Aguilar, A., et al., 2008, *ApJ*, 687, 1145
 Sicilia-Aguilar, A., et al., 2009, *ApJ*, 701, 1188
 Sicilia-Aguilar, A., Henning, Th., Hartmann, L., 2010, *ApJ*, 710, 597
 Simon, M., Prato, L., 1995, *ApJ*, 450, 824
 Strom, K., Strom, S., et al., 1989, *AJ*, 97, 1451
 Skrutskie, M., 1990, *AJ*, 99, 1187
 Skrutskie, M., et al., 2006, *AJ*, 131, 1163
 Thalmann, C., et al., 2010, *ApJ*, 718, 87L
 Torres, C., et al., 2006, *A&A*, 460, 695
 Valenti, J., et al., 1993, *AJ*, 106, 2024
 White, R. J., Ghez, A. M., 2001, *ApJ*, 556, 265
 White, R. J., Hillenbrand, L. A., 2004, *ApJ*, 616, 998
 Whitney, B., et al., 2003a, *ApJ*, 591, 1049
 Whitney, B., et al., 2003b, *ApJ*, 598, 1079
 Wilking, B., et al., 1985, *ApJ*, 293, 165
 Wilking, B., et al., 1992, *ApJ*, 397, 520
 Willner, S., et al., 1982, *ApJ*, 253, 174
 Wolk, S. J., Walter, F., 1996, *AJ*, 111, 2066
 Wood, K., et al., 2002, *ApJ*, 567, 1183

TABLE 1
MEMBERS LISTED IN FORBRICH AND
PREIBISCH (2007) AND INCLUDED IN THIS
WORK

| Name | RA (2000) | DEC (2000) |
|------------|-------------|-------------|
| S-CrA | 19:01:08.60 | -36:57:21.3 |
| F-3 | 19:01:15.86 | -37:03:44.3 |
| FP-6 | 19:01:19.39 | -37:01:42.0 |
| FP-8 | 19:01:22.40 | -37:00:55.4 |
| CrA-134 | 19:01:25.75 | -36:59:19.3 |
| CrA-135 | 19:01:27.15 | -36:59:8.6 |
| V709 | 19:01:34.84 | -37:00:56.7 |
| HD176386B | 19:01:39.15 | -36:53:29.6 |
| FP-18 | 19:01:39.34 | -37:02:07.8 |
| TY-CrAabcd | 19:01:40.81 | -36:52:34.0 |
| IRS2 | 19:01:41.55 | -36:58:31.6 |
| HBC677 | 19:01:41.62 | -36:59:53.1 |
| FP-23 | 19:01:43.12 | -36:50:20.9 |
| IRS5ab | 19:01:48.02 | -36:57:22.4 |
| FP-25 | 19:01:48.46 | -36:57:14.5 |
| IRS6A | 19:01:50.45 | -36:56:38.1 |
| V710 | 19:01:50.66 | -36:58:09.9 |
| IRS8 | 19:01:51.11 | -36:54:12.5 |
| IRS9 | 19:01:52.63 | -36:57:00.2 |
| RCrA | 19:01:53.67 | -36:57:08.3 |
| IRS7w | 19:01:55.31 | -36:57:22.0 |
| FP-33 | 19:01:55.61 | -36:56:51.1 |
| FP-34 | 19:01:55.76 | -36:57:27.7 |
| FP-35 | 19:01:55.85 | -36:52:04.3 |
| IRS-7e | 19:01:56.39 | -36:57:28.4 |
| FP-37 | 19:01:57.46 | -37:03:11.9 |
| FP-38 | 19:01:58.32 | -37:00:27.5 |
| T-CrA | 19:01:58.79 | -36:57:50.1 |
| V702 | 19:02:01.92 | -37:07:43.0 |
| B1858 | 19:02:01.94 | -36:54:00.1 |
| HBC-679 | 19:02:22.13 | -36:55:41.0 |
| CrA-159 | 19:02:33.07 | -36:58:21.1 |

NOTE. — Sources with an “FP” prefix followed by a number identify Coronet Cluster members uniquely identified by Forbrich and Preibisch (2007). The number following “FP” identifies the row number of the source in Table 2 of that paper.

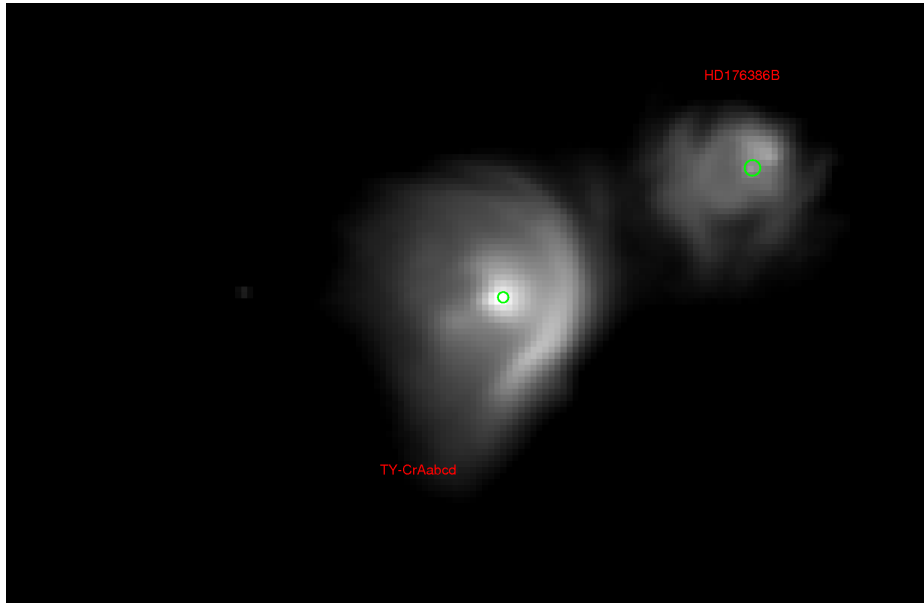


FIG. 1.— Region of the IRAC [5.8] mosaic showing nebular emission surrounding TY CrA and HD 176386b. The positions of both sources are shown as green circles. Nebular emission contaminates both stars and is responsible for positional offsets between the 2.2–4.5 μm centroids and 5.8–8 μm centroids.

TABLE 2
PHOTOMETRY FOR MEMBERS LISTED IN FORBRICH AND PREIBISCH (2007)

| Name | J | $\sigma(J)$ | H | $\sigma(H)$ | K_s | $\sigma(K_s)$ | [3.6] | $\sigma([3.6])$ | [4.5] | $\sigma([4.5])$ | [5.8] | $\sigma([5.8])$ | [8] | $\sigma([8])$ | [24] | $\sigma([24])$ |
|---------------------|--------|-------------|--------|-------------|--------|---------------|--------|-----------------|--------|-----------------|--------|-----------------|--------|---------------|-------|----------------|
| S-CrA | 8.19 | 0.02 | 7.05 | 0.024 | 6.10 | 0.02 | 5.060 | 0.005 | 4.386 | 0.005 | 3.699 | 0.005 | 2.969 | 0.004 | - | - |
| FP-3 | - | - | - | - | - | - | 13.971 | 0.014 | 13.371 | 0.012 | 12.092 | 0.020 | 11.616 | 0.029 | - | - |
| FP-6 | - | - | - | - | - | - | - | - | - | - | 12.299 | 0.017 | 11.458 | 0.033 | 6.106 | 0.00 |
| FP-8 | - | - | - | - | - | - | - | - | - | - | - | - | 12.697 | 0.092 | - | - |
| CrA-134 | 11.61 | 0.02 | 9.78 | 0.03 | 8.77 | 0.023 | 7.876 | 0.002 | 7.367 | 0.002 | 6.862 | 0.003 | 6.537 | 0.002 | - | - |
| CrA-135 | 10.81 | 0.02 | 10.11 | 0.02 | 9.89 | 0.02 | 9.599 | 0.005 | 9.601 | 0.004 | 9.551 | 0.007 | 9.611 | 0.007 | - | - |
| V709 | 8.67 | 0.03 | 7.97 | 0.04 | 7.71 | 0.02 | 7.863 | 0.002 | 7.717 | 0.003 | 7.533 | 0.004 | 7.512 | 0.004 | 6.794 | 0.00 |
| ¹ HD | 7.60 | - | 7.49 | 0.09 | 7.14 | 0.08 | 7.837 | 0.003 | 7.781 | 0.003 | 6.243 | 0.003 | 4.706 | 0.003 | - | - |
| 176386 | - | - | - | - | - | - | - | - | - | - | - | - | - | - | - | - |
| FP-18 | 11.34 | 0.03 | 10.66 | 0.03 | 10.37 | 0.03 | 10.110 | 0.005 | 10.097 | 0.005 | 9.979 | 0.007 | 9.927 | 0.010 | 9.364 | 0.10 |
| ¹ TY CrA | 7.49 | 0.02 | 6.97 | 0.03 | 6.67 | 0.02 | 6.217 | 0.005 | 6.085 | 0.005 | 4.478 | 0.004 | - | - | - | - |
| abcd | - | - | - | - | - | - | - | - | - | - | - | - | - | - | - | - |
| IRS-2 | 13.75 | 0.02 | 9.74 | 0.02 | 7.07 | 0.02 | 5.181 | 0.004 | 4.281 | 0.003 | - | - | 2.230 | 0.003 | - | - |
| HBC 677 | 10.47 | 0.02 | 9.04 | 0.02 | 8.09 | 0.03 | 7.725 | 0.003 | 7.201 | 0.003 | 6.528 | 0.004 | 5.859 | 0.004 | - | - |
| FP-23 | 16.92 | 0.18 | 15.23 | 0.11 | 14.77 | 0.10 | - | - | - | - | - | - | - | - | - | - |
| IRS-5ab | 16.9 | - | 13.73 | 0.01 | 10.59 | 0.01 | 7.456 | 0.002 | 6.293 | 0.001 | - | - | 3.937 | 0.003 | - | - |
| FP-25 | 15.56 | - | 13.14 | - | 12.49 | 0.15 | - | - | 9.115 | 0.003 | - | - | 7.017 | 0.003 | - | - |
| IRS-6A | 16.39 | 0.20 | 12.14 | - | 10.31 | - | 8.480 | 0.003 | 7.687 | 0.004 | - | - | 6.286 | 0.003 | - | - |
| V710 | 15.96 | 0.10 | 11.13 | 0.03 | 7.62 | 0.04 | - | - | 3.659 | 0.003 | - | - | - | - | - | - |
| IRS-8 | 14.92 | 0.04 | 12.69 | 0.03 | 11.37 | 0.02 | 9.911 | 0.005 | 9.358 | 0.005 | 8.744 | 0.006 | 7.946 | 0.005 | - | - |
| IRS-9 | - | - | - | - | - | - | 8.031 | 0.003 | 7.313 | 0.003 | - | - | - | - | - | - |
| R CrA | 6.952 | 0.021 | 4.955 | 0.024 | 2.910 | 0.318 | - | - | - | - | - | - | - | - | - | - |
| IRS-7w | 12.55 | - | 13.25 | 0.32 | 10.76 | - | 8.635 | 0.004 | 7.073 | 0.003 | - | - | - | - | - | - |
| FP-33 | - | - | - | - | - | - | 10.181 | 0.005 | 9.025 | 0.004 | - | - | 6.860 | 0.004 | - | - |
| FP-34 | - | - | - | - | - | - | 9.730 | 0.004 | 8.293 | 0.004 | - | - | - | - | - | - |
| FP-35 | - | - | - | - | - | - | - | - | 13.387 | 0.016 | 11.660 | 0.018 | 10.921 | 0.020 | 7.532 | 0.00 |
| IRS-7e | - | - | - | - | - | - | 9.417 | 0.004 | - | - | - | - | - | - | - | - |
| FP-37 | 15.58 | 0.07 | 14.02 | 0.04 | 13.19 | 0.04 | 12.320 | 0.007 | 12.264 | 0.006 | 11.925 | 0.089 | 12.086 | 0.037 | - | - |
| FP-38 | 16.961 | - | 15.275 | 0.139 | 13.704 | 0.060 | 12.426 | 0.007 | 12.102 | 0.008 | 11.508 | 0.017 | 12.008 | 0.050 | - | - |
| T-CrA | 8.93 | 0.03 | 7.70 | 0.04 | 6.60 | 0.02 | - | - | 4.819 | 0.005 | 4.217 | 0.005 | - | - | - | - |
| V702 | 8.90 | 0.02 | 8.48 | 0.04 | 8.35 | 0.03 | 8.444 | 0.004 | 8.329 | 0.003 | 8.282 | 0.0048 | 8.280 | 0.003 | 8.122 | 0.00 |
| B185839.6 | - | - | - | - | - | - | 14.099 | 0.019 | 14.766 | 0.054 | - | - | - | - | 8.617 | 0.00 |
| -3658 | - | - | - | - | - | - | - | - | - | - | - | - | - | - | - | - |
| HBC-679 | 10.33 | 0.03 | 9.50 | 0.04 | 9.23 | 0.03 | 9.031 | 0.003 | 8.967 | 0.004 | 8.901 | 0.005 | 8.868 | 0.006 | 8.258 | 0.00 |
| CrA-159 | 10.59 | 0.03 | 9.26 | 0.02 | 8.45 | 0.020 | 7.565 | 0.002 | 7.016 | 0.003 | 6.372 | 0.003 | 5.887 | 0.004 | 3.704 | 0.00 |

NOTE. — Notes – 1) Inspection of the IRAC mosaic shows that TY CrAabcd and HD 176386B are contaminated by nebular emission at 5.8 μm and 8 μm . 2).

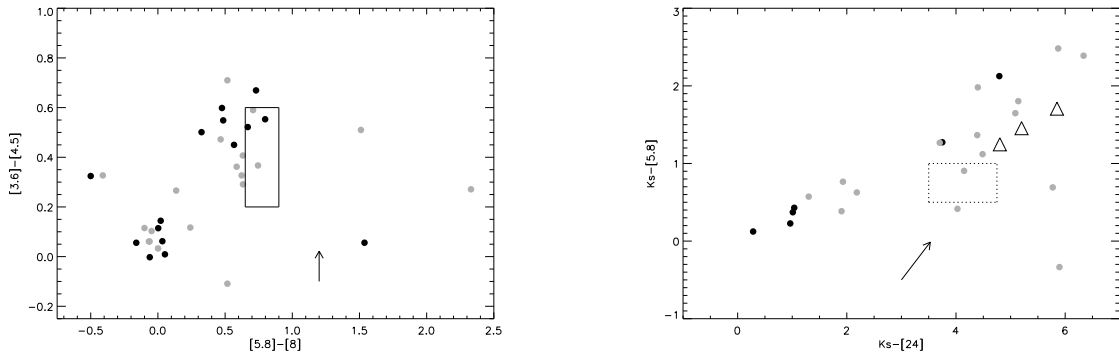


FIG. 2.— (Left panel) IRAC color-color diagram of Coronet Cluster stars with new photometry (black circles) and those analyzed in Sicilia-Aguilar et al. (2008) (grey circles). (Right panel) K_s -[5.8] vs. K_s -[24] color-color diagram for Coronet Cluster stars. In each panel, we overplot a reddening vector of $A_V = 10$, assuming the extinction relations of Indebetouw et al. (2005) for 2MASS and IRAC and Flaherty et al. (2007) for MIPS. In the left panel, the box corresponds to the range of colors for most stars in Taurus (Hartmann et al. 2005); the dotted box in the right-hand panel corresponds to the range of colors for most homologously depleted transitional disks in NGC 2362 identified by Currie et al. (2009). The triangles in the right panel correspond to (from bottom to top) the lower-quartile Taurus SED, median Taurus SED, and upper-quartile Taurus SED for K5–M2 stars from Furlan et al. (2006).

TABLE 3
 PROVISIONAL EVOLUTIONARY STATES FOR CORONET CLUSTER DISKS WITH NEW SPITZER PHOTOMETRY
 BASED ON 1–24 μm DATA

| ID | ST | ST Ref | $A_V(\text{best})$ | $\tau_{\text{mid-IR}}$ | Inner Hole? (R_{sub}) | Disk Class |
|------------|--------------------|--------|--------------------|------------------------|----------------------------------|-----------------|
| S-CrA | G5/K5 ¹ | 1 | 2 | thick | n | PD |
| CrA-159 | M2 ² | est. | 3 | thick | n | PD |
| IRS-2 | K2 | 2 | - | thick | n | PS |
| CrA-134 | K3 | 2 | 11 | thick | n | PD |
| CrA-135 | M4 | 2 | 0.5 | - | - | Star |
| V709 | K1 | 7 | 0.5 | thin/- | - | Star/TD(HD)/DD? |
| HD 176396B | K7 | 2 | 0.75 | ? | n | ? |
| FP-18 | M3 | est. | 0.4 | - | - | Star |
| TY-CrA | B8/K2 | 3,4 | 3.5 | ? | n | ? |
| HBC-677 | M2 | 2 | 3.9 | thick | n | PD |
| IRS-5ab | K5 | 2,5 | - | thick | n | PS |
| FP-25 | M? | 7 | - | thick | n | PS |
| IRS-6 | M1 | 2 | 10.5 | thick | n | PD |
| V710 | K5-M0 | 5 | - | thick | n | PS |
| IRS-7 | ? | - | - | thick | n | PS |
| IRS-8 | M2 | est. | 13.5 | thick | n | PD |
| R-CrA | A5 | 7 | ? | thick | n | PD |
| T-CrA | F0 | 6 | 0.3 | thick | n | PD |
| V702 | G5 | 7 | 0.25 | - | - | Star |
| HBC-679 | K2 | 7 | 1.5 | - | - | Star |

NOTE. — The disk states are identified as follows: PS=Protostar, PD = Primordial Disk, and TD = Transitional Disk, Star = Stellar Photosphere (no circumstellar material). The transitional disks are further divided into those with inner holes (IH) and those that are homogeneously depleted (HD). The disk states here are considered to be provisional since these Coronet Cluster stars lack sensitive far-IR/submm data. The spectral type references are the following: 1) Carmona et al. (2007), 2) Meyer and Wilking (2009), 3) Marraco and Rydgren (1981), 4) Casey et al. (1998), 5) Nisini et al. (2005), 6) Patten (1998), and 7) Forbrich and Preibisch (2007). "Est" means that the spectral type was estimated by modeling the optical to near-IR SED using the Robitaille et al. (2006) grid and the Currie et al. (2010) effective temperature scale. Note (1) – The fit to the photosphere for this star is generally poor; the best-fit A_V corresponds to a K0 stellar photosphere model. However, the exact value has no bearing on our classification. Note (2) – Patten (1998) list the spectral type for this star as M3–M5. However, we cannot reproduce the observed optical to near-IR SED with a M3–M5 photosphere using either the Currie et al. (2011) Te scale and dwarf colors or with the Robitaille et al. (2006) grid: all good-fitting models ($\chi^2 - \chi_{\text{best}}^2 < 3$) predict that its photosphere is hotter than ~ 3800 K and thus its spectral type is earlier than M0–M2. Since other stars classified as M3–M5 by Patten (1998) are reclassified as M0–M2 by Meyer and Wilking (2009) based on higher signal-to-noise data, we list this star as an M2 star.

TABLE 4
PROVISIONAL EVOLUTIONARY STATES FOR CORONET CLUSTER DISKS STUDIED IN SICILIA-AGUILAR ET AL. (2008) BASED ON
1–70 μm DATA

| ID | ST | ST Ref. | A_V (best) | τ_{mid-IR} | Inner Hole?(R_{sub}) | Disk Class (Si08) | Disk Class (Er09) | Disk Class (This Work) |
|----------|-------------|---------|--------------|-----------------|--------------------------|-------------------|-------------------|------------------------|
| CrA-205 | M4–M6 | 8,9 | 0.25 | thin | y,2000 | TD(IH) | PD | TD(IH) |
| CrA-432 | M5–M7 | 8,9 | 0.5 | thick | n | PD | – | PD |
| CrA-453 | M4.5 | 10 | 1.5 | – | – | Star | – | Star |
| CrA-465 | M5–M7.5 | 8,10 | 0 | thick | n | PD | – | PD |
| CrA-466 | M2 | 10 | 6.6 | thick | n | TD(IH) | PD | PD |
| CrA-4107 | \geq M4.5 | 8,9 | 1 | thick | n | PD | – | PD |
| CrA-4109 | $>$ M5 | 9, est | 1 | thin | y,300 | TD(IH) | TD(IH) | TD(IH) |
| CrA-4110 | M5 | 9 | 0.4 | thick | n | PD | – | PD |
| CrA-4111 | M4.5 | 9 | 0 | thin | y,70 | TD(IH) | TD(IH) | TD(IH) |
| G-1 | M0 | 9,est. | 3 | thin | 2 | PD | – | TD(HD) |
| G-14 | M4.5 | 10 | 1.9 | thin | n | TD(IH) | PD | TD(HD) |
| G-30 | M3.5 | 10 | 0.09 | thin | n | TD(IH)/DD | – | TD(HD) |
| G-32 | $>$ M5 | 10,est. | 8–15 | thick | n | PD | – | PD |
| G-49 | M4 | 10 | 0.07 | – | – | Star | – | Star |
| G-65 | M1–M2 | 10 | 14–15 | thick | n | TD(IH) | PD | PD |
| G-85 | M0.5 | 9, est. | 17 | thick | n | PD | – | PD |
| G-87 | M1.5 | 10 | 14 | thin | 1 | TD(IH) | PD | TD(HD) |
| G-94 | M3.5 | 10 | 0.6 | thin | n | TD(IH)/DD | – | TD(HD)/DD |
| G-95 | M1 | 10 | 5 | thin | y,20 | TD(IH)/DD | – | TD(IH)/DD |
| G-102 | M5 | 10 | 0.7 | thin | n | TD(IH)/DD | – | TD(HD)/DD |

NOTE. — References for spectral types are the following: 8) López-Martí et al. (2005), 9) Sicilia-Aguilar et al. 2010, in prep., 10) Sicilia-Aguilar et al. (2008). "Est" means that the spectral type was estimated by modeling the optical to near-IR SED using the Robitaille et al. (2006) grid and the Currie et al. (2010) effective temperature scale.

TABLE 5
IRS FLUX DENSITY MEASUREMENTS USED IN MODELING CORONET CLUSTER STARS FROM SICILIA-AGUILAR ET AL. (2008)

| ID | Wavelengths Sampled (μm) | Flux Density (mJy) |
|---------|---------------------------------------|---|
| CrA-205 | 9,13,17,21,27 | 1.03 ± 0.06 , 0.70 ± 0.08 , 0.91 ± 0.30 , 1.10 ± 0.30 , 2.08 ± 0.26 |
| G-14 | " | 4.95 ± 0.20 , 4.70 ± 0.15 , 5.53 ± 0.45 , 4.75 ± 0.34 , 3.62 ± 0.49 |
| G-65 | 6,7,9, 10, 11, 12 | 53.06 ± 12.80 , 48.30 ± 30.30 , 49.96 ± 13.27 , 47.9 ± 12.30 , 48.10 ± 23.98 , 43.1 ± 32.70 |
| G-87 | 9, 13, 17, 21, 27 | 10.02 ± 0.31 , 12.56 ± 0.29 , 15.55 ± 4.84 , 19.04 ± 4.88 , 25.37 ± 6.19 |

NOTE. — The wavelength sampling for G-65 is different than the others because G-65 lacks data longwards of $\sim 15 \mu\text{m}$.

TABLE 6
PROPERTIES OF SELECTED TAURUS SOURCES

| Name | ST | M_* (M_\odot) | A_V | A_V range | K_s -[8] | K_s -[24] | τ_{mid-IR} | Inner Hole? |
|-----------|-------|------------------------|-------|-------------|------------|-------------|-----------------|-------------|
| UX Tau | K5 | 1.0 | 0.75 | 0.25-1.25 | 1.56 | 5.42 | thin | y |
| V807 Tau | K5 | 1.0 | 1.4 | 0.9-1.9 | 1.46 | 3.91 | thin | n |
| LkCa 15 | K5 | 1.0 | 1.2 | 0.7-1.7 | 1.58 | 5.06 | thin | y |
| FY Tau | K5 | 1.0 | 5 | 4-6 | 1.68 | 3.93 | thin | n |
| JH 112 | K6 | 0.95 | 3.4 | 2.72-4.08 | 1.97 | 5.34 | thick | n |
| V836 Tau | K7 | 0.85 | 1.05 | 0.55-1.55 | 1.76 | 4.77 | thin | n |
| DN Tau | M0 | 0.75 | 0.7 | 0.2-1.2 | 1.99 | 5.00 | thin | n |
| VY Tau | M0 | 0.75 | 1.1 | 0.6-1.6 | 1.53 | 4.35 | thin | n |
| GO Tau | M0 | 0.75 | 2 | 1.5-2.5 | 1.85 | 4.93 | thin | n |
| IP Tau | M0 | 0.75 | 0.6 | 0.1-1.1 | 1.68 | 4.74 | thick | n |
| HO Tau | M0.5 | 0.65 | 1.3 | 0.8-1.8 | 1.90 | 4.79 | thick | n |
| DH Tau | M1 | 0.6 | 1.9 | 1.4-2.4 | 1.28 | 4.79 | thin | ? |
| FX Tau | M1.5 | 0.57 | 2 | 1.5-2.5 | 1.90 | 4.85 | thick | n |
| CY Tau | M1.5 | 0.57 | 1.7 | 1.2-2.2 | 1.89 | 4.11 | thick | n |
| 04333905 | M1.75 | 0.57 | 7.9 | 2.4-3.6 | 1.49 | 5.81 | thin | y |
| +2227207 | | | | | | | | |
| JH-223 | M2 | 0.55 | 2.2 | 1.6-2.6 | 1.72 | 4.27 | thin | n |
| GH Tau | M2 | 0.55 | 1 | 0.5-1.5 | 1.79 | 4.51 | thick | n |
| ZZ Tau | M3 | 0.4 | 1.2 | 0.7-1.7 | 1.39 | 3.91 | thin | n |
| XEST13-10 | M3 | 0.4 | 6 | 4.8-7.2 | 1.52 | 4.40 | thin | n |
| CIDA 8 | M3.5 | 0.3 | 2.25 | 1.75-2.75 | 1.49 | 4.30 | thin | n |
| 04231822 | M3.5 | 0.3 | 8 | 6.4-9.6 | 1.53 | 5.11 | thin | n |
| +2641156 | | | | | | | | |
| 04153916 | M3.75 | 0.275 | 2 | 1.5-2.5 | 1.62 | 4.93 | thin | n |
| +2818586 | | | | | | | | |
| FP Tau | M4 | 0.25 | 0.5 | 0-1 | 1.52 | 4.53 | thin | n |
| ITG-15 | M5 | 0.175 | 3.25 | 2.6-3.9 | 1.62 | 4.79 | thin | n |
| 04202555 | M5.25 | 0.15 | 2.1 | 1.6-2.6 | 1.69 | 5.37 | thin | ? |
| +2700355 | | | | | | | | |

NOTE. — The K_s -[8] and K_s -[24] colors listed are dereddened colors as determined by Luhman et al. (2010). The stellar masses are computed using the Currie et al. (2011) effective temperature scale for K5-M2 stars and the Luhman et al. (2003) scale for later stars and the Baraffe et al. (1998) isochrones. A_V was determined individually by fitting the optical-to-near-IR SED for stellar photospheres using the Currie et al. (2011) intrinsic colors for a given effective temperature and using the Currie et al. (2011) and Luhman et al. (2003) effective temperature scales. The range in A_V assumes a nominal 20% extinction uncertainty with a minimum uncertainty of 0.5 mags.

TABLE 7
DISK EVOLUTIONARY STATES FOR SELECTED TAURUS SOURCES

| Name | M_{disk} | $\frac{M_{disk}}{M_{\star}}$ | $\frac{M_{disk}}{M_{\star}}$ (IQR) | $f(< 1,3 \times 10^{-3})$ | Submm. Ref. | M_{disk} ($M_{\odot, submm}$) | $\frac{M_{disk}}{M_{\star}}$ (submm) | Disk Class |
|----------------------|----------------------|------------------------------|--|---------------------------|----------------|--------------------------------------|---|------------|
| UX Tau | 0.02 | 0.02 | [0.017,0.022] | 0,0 | 1 | 5.1×10^{-3} | 5.1×10^{-3} | TD(IH) |
| V807 Tau | 3×10^{-3} | 3×10^{-3} | $[3 \times 10^{-3}, 4 \times 10^{-3}]$ | 0,0.5 | 1 | 10^{-3} | 10^{-3} | PD/TD(HD) |
| LkCa 15 | 0.01 | 0.01 | [0.01,0.025] | 0,0 | 1 | 0.05 | 0.05 | TD(IH) |
| FY Tau | 10^{-4} | 10^{-4} | $[6 \times 10^{-6}, 1 \times 10^{-3}]$ | 0.76,0.82 | 1 | 7×10^{-4} | 7×10^{-4} | TD(HD) |
| JH 112 | 8×10^{-3} | 9.4×10^{-3} | $[4 \times 10^{-3}, 0.01]$ | 0.06,0.12 | 1 | 10^{-3} | 1.05×10^{-3} | PD |
| V836 Tau | 0.01 | 0.012 | [0.012,0.014] | 0,0 | 1 | 0.01 | 0.012 | PD |
| DN Tau | 0.01 | 0.013 | [0.013,0.03] | 0,0 | 1,4 | 3×10^{-2} | 4×10^{-2} | PD |
| VY Tau | 2×10^{-4} | 2.7×10^{-4} | $[3.4 \times 10^{-5}, 9 \times 10^{-4}]$ | 0.76,0.91 | 1 | $< 5 \times 10^{-4}$ | $< 6.7 \times 10^{-4}$ | TD(HD) |
| GO Tau | 6×10^{-3} | 8×10^{-3} | $[5 \times 10^{-3}, 0.023]$ | 0,0 | 1 | 0.07 | 0.09 | PD |
| IP Tau | 8×10^{-3} | 0.011 | $[7 \times 10^{-3}, 0.016]$ | 0,0.05 | 1 | 3×10^{-3} | 4×10^{-3} | PD |
| HO Tau | 8×10^{-3} | 0.012 | [0.013,0.013] | 0,0 | 1 | 2×10^{-3} | 3.1×10^{-3} | PD |
| DH Tau | 5×10^{-3} | 0.01 | [0.01,0.018] | 0,0.27 | 1 | 3×10^{-3} | 5×10^{-3} | PD/TD(IH) |
| FX Tau | 4×10^{-3} | 7×10^{-3} | $[5 \times 10^{-3}, 0.013]$ | 0.09,0.22 | 1 | 9×10^{-4} | 1.5×10^{-3} | PD |
| CY Tau | 8×10^{-3} | 0.014 | [0.014,0.025] | 0,0 | 1,4 | 6×10^{-3} | 0.015 | PD |
| 04333905 +2227207 | 4×10^{-4} | 7×10^{-4} | $[1.7 \times 10^{-4}, 2.7 \times 10^{-3}]$ | 0.63,0.68 | – | – | – | TD(IH) |
| JH 223 | 7.9×10^{-5} | 1.4×10^{-4} | $[8.5 \times 10^{-5}, 1 \times 10^{-3}]$ | 0.75,0.82 | 1 | $< 3 \times 10^{-4}$ | $< 5.5 \times 10^{-4}$ | TD(HD) |
| GH Tau | 4.1×10^{-3} | 7.5×10^{-3} | $[4 \times 10^{-3}, 0.01]$ | 0.03,0.16 | 1 | 7×10^{-4} | 1.3×10^{-3} | PD |
| ZZ Tau | 1×10^{-4} | 2.5×10^{-4} | $[2 \times 10^{-5}, 8 \times 10^{-4}]$ | 0.77,0.86 | 1,3 | $< 4 \times 10^{-4}$ | $< 10^{-3}$ | TD(HD) |
| XEST13-10 | 4×10^{-4} | 1×10^{-3} | $[2.5 \times 10^{-4}, 3 \times 10^{-3}]$ | 0.5,0.72 | – | – | – | TD(HD) |
| CIDA 8 | 8×10^{-3} | 0.03 | [0.03,0.04] | 0,0 | 1 | 10^{-3} | 3.3×10^{-3} | PD |
| 04231822 +2641156 | 5×10^{-4} | 1.7×10^{-3} | $[3 \times 10^{-4}, 5 \times 10^{-3}]$ | 0.43,0.66 | – | – | – | PD/TD(HD) |
| 04153916 +2818586 | 4×10^{-4} | 1.5×10^{-3} | $[4 \times 10^{-4}, 6 \times 10^{-3}]$ | 0.39,0.59 | – | – | – | PD/TD(HD) |
| FP Tau | 2.5×10^{-4} | 1×10^{-3} | $[4 \times 10^{-4}, 4 \times 10^{-3}]$ | 0.53,0.68 | 2 | $< 1.3 \times 10^{-4}$ | $< 5.2 \times 10^{-4}$ | TD(HD) |
| ITG-15 | 3×10^{-4} | 1.7×10^{-3} | $[3.6 \times 10^{-4}, 9 \times 10^{-3}]$ | 0.49,0.65 | – | – | – | PD/TD(HD) |
| 04202555 +2700355 | 4×10^{-4} | 2.7×10^{-3} | $[1 \times 10^{-3}, 3 \times 10^{-3}]$ | 0.07,0.53 | – | – | – | PD/TD(IH) |

NOTE. — IQR refers to the interquartile range of fractional disk masses from best-fit models. The identification "Lu10" refers to Luhman et al. (2010), where the classification listed is based on applying the Luhman et al. (2010) color criteria. The references for submillimeter data and (sub)millimeter-derived disk masses are the following: (1) Andrews and Williams (2005), (2) Jewitt et al. (1994), (3) Jensen et al. (1994), and (4) Beckwith and Sargent (1991). The fractional disk masses are computed using the Currie et al. (2011) effective temperature scale for K5–M2 stars and the Luhman et al. (2003) scale for later stars and the Baraffe et al. (1998) isochrones. Sources with disk evolutionary states listed as PD/TD(IH) or PD/TD(HD) have uncertain states: either SED modeling is inconclusive as to whether the disks likely have inner holes (PD/TD(IH)) or the classification depends on whether the full range or interquartile range of disk masses is used to identify primordial disks (PD/TD(HD)). Luhman et al. (2010) label all of these disks as primordial disks.

TABLE 8
OPTICALLY-THICK PRIMORDIAL DISKS AROUND K5–M6 STARS IN TAURUS LISTED AS HAVING LOW MASSES IN
ANDREWS AND WILLIAMS (2005)

| Name | ST | M_{\star} | M_{disk} (M_{\odot})(AW05) | M_{disk}/M_{\star} (AW05) ¹ | M_{disk} (M_{\odot} , this work) | M_{disk}/M_{\star} (this work) |
|---------------------|----|-------------|----------------------------------|--|---------------------------------------|----------------------------------|
| HN Tau | K5 | 1.0 | 8×10^{-4} | 8×10^{-4} | 6×10^{-3} | 6×10^{-3} |
| V955 Tau | K7 | 0.85 | 5×10^{-4} | 5.9×10^{-4} | 4×10^{-3} | 5×10^{-3} |
| DF Tau | M2 | 0.55 | 4×10^{-4} | 7.3×10^{-4} | 5×10^{-3} | 9×10^{-3} |
| CoKu Tau/3 | M1 | 0.6 | $< 4 \times 10^{-4}$ | $< 6.7 \times 10^{-4}$ | 5×10^{-3} | 8×10^{-3} |
| DP Tau | M1 | 0.6 | $< 5 \times 10^{-4}$ | $< 8.3 \times 10^{-4}$ | 2×10^{-3} | 3×10^{-3} |
| CIDA-3/V410 X-Ray 1 | M2 | 0.55 | $< 4 \times 10^{-4}$ | $< 7.3 \times 10^{-4}$ | 2×10^{-5} | 4×10^{-5} |
| CZ Tau | M3 | 0.4 | $< 4 \times 10^{-4}$ | $< 10^{-3}$ | 2×10^{-5} | 5×10^{-5} |

NOTE. — Notes (1) – Fractional disk mass is derived using our estimates for stellar mass.

TABLE 9
PROVISIONAL DISK EVOLUTIONARY STATES FOR SELECTED LATE-TYPE IC 348 MEMBERS BASED ON 1–24 μm DATA

| ID | ST | $A_V(\text{Best})$ | $K_s-[8]$ | $K_s-[24]$ | τ_{mid-IR} | Inner Hole? | CK09 | Disk Class | |
|-------|-------|--------------------|-----------|------------|-----------------|-------------|--------|------------|----------------|
| | | | | | | | | Lu10 | This Work |
| 21 | K0 | 5.4 | 1.03 | 5.43 | thin | y | TD(IH) | TD | TD(IH) |
| 26 | K7 | 8 | 2.03 | 4.90 | thick | n | PD | PD | PD |
| 32 | K7 | 4.6 | 1.95 | 4.81 | thick | n | PD | PD | PD |
| 40 | K8 | 4 | 1.58 | 5.68 | thin | ? | PD | PD | TD(HD)/TD(IH) |
| 55 | M0.5 | 11 | 1.93 | 4.86 | thick | n | PD | PD | PD |
| 58 | M1.25 | 3.7 | 1.81 | 5.81 | thin | ? | PD | PD | TD(HD)/TD(IH)? |
| 67 | M0.75 | 1.2 | 1.14 | 6.12 | thin | y | TD(IH) | TD | TD(IH) |
| 68 | M3.5 | 2.25 | 1.43 | 4.14 | thin | ? | PD | PD | TD(HD)/TD(IH)? |
| 72 | M2.5 | 1.7 | 0.75 | 5.65 | thin | y | TD(IH) | TD | TD(IH) |
| 76 | M3.75 | 3.0 | 1.48 | 4.41 | thin | n | PD | TD | TD(HD) |
| 97 | M2.25 | 5.5 | 1.30 | 4.85 | thin | y | PD | PD | TD(IH) |
| 110 | M2 | 5.0 | 1.62 | 5.90 | thin | y | PD | PD | TD(IH) |
| 128 | M2 | 2.75 | 1.47 | 3.54 | thin | n | PD | PD | TD(HD) |
| 129 | M2 | 2.0 | 1.88 | 4.32 | thin | n | PD | PD | TD(HD) |
| 135 | M4.5 | 0.9 | 1.41 | 3.48 | thin | n | PD | TD | TD(HD) |
| 153 | M4.75 | 2.85 | 1.84 | 4.76 | thick | n | PD | PD | PD |
| 194 | M4.75 | 3.1 | 1.46 | 4.88 | thin | n | PD | PD | TD(HD) |
| 213 | M4.75 | 1.4 | 1.48 | 4.04 | thin | n | PD | PD | TD(HD) |
| 214 | M4.75 | 1.1 | 1.48 | 4.69 | thin | n | PD | PD | TD(HD) |
| 301 | M4.75 | 6.2 | 1.24 | 4.93 | thin | y | TD | TD | TD(IH) |
| 308 | M4 | 11.8 | 1.31 | 4.92 | thin | y | PD | TD | TD(IH) |
| 1928 | M5.5 | 1.4 | 1.74 | 3.68 | thick | n | PD | PD | PD |
| 8078 | M0.5 | 5.8 | 1.82 | 5.22 | thick | n | PD | PD | PD |
| 9024 | M0 | 3.75 | 1.94 | 4.72 | thick | n | PD | PD | PD |
| 10352 | M1 | 3.5 | 1.88 | 5.24 | thick | n | PD | PD | PD |

NOTE. — $A_V(\text{Best})$ corresponds to the extinction that produces the best fit to the observed SED. The range in A_V used for SED modeling with the Robitaille models follows the method described for Taurus stars. The identification "Lu10" refers to Luhman et al. (2010), where the classification listed is based on applying the Luhman et al. (2010) color criteria. The classification listed for CK09, Currie and Kenyon (2009), is based on applying their color-criteria. The disk states listed here are considered to be "provisional" since IC 348 lacks sensitive far-IR and submm data.

TABLE 10
PROVISIONAL DISK EVOLUTIONARY STATES FOR LATE-TYPE NGC 2362 MEMBERS BASED ON 1–24 μm DATA

| ID | ST | $A_V(\text{Best})$ | $K_s-[8]$ | $K_s-[24]$ | τ_{mid-IR} | Inner Hole? (R_{sub}, AU) | CL09 | Disk Class | |
|-----------------|-----------------|--------------------|-----------|------------|-----------------|--------------------------------------|--------|------------|-------------------|
| | | | | | | | | Lu10 | This Work |
| 3 | M2 ¹ | 0.6 | 1.45 | 5.89 | thin | y,4.10 | TD(IH) | PD | TD(IH) |
| 36 | K5 ¹ | 0.5 | 1.70 | 4.51 | thin | n | TD(HD) | PD | TD(HD) |
| 41 ² | K1 | 0.3 | 0.19 | 1.34 | thin | n | TD(HD) | - | TD(HD) |
| 63 ² | M0 ¹ | 0.7 | 0.52 | 2.76 | thin | n | TD(HD) | - | TD(HD) |
| 85 | M2 ¹ | 1.5 | 1.55 | 4.58 | thin | n | TD(HD) | PD | TD(HD) |
| 111 | K7 | 0.75 | 2.5 | 5.34 | thick | n | PD | PD | PD |
| 139 | M2 | 0.4 | 3.48 | 6.82 | thick | n | PD | PD | PD |
| 168 | K3 | 0.5 | 0 | 3.48 | thin | y,5.20 | TD(IH) | TD | TD(IH) |
| 177 | M0 ¹ | 0.8 | 1.82 | 5.33 | thin | ? ³ | TD(HD) | PD | PD/TD(HD)/TD(IH)? |
| 187 | M0.5 | 1.5 | 2.64 | 4.81 | thick | n | PD | PD | PD |
| 194 | K5 | 1.2 | 1.06 | 5.46 | thin | y,7.57 | TD(IH) | TD | TD(IH) |
| 196 | K5 ¹ | 0.1 | 0.22 | 2.35 | thin | y,3.63 | TD(IH) | TD | TD(IH) |
| 202 | M2.5 | 0.9 | 2.53 | 5.92 | thick | n | PD | PD | PD |
| 204 | M2.5 | 2 | 1.46 | 4.69 | thin | n | TD(HD) | PD | TD(HD) |
| 213 | M3 ¹ | 0.8 | 1.28 | 3.84 | thin | n | TD(HD) | TD | TD(HD) |
| 214 | K7 ¹ | 0.35 | 1.5 | 4.17 | thin | n | TD(HD) | PD | TD(HD) |
| 219 | M0 | 0.8 | 1.65 | 3.87 | thin | n | TD(HD) | PD | TD(HD) |
| 229 | M1.5 | 0.95 | 1.38 | 3.92 | thin | n | TD(HD) | PD | TD(HD) |
| 251 | M2 ¹ | 1.25 | 1.7 | 4.68 | thin | n | TD(HD) | PD | TD(HD) |
| 267 | M2 ¹ | 0.85 | 1.33 | 4.19 | thin | n | TD(HD) | PD | TD(HD) |
| 295 | M2 ¹ | 0.4 | 0.34 | 4.20 | thin | y,1.29 | TD(IH) | TD | TD(IH) |

NOTE. — The identification "Lu10" refers to Luhman et al. (2010), where the classification listed is based on applying the Luhman et al. (2010) color criteria. The identification CL09 refers to the disk evolutionary states listed in Currie et al. (2009). The disk states listed from this work are considered to be provisional since NGC 2362 lacks sensitive far-IR/submm data. To compare our results with those presented in Currie et al. (2009), we list the inner hole sizes in AU. (1) Denotes approximate spectral types assigned based on fitting the optical and near-IR data. Likewise, $A_V(\text{Best})$ is corresponds to the extinction that produces the best fit to the observed SED. (2) The detections of these sources were confirmed by a re-reduction of the MIPS-24 μm data and PRF-fitting photometry. (3) The best-fit models are evenly divided between those that have an AU-scale inner hole and those that don't. For members with disks that have an inner hole (marked "y"), we add the inner hole size in AU as determined in Currie et al. (2009).

TABLE 11
DISK EVOLUTIONARY STATES FOR LATE-TYPE η CHA SOURCES

| Name | ST ¹ (M _⊙) | M _★ | K _s -[8] | K _s -[24] | τ_{mid-IR} | Inner Hole? | M_{disk} | $\frac{M_{disk}}{M_{★}}$ | Disk Class f(< 1,3×10 ⁻³) | Si09 | Lu10 | This Work |
|---------|--------------------------------------|----------------|---------------------|----------------------|-----------------|----------------|----------------------|--------------------------|--|--------|------|------------------------|
| RECX-1 | K7+M0,K6 | 0.95 | 0.23 | 0.38 | - | n | - | - | - | star | star | star |
| RECX-3 | M3,M3.25 | 0.35 | 0.26 | 0.92 | thin | y | 3.5×10 ⁻⁸ | 1×10 ⁻⁷ | 1,1 | TD(IH) | TD | TD(IH) |
| RECX-4 | M1.75,M1.3 | 0.6 | 0.30 | 0.89 | thin | y | 1.8×10 ⁻⁷ | 3×10 ⁻⁷ | 1,1 | TD(IH) | TD | TD(IH) |
| RECX-5 | M3.8,M4 | 0.25 | 0.97 | 4.81 | thin | y | 7×10 ⁻⁴ | 2.8×10 ⁻³ | 0.14,0.73 | TD(IH) | TD | TD(IH) |
| RECX-6 | M3,M3 | 0.375 | 0.25 | 0.41 | - | n | - | - | - | star | star | star |
| RECX-7 | K6.9+M1,K6 | 0.95 | 0.17 | 0.26 | - | n | - | - | - | star | star | star |
| RECX-9 | M4.4+M4.7, M4.5 | 0.225 | 1.37 | 3.96 | thin | n | 1.4×10 ⁻⁴ | 6×10 ⁻⁴ | 0.53,0.75 | TD(HD) | PD | TD(HD) |
| RECX-10 | M0.3,M1 | 0.6 | 0.24 | 0.28 | - | n | - | - | - | star | star | star |
| RECX-11 | K6.5,K5.5 | 1 | 1.69 | 3.98 | thin | n | 3.3×10 ⁻³ | 3.3×10 ⁻³ | 0.13,0.50 | PD | PD | PD |
| RECX-12 | M3.2,M3.25 | 0.35 | 0.34 | 0.46 | - | n | - | - | - | star | star | star |
| J0841 | M5.5,M4.75 | 0.2 | 1.50 | 3.91 | thin | n | 3×10 ⁻⁵ | 2×10 ⁻⁴ | 1,1 | TD(HD) | PD | TD(HD) |
| J0843 | M5,M3.25 | 0.35 | 2.92 | 5.91 | thick | n | 1×10 ⁻³ | 3×10 ⁻³ | 0.31,0.50 | PD | PD | PD |
| J0844 | M5.3, M5.75 | 0.1 | 1.86 | 4.51 | thin? | n | - | - | - | PD | ? | PD/TD(HD) ² |
| J0838 | M5, M5.25 | 0.15 | 0.53 | - | - | n | - | - | - | star | star | star |
| J0836 | M5.3, M5.5 | 0.12 | 0.58 | - | - | n | - | - | - | star | star | star |

scriptsize

NOTE. — The identification "Lu10" refers to Luhman et al. (2010), where the classification listed is based on applying the Luhman et al. (2010) color criteria. The identification "Si09" refers to Sicilia-Aguilar et al. (2009)'s disk classification translated into our nomenclature. 1) The first entry for spectral type comes from Lyo et al. (2004) and the second one comes from Luhman and Steeghs (2004). We compute the stellar masses and fractional disk masses using the Luhman and Steeghs (2004) spectral types and the stellar masses for a given effective temperature at 6 Myr from the Baraffe et al. (1998) isochrones. Our results do not leverage on whose spectral types we adopt. 2) For our statistics, we classify this disk as a primordial disk since it lacks far-IR data to needed to derive a meaningful disk mass estimate. We omit a column for optical extinction since it is negligible for this cluster (e.g. Lyo et al. 2004; Luhman and Steeghs 2004).

TABLE 12
FREQUENCY OF TRANSITIONAL DISKS WITH TIME (CORRECTED FOR
CONTAMINATION)

| Cluster | Age (Myr) | Spectral Type Range | f(TD) _{lower} | f(TD) _{upper} |
|------------|-----------|---------------------|------------------------|------------------------|
| Taurus | 1-2 | K5-M6 | 0.18 (25/143) | 0.22 (32/145) |
| | | K5-M2 | 0.17 (13/75) | 0.21 (16/77) |
| | | M2.5-M6 | 0.18 (12/68) | 0.24 (16/68) |
| Coronet | 1-3 | K5-M6 | 0.21 (4/19) | 0.36 (8/22) |
| | | K5-M2 | 0.12 (1/9) | 0.22 (2/9) |
| | | M2.5-M6 | 0.30 (3/10) | 0.50 (6/12) |
| IC 348 | 2.5 | K5-M6 | 0.32 (40/124) | 0.40 (49/124) |
| | | K5-M2 | 0.18 (6/33) | 0.24 (8/33) |
| | | M2.5-M6 | 0.42 (34/81) | 0.51 (41/81) |
| NGC 2362 | 5 | K5-M3 | 0.58 (11/19) | 0.63 (12/19) |
| η Cha | 6-8 | K5-M6 | 0.63 (5/8) | " |

NOTE. — The transitional disk frequency is defined as $f(\text{TD})/(f(\text{TD})+f(\text{PD}))$. The range in transitional disk frequencies ($f(\text{TD})$) for Taurus accounts for disks with uncertain/indeterminable states. The range in frequencies for the Coronet, IC 348, and NGC 2362 also account for the range of contamination estimates based on SED modeling of Taurus data.

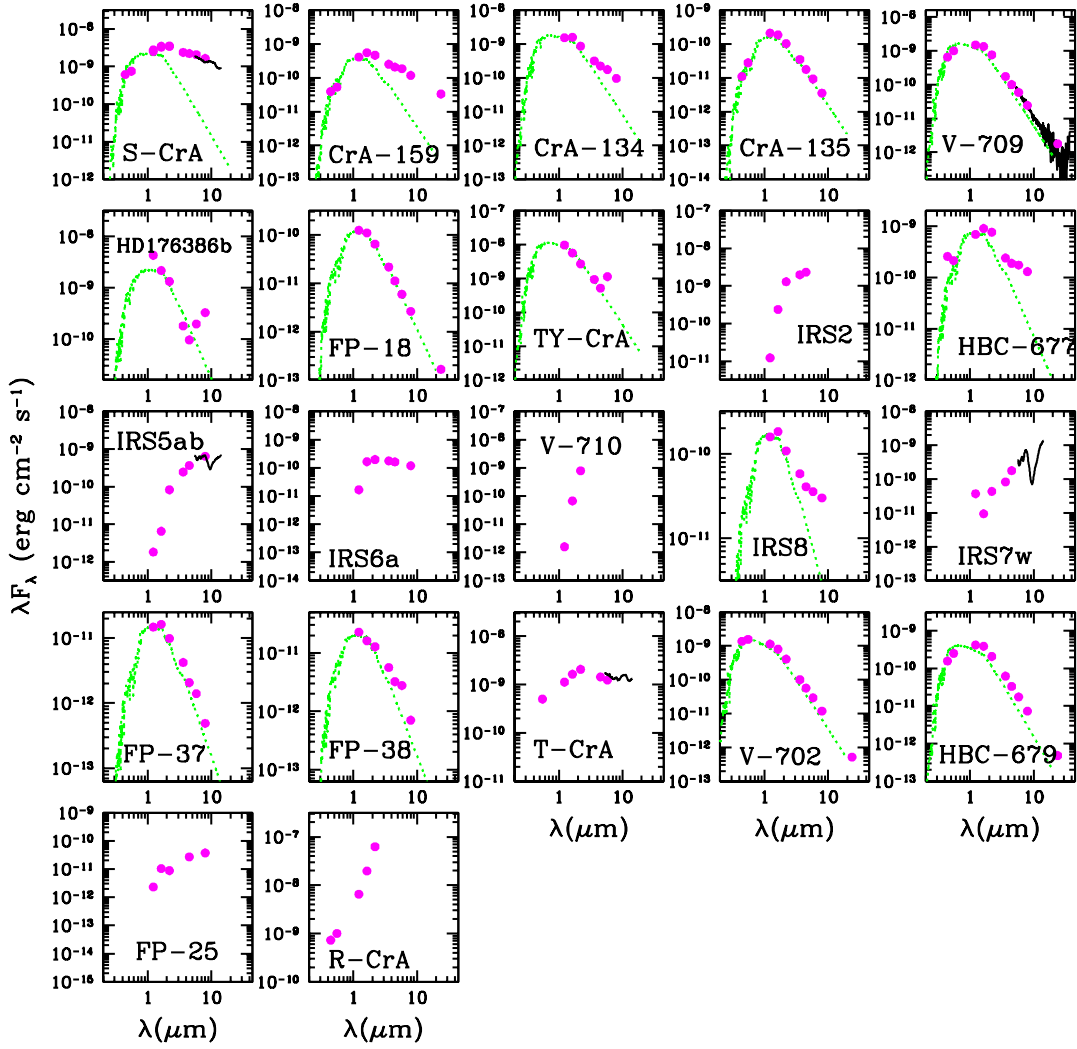


FIG. 3.— Spectral energy distributions of Coronet Cluster stars with new Spitzer photometry. In most cases, the SEDs can be modeled as a stellar photosphere (green) plus excess emission from a disk. The stellar photospheres plotted come from the MARCS stellar atmosphere models (Gustafsson et al. 2008, and references therein). Sources not shown lack near-to-mid IR data required to constrain their SEDs.

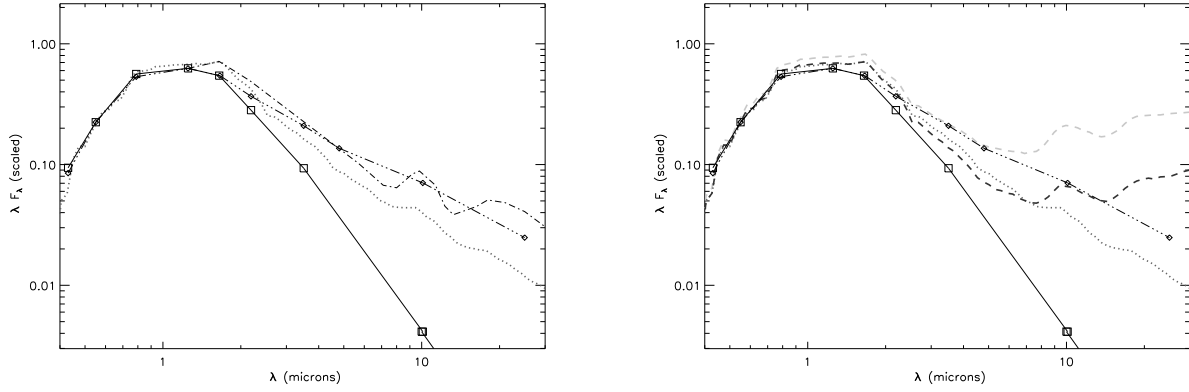


FIG. 4.— Comparisons between various empirical and theoretical SEDs and our fiducial flat disk models used for analysis— the Kenyon and Hartmann (1987) flat, reprocessing disk and our non-flaring, optically thick reprocessing disk from the Whitney et al. (2003a) Monte Carlo radiative transfer code. The models shown are for M0, $T_e = 3850$ K stars. In both panels, the Kenyon and Hartmann (1987) disk is shown as a dashed-three dots–diamonds locus, the Whitney et al. model is shown as a grey dotted line, and the stellar photosphere is shown as a solid line connected by squares. (left) Comparisons with the lower-quartile Taurus SED from Furlan et al. (dash/dots 2006). (right) Comparisons with a standard flared disk model (grey dashed line) and a flared but "settled"/shadowed disk model (black dashed line). The Whitney radiative transfer models deviate from the stellar photosphere and Kenyon and Hartmann flat disk in the near-IR because it includes strong, hot, optically-thick emission from the puffed up inner disk regions.

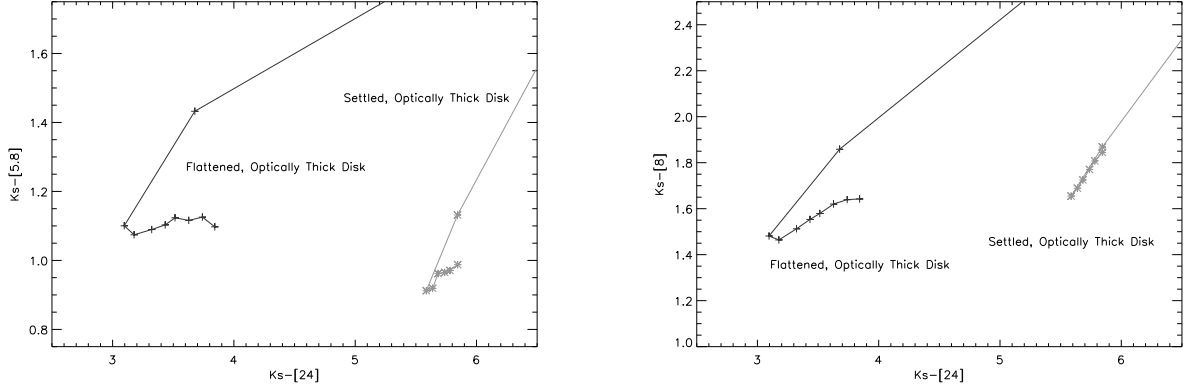


FIG. 5.— Loci of colors for an optically-thick flattened disk around a M0 star (black solid line) and an optically-thick "settled" disk around a M0 star (grey solid line) as a function of disk inclination. Disks viewed edge on have extremely red colors and lie off the boundary of the plot. The right-most point in each plot corresponds to the face-on case. Note that since the model predicts some K-band excess, the colors compared to that of the stellar photosphere are redder by an additional ~ 0.1 – 0.2 mags.

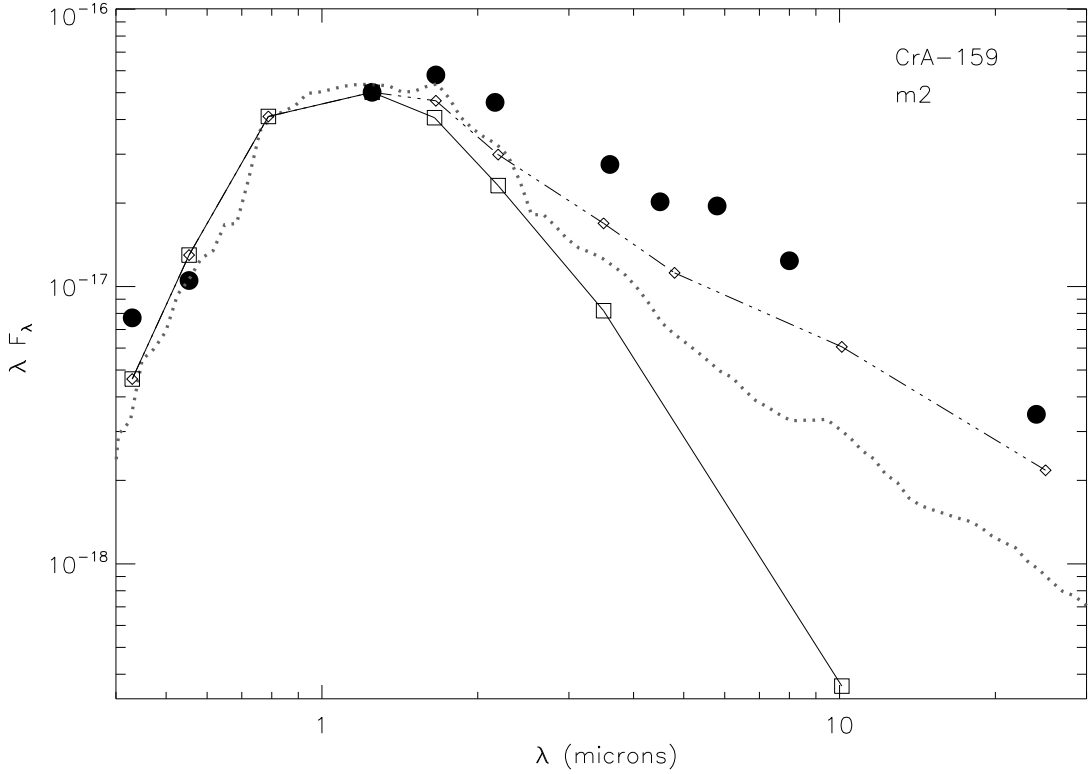


FIG. 6.— SED analysis for CrA-159, comparing its emission to the razor-thin flat optically thick disk model (e.g. Kenyon and Hartmann 1987, dash-three dots/diamonds) and a flat, optically-thick disk model constructed from the Whitney radiative transfer code (dotted line). For reference we overplot the stellar photosphere as a solid line. CrA-159 has disk emission consistently lying above the Whitney flat disk model and thus we classify it as having a primordial disk.

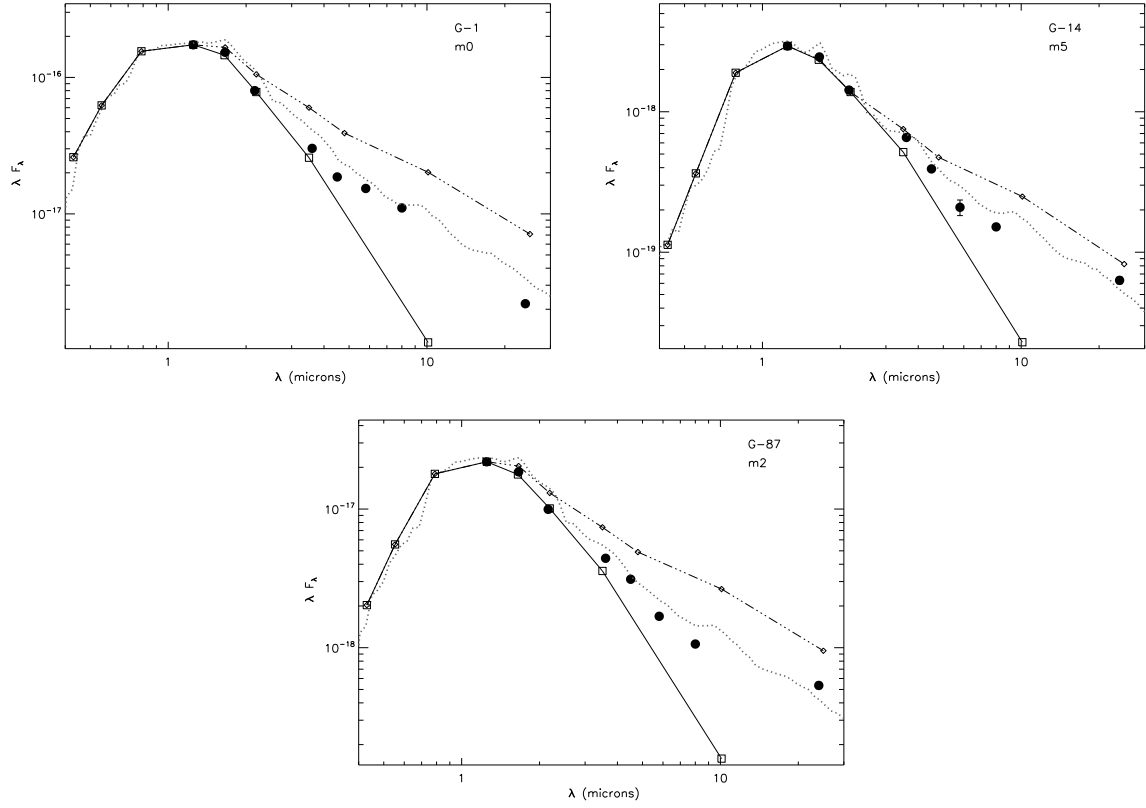


FIG. 7.— SEDs G-1 (top), G-14 (middle), and G-87 (bottom). We fit the optical/near-IR portion of the SED to a stellar SED constructed from the Currie et al. (2011) intrinsic colors (solid line), overplot the flat, optically-thick disk model constructed from the Whitney radiative transfer code (dotted line) and overplot the flat, reprocessing disk SED from Kenyon and Hartmann (1987, dash-three dots). All three stars have homologously depleted transitional disks.

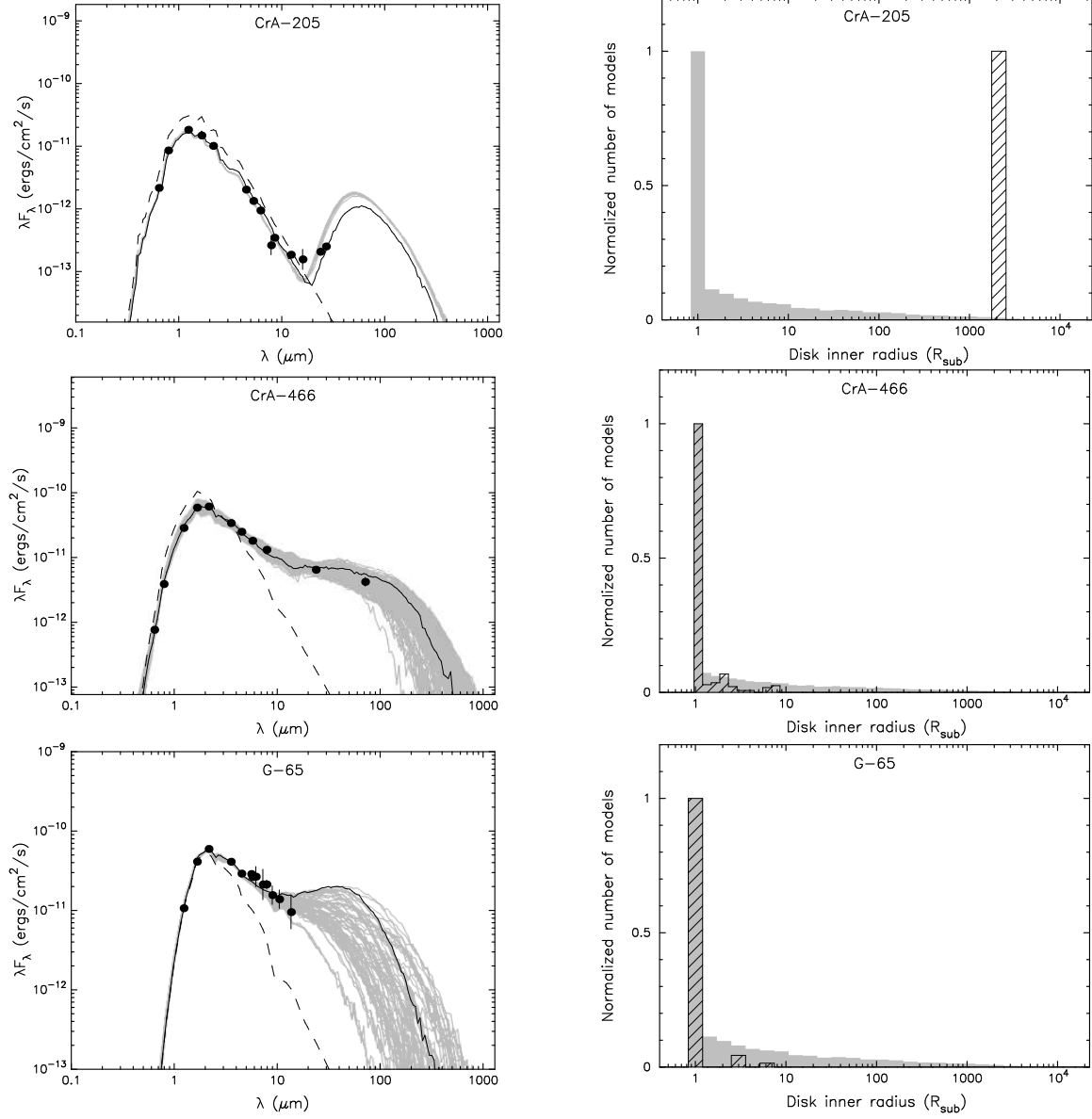


FIG. 8.— Spectral energy distributions and histograms of inner disk radii for CrA-205, CrA-466, and G-65. For the righthand panels, the hatched region shows the distribution of disk inner radii from best-fit models; the grey shaded region shows the normalized distribution of inner radii from all models. CrA-466 and G-65 do not show evidence for an inner hole, in agreement with Ercolano et al. (2009). CrA-205 has an inner hole and thus is a transitional disk, in agreement with Sicilia-Aguilar et al. (2008).

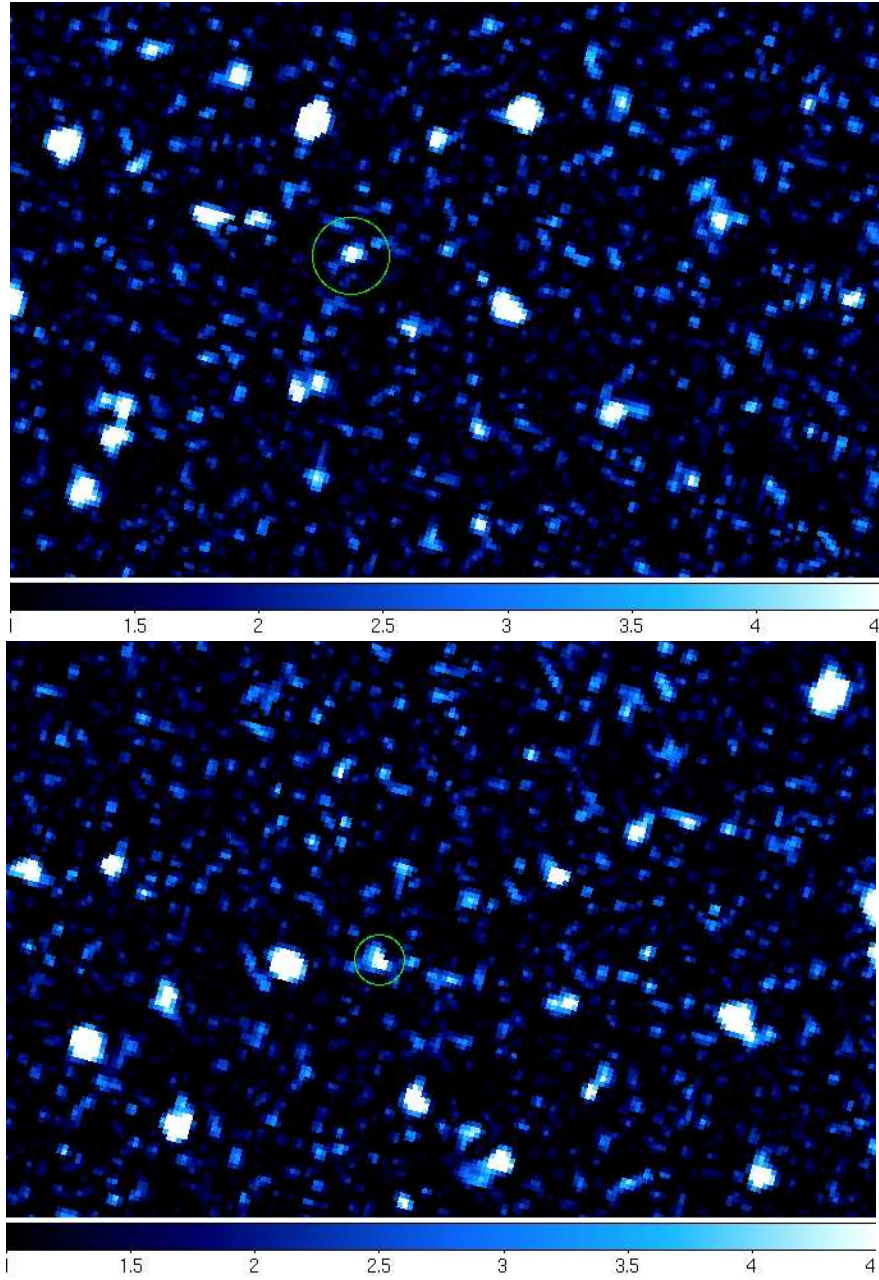


FIG. 9.— Signal-to-noise maps constructed from our reduced NGC 2362 MIPS mosaic image with the positions of ID-41 (top) and ID-63 (bottom) circled. The color stretch in each panel goes from 1 to 4.5 σ (black to blue to white). The signal-to-noise for the integrated flux is ~ 5 for both ID-41 and 63. Luhman et al. (2010) claim “from inspection of the mosaic” that both of these sources have $\text{SNR} < 3$. If that were the case, none of the pixels centered on these targets would be light blue or white. However, their removal of two stars (IDs 663 and 1091 but not IDs 809 or 931) from the Irwin et al. sample not considered here is better justified: one does have a low signal-to-noise and the other is blended with a different source.

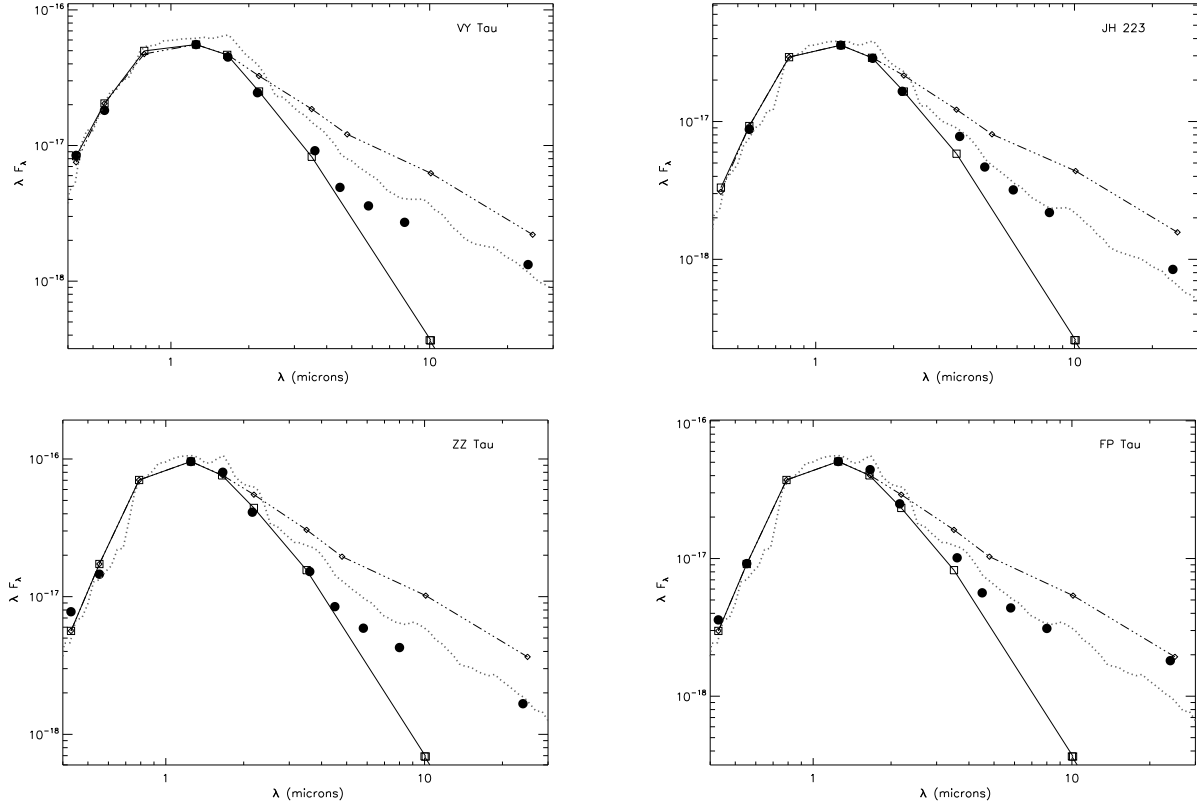


FIG. 10.— SEDs for four homologously depleted transitional disks in Taurus, showing optical to mid-IR photometric data compared to the flat, optically-thick reprocessing disk limit and the lower-quartile Taurus SED.

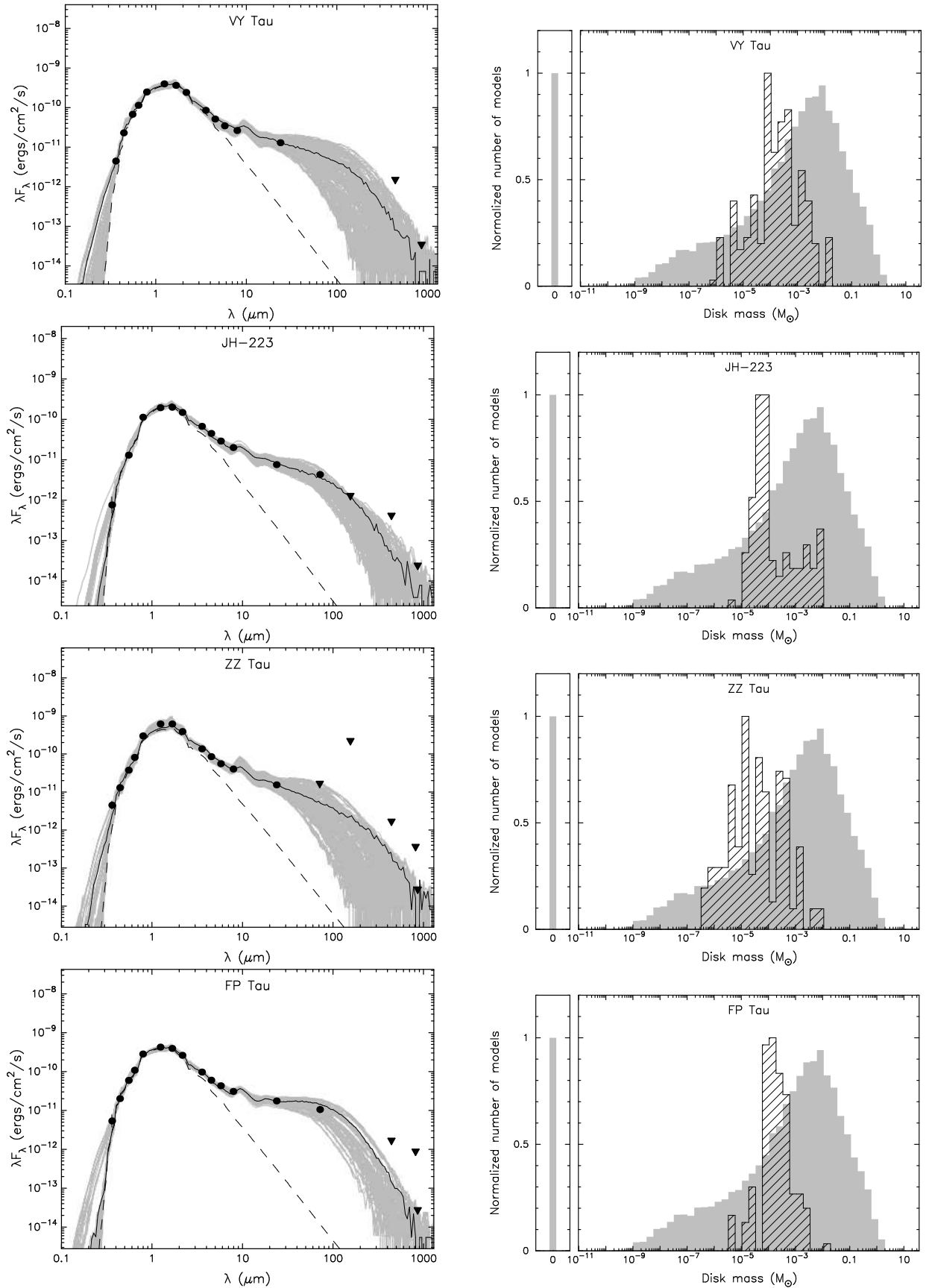


FIG. 11.— SED modeling of sources shown in previous figure, displaying the best-fit SEDs from the Robitaille grid along with the corresponding masses for the best-fit models. For the righthand panels, the hatched region shows the normalized distribution of masses from best-fit models; the shaded grey region shows the normalized distribution of masses from all available models. The x-axis of the righthand side figures lists the disk mass, not the fractional disk mass. The division corresponding to $M_{disk}/M_{\star} = 10^{(-3)}$ for VY Tau, JH-223, ZZ Tau, and FP Tau occurs at $M_{disk} = 7.5 \times 10^{-4}$, 5.5×10^{-4} , 4×10^{-4} , and 2.5×10^{-4} , respectively

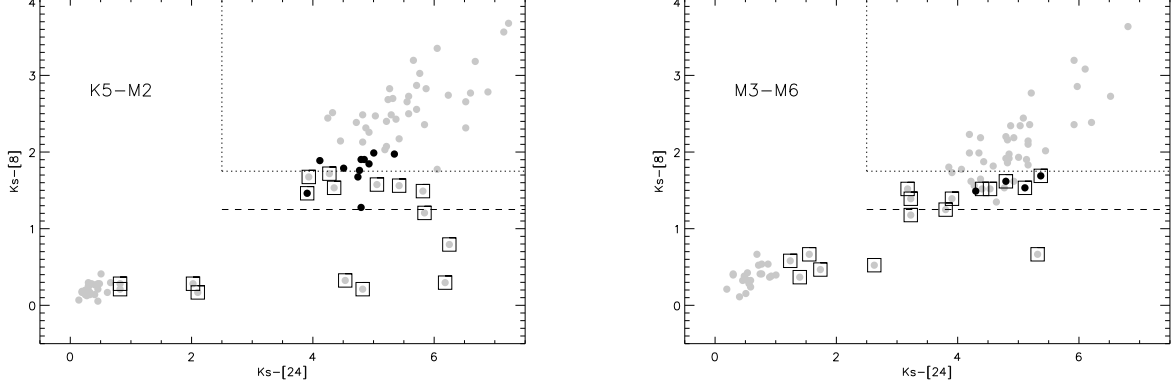


FIG. 12.— $K_s-[8]$ vs. $K_s-[24]$ colors for K5–M2 (left panel) and M3–M6 (right panel) Taurus members with data from Luhman et al. (2010) and Rebull et al. (2010). Grey circles surrounded by squares represent transitional disks identified from SED modeling, black dots represent primordial disks identified from SED modeling, and black dots surrounded by squares identify disks that could either be primordial or transitional. SED modeling was not performed for members represented as grey dots only. Sources between the horizontal dashed line ($K_s-[8]=1.25$) and the horizontal dotted line ($K_s-[8]=1.75$) include both primordial disks and transitional disks. Those above the horizontal dotted line include only primordial disks while primordial disks are absent below the horizontal dashed line.

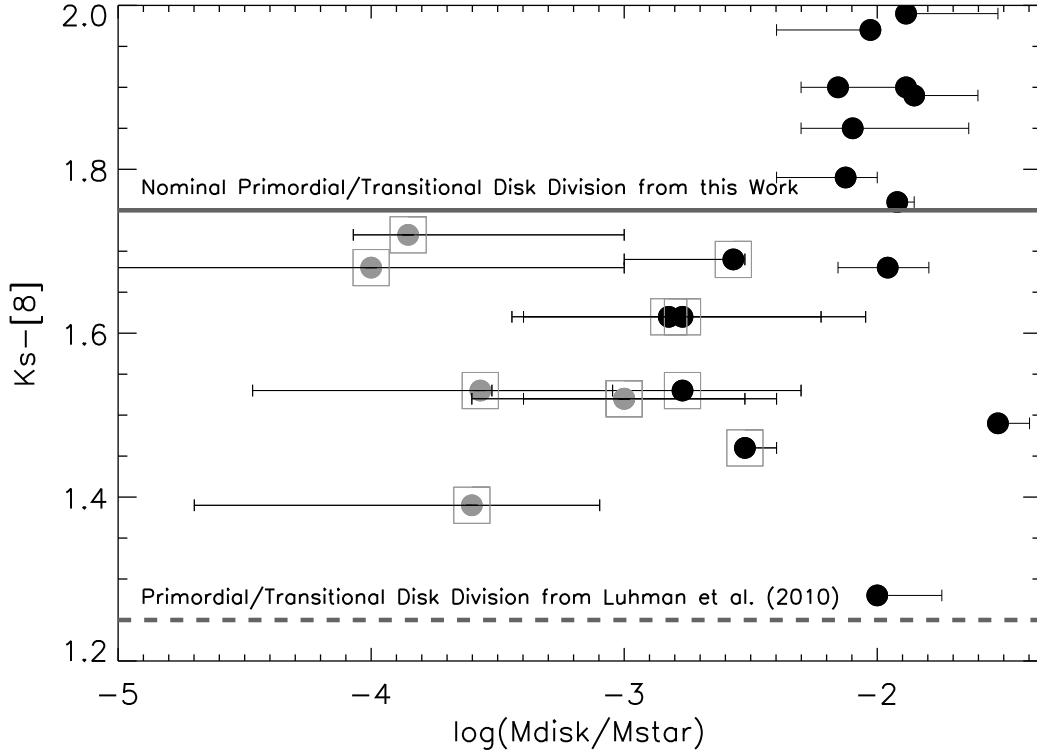


FIG. 13.— $K_s-[8]$ vs. fractional disk mass for homologously depleted transitional disks (grey circles surrounded by squares), “borderline” cases (black dots surrounded by squares), and primordial disks (black circles). The error bars identify the the interquartile range of disk masses for each star. For reference, we show the threshold in $K_s-[8]$ color below which the Taurus transitional disk population begins (horizontal grey line, $K_s-[8] = 1.75$) and that assumed in Luhman et al. (2010) for K5–M2 stars (horizontal black dotted line, $K_s-[8]=1.25$). This plot shows that the ranges of disk masses for the homologously depleted transitional disk and primordial disk populations are distinct. The interquartile range of disk masses for the borderline cases slightly overlaps with the range for primordial disks.

APPENDIX

IDENTIFYING TRANSITIONAL DISKS

Wavelength Range Required to Meaningfully Constrain Disk Masses

To determine the wavelength range necessary to meaningfully constrain disk masses, we follow Robitaille et al. (2007) and display SED modeling results for AA Tau, a “typical” optically-thick primordial disk (Figure 20). For modeling,

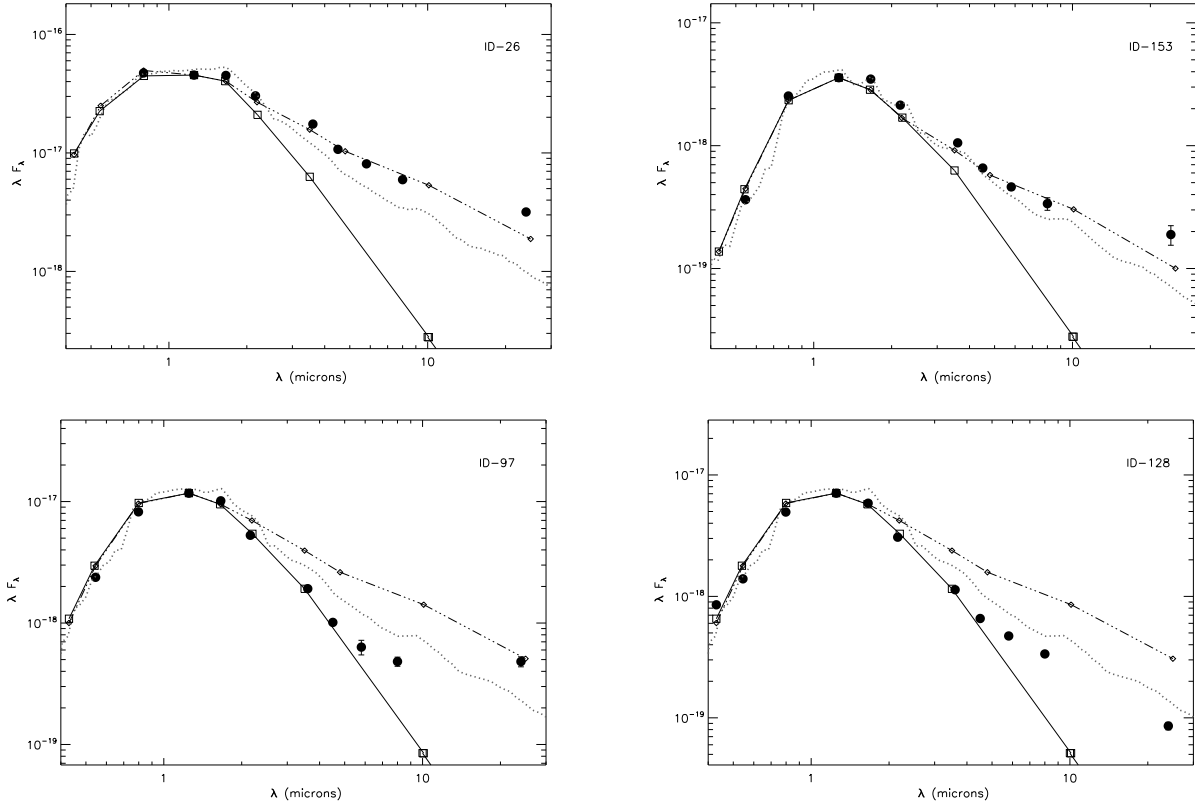


FIG. 14.— Representative SEDs for IC 348 sources. The provisional disk states for these members are (clockwise from top-left): primordial disk, primordial disk, homologously depleted transitional disk, and transitional disk with an inner hole.

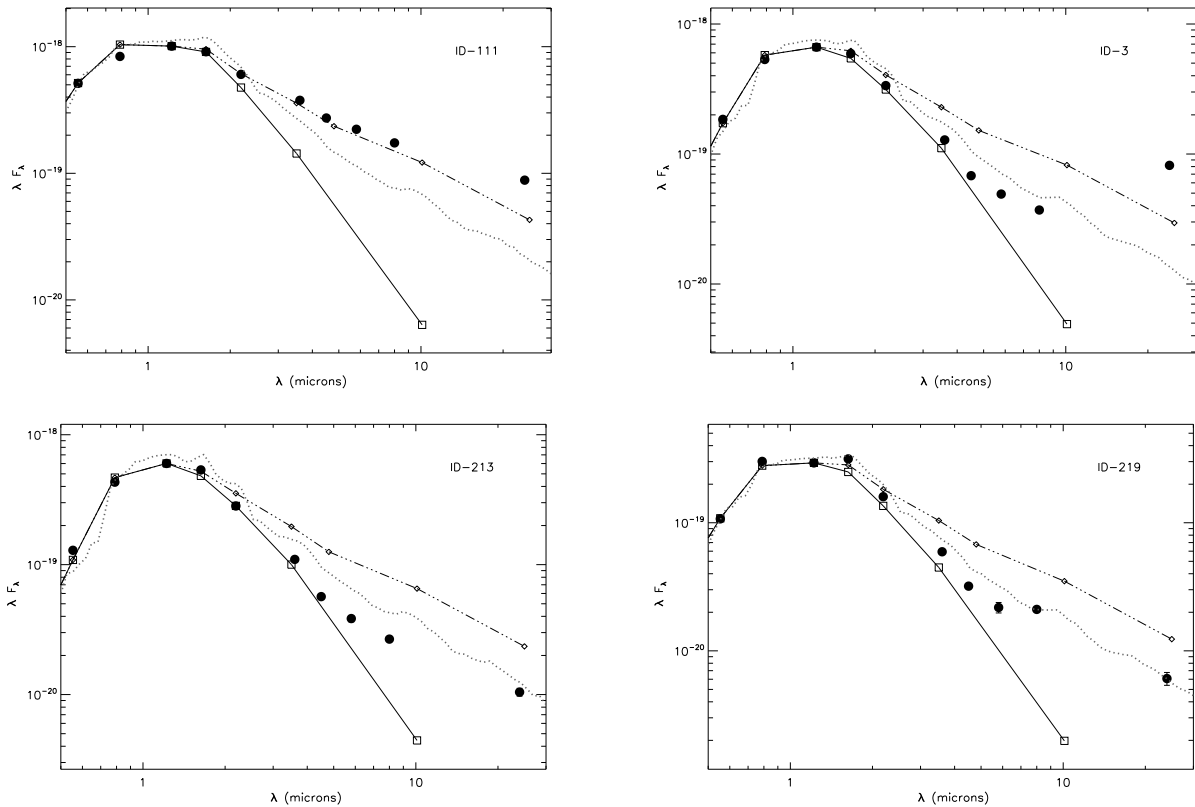


FIG. 15.— Representative SEDs for NGC 2362 sources. The provisional disk states for these members are (clockwise from top-left): primordial disk, transitional disk with inner hole, homologously depleted transitional disk, and homologously depleted transitional disk.

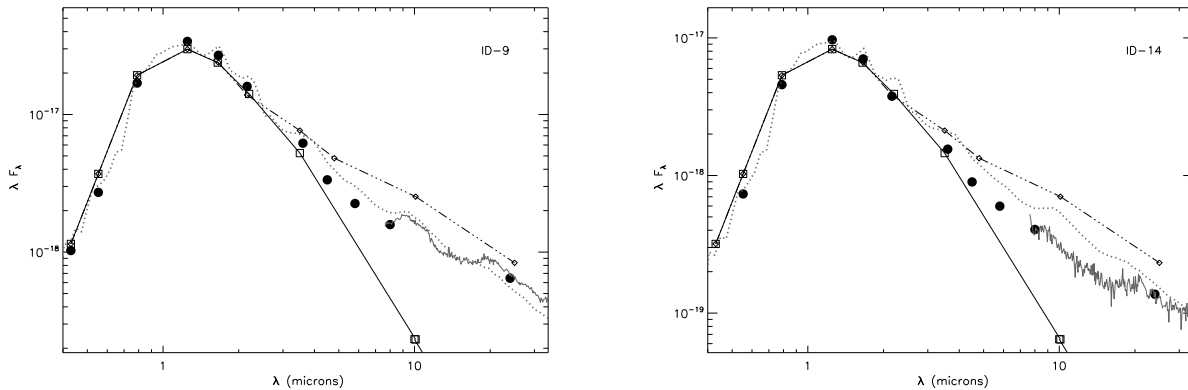


FIG. 16.— SEDs for two η Cha members identified as having homologously depleted transitional disks based in their photometric and spectroscopic flux densities (dots and thick grey line, respectively) compared to the appropriate flat, reprocessing disk models.

we assume an extinction range of $A_V = 1.45$ to 2.45 – the average between the Furlan et al. (2006) and Rebull et al. (2010) estimates ± 0.5 mags – and use the optical, 2MASS, Spitzer-IRAC/MIPS, and submillimeter data as listed by Robitaille et al. (2007). We adopt the same photometric errors as well.

The best-fit SED including all these data (top-left panel) reproduces the Robitaille et al. results. Our distribution of masses (top-right) is sharply peaked about $M_{disk} = 0.015 M_\odot$ with a median value of $\sim 0.02 M_\odot$, perfectly overlapping with their results. Now we remove longer wavelength data to see if the predicted range of disk masses changes. Restricting ourselves to data equal to or shortward of $70 \mu m$, the dispersion in disk masses is larger, but clearly and sharply peaked about $M_{disk} \sim 0.015 M_\odot$ (bottom-left) with a median value of $\sim 0.01 M_\odot$. Modeling optical through MIPS-24 data yields a peak noticeably shifted towards slightly lower disk masses ($\sim 8 \times 10^{-3} M_\odot$). More generally, the distribution of disk masses traces the shape of the distribution for all possible models (light grey shaded region).

While submillimeter data is required to yield the most precise disk mass estimates, this exercise indicates that far-IR wavelengths effectively probe the bulk disk mass. Disk mass estimates derived from modeling optical through far-IR data (e.g. $70 \mu m$) show good agreement with modeling that includes submillimeter data. Therefore, we conclude that a submillimeter detection is preferred but not required to estimate disk masses with a precision useful for our study. On the other hand, if far-IR/submm data is not available, disk mass estimates are very imprecise and likely not useful for our study.

Masses of Primordial Disks and Transitional Disks

SED modeling of optical-to-submm data for stars in 1–2 Myr-old clusters like Taurus provides useful benchmark values for disk properties that can be utilized to assess disk evolution. For instance, comparing near-to-mid IR emission from disks to the median and upper/lower-quartile Taurus SED is often used to identify sources showing evidence for warm dust depletion and/or settling in the inner disk (cf. Hartmann et al. 2005; Furlan et al. 2006; Currie et al. 2009). Similarly, the median and upper/lower quartile of masses for optically-thick primordial disks compared to stellar masses as inferred from submillimeter measurements (“fractional disk masses”) can be used to assess dust depletion in the outer disk, which traces the total mass of dust (Beckwith and Sargent 1991; Wood et al. 2002; Andrews and Williams 2005). Submillimeter data is particularly important in this paper since identifying homologously depleted transitional disks – those with low disk masses compared to primordial disks – presupposes that we can identify appropriate lower limits for primordial disk masses. In this section, we revisit and expand upon the study of Andrews and Williams (2005) to identify the range of fractional disk masses for primordial disks, showing that the appropriate lower limit is $M_{disk} = 0.001\text{--}0.003 M_\star$.

The Andrews and Williams (2005) study includes data for 153 Taurus members (their Table 1). Andrews and Williams (2005) estimated disk masses for 44 of the members from SED modeling (their Table 2), since they have submillimeter detections and high-quality near-to-far IR photometry: we hereafter refer to this sample as the ‘Table 2 sample’. Disk masses for the other 109 members were estimated solely from their submillimeter fluxes/upper limits: we hereafter refer to this sample as the ‘Table 1-only sample’.

To determine fractional disk masses for disks in both samples, we adopt spectral types from Luhman et al. (2010), use our stellar mass estimates, and restrict the samples to K5–M6 stars. Because our goal is identifying the masses of optically-thick primordial disks, we further trim the sample of Class I protostars, Class III diskless stars, known transitional disks with inner holes (e.g. GM Aur, UX Tau), and other disks with optically-thin near-to-mid IR emission listed in Table 6 (e.g. V836 Tau, JH 223). Finally, we remove foreground nonmembers (St 34) and other stars lacking MIPS data reported in Luhman et al. (2010) and Rebull et al. (2010) that is necessary for SED modeling (e.g. CIDA-11, CIDA-12, and FV Tau/c).

Our selection criteria leaves 22 stars in the Table 1-only sample and 26 in the Table 2 sample. The sample of stars that were not modeled by Andrews and Williams (2005), and thus listed in Table 2, is dominated by Class III diskless

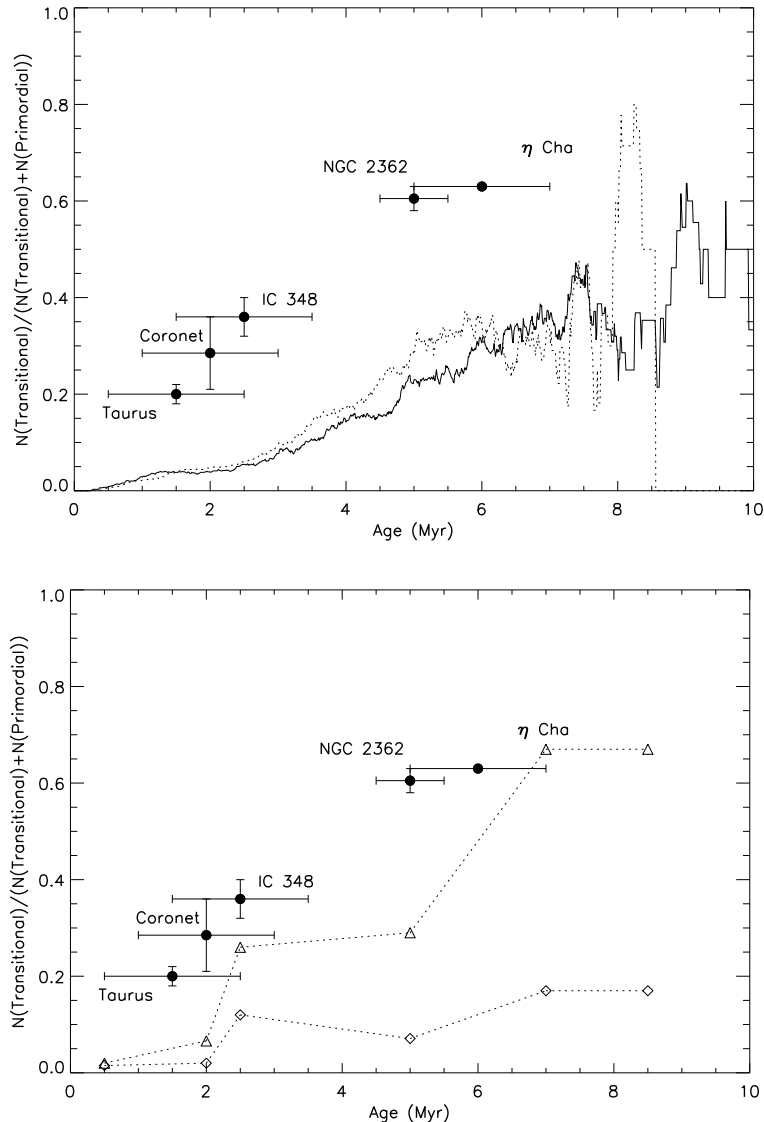


FIG. 17.— Frequency of transitional disks vs. time. (Top panel) We compare our frequencies to the theoretical models of Alexander and Armitage (2009) who determine the frequency of transitional disks vs. time from a disk evolution/planet formation model with a disk clearing timescale of 0.5 Myr. The dashed line corresponds to the reference model, while the solid line includes a dispersion in disk properties (initial angular momentum, disk lifetime, disk mass). See Alexander and Armitage (2009) for details. (Bottom panel) Our frequencies compared to those derived by Muzerolle et al. (2010). Their loci correspond to frequencies assuming that all transitional disks have inner holes and optically thick outer regions (lower dashed line/diamonds) and allowing for a broader definition of transitional disk that would include many identified from this work (upper dashed line/triangles). In this figure and the next one, the dots identify the average of the lower and upper limits for the transitional disk frequency as listed in Table 12.

members. This characteristic explains the precipitous drop in the number of Table 1-only stars analyzed (22) compared to the nominal sample (109).

Figure 21 shows the cumulative distribution functions for both samples, adopting Andrews and Williams (2005) disk mass estimates and our stellar mass estimates. For the Table 2, the median and mean fractional disk masses are $M_{\text{disk}} \sim 0.011 M_{\star}$ and $M_{\text{disk}} \sim 0.039 M_{\star}$. The interquartile range covers $0.003 M_{\star}$ to $0.033 M_{\star}$. About 88% (23/26) have masses greater than or equal to $0.001 M_{\star}$: the low-mass outliers are DF Tau, HN Tau, and V955 Tau. For the Table 1-only sample, about 82% (18/22) have masses greater than or equal to $0.001 M_{\star}$: the low-mass outliers are CIDA-3, CoKu Tau/3, CZ Tau, and DP Tau. To more definitively determine whether any member in either sample has a low-mass disk, we fit their SEDs using the Robitaille et al. (2007) model grid and data reported from Spitzer (Luhman et al. 2010; Rebull et al. 2010) and ground-based studies, following the methods described in §4 of the main text.

As listed in Table 8 and shown by Figure 22, inferred disk masses for DF Tau, HN Tau, and V955 Tau using the Robitaille models are substantially higher than values listed by Andrews and Williams (2005). The median masses of the best-fit models are $5\text{--}9 \times 10^{-3} M_{\star}$, exceeding both the $0.001 M_{\star}$ limit and the previously quoted lower-quartile frac-

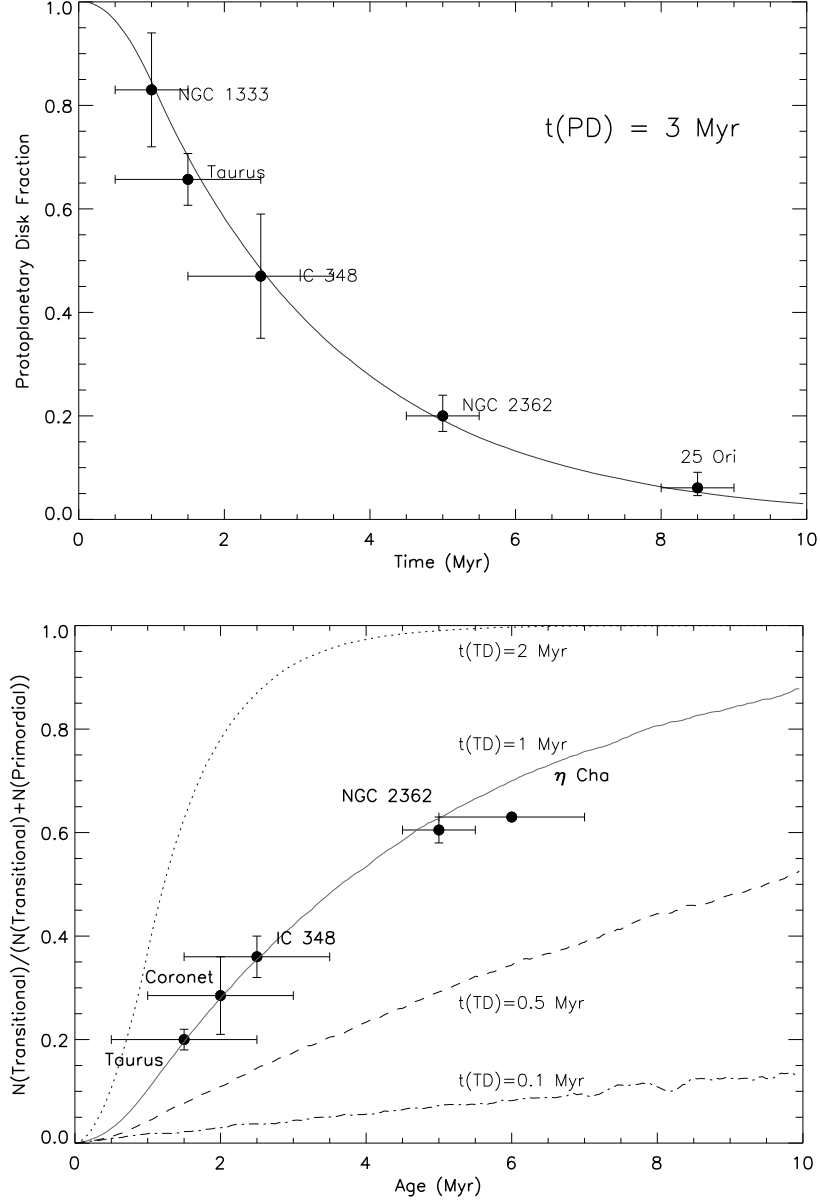


FIG. 18.— (Top) The frequency of protoplanetary disks vs. time as probed by Spitzer observations. For NGC 1333, IC 348, and 25 Ori the frequencies are taken from the literature (Gutermuth et al. 2008; Lada et al. 2006; Hernandez et al. 2007b). The frequency for Taurus is taken from the number of “Class II” objects in Taurus reported by Luhman et al. (2010) and the number of “Class III” objects showing evidence for weak IR excess (e.g. FW Tau). The frequency for NGC 2362 is taken from data presented in Currie et al. (2009), which is in agreement with estimates from Dahm and Hillenbrand (2007). (Bottom) The transitional disk frequency vs. time for different clusters in our study. Overplotted are the predicted transitional disk frequencies from our parametric model, assuming a typical protoplanetary disk lifetime of 3 Myr and varying amounts of that time spent as transitional disks (0.1–2 Myr).

tional disk mass. Thus, we conclude that all of the optically-thick primordial disks modeled by Andrews and Williams (2005) have inferred masses greater than $M_{\text{disk}} = 0.001 M_{\star}$.

We obtain similar results for the low-mass outliers in our second sample. Figure 23 shows the SEDs and distribution of masses from best-fit Robitaille models for CIDA-3, CoKu Tau/3, CZ Tau, and DP Tau. CoKu Tau/3 and DP Tau have inferred masses greater than $0.001 M_{\star}$. CZ Tau and CIDA-3 have much lower masses and represent the only optically-thick primordial disks from the Andrews and Williams (2005) sample with inferred masses lower than $0.001 M_{\star}$.

Figure 24 shows the revised cumulative distribution functions for the fractional masses of optically-thick primordial disks surrounding K5–M6 stars in Taurus. Except for the sources individually modeled in this section (listed in Table 8), we adopt disk mass values from Andrews and Williams (2005) for simplicity. Of these members, $\sim 96\%$ (46/48) have masses greater than or equal to $0.001 M_{\star}$. The median and interquartile range for the Table 2 sample is $0.011 M_{\star}$ and $0.006\text{--}0.033 M_{\star}$. For the combined sample of 48 stars, these values are $5 \times 10^{-3} M_{\star}$ and $0.0024\text{--}0.015 M_{\star}$;

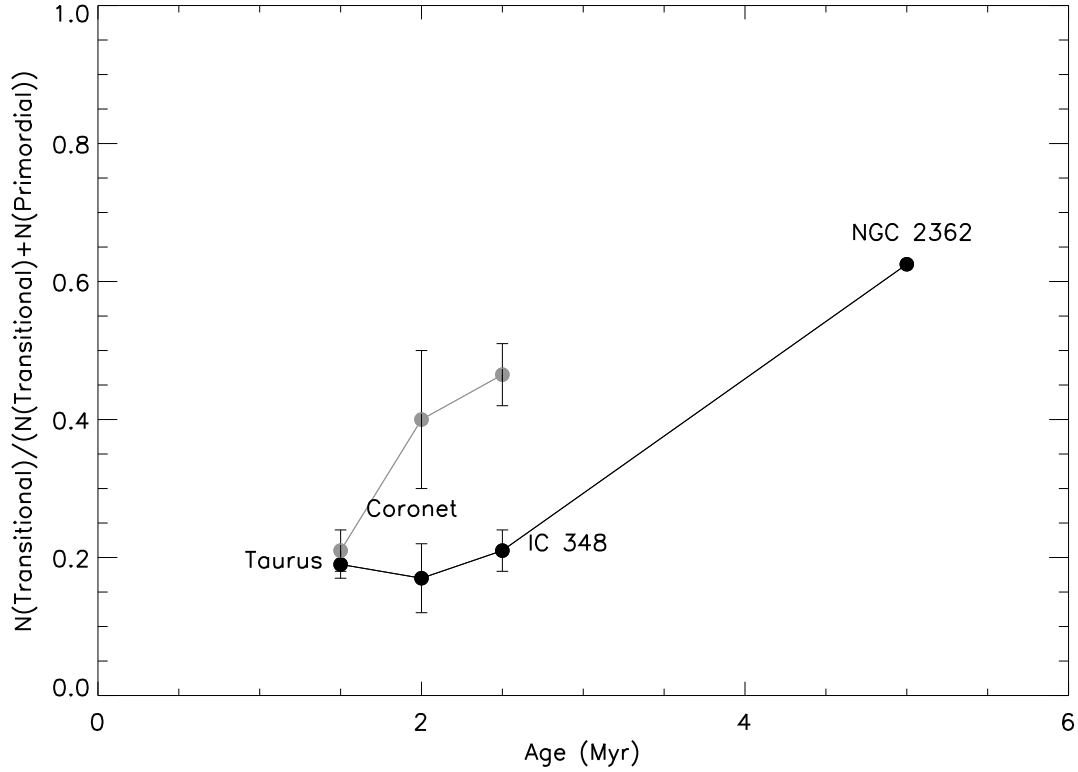


FIG. 19.— The transitional disk frequency vs. time for different clusters separated by spectral type: K5–M2 stars (lower locus) and later stars (upper locus). The error bars simply define the range in values from Table 12, taking into account disks with uncertain states.

however, most of the masses are derived from submillimeter fluxes alone, so individual mass estimates accounting for the entire disk should be larger and the median and quartile disk masses should likewise be larger.

Since nearly all primordial disks in the Andrews and Williams (2005) sample have masses greater than $0.001 M_{\star}$ and the lower quartile disk mass for the modeled sample is $> 0.003 M_{star}$, we conclude that disks with masses lying below $0.001\text{--}0.003 M_{\star}$ lie below the range expected for primordial disks. Thus, based on modeling current optical through submillimeter data, defining the lower mass limit for optically-thick primordial disks at $0.001\text{--}0.003 M_{\star}$ is justified.

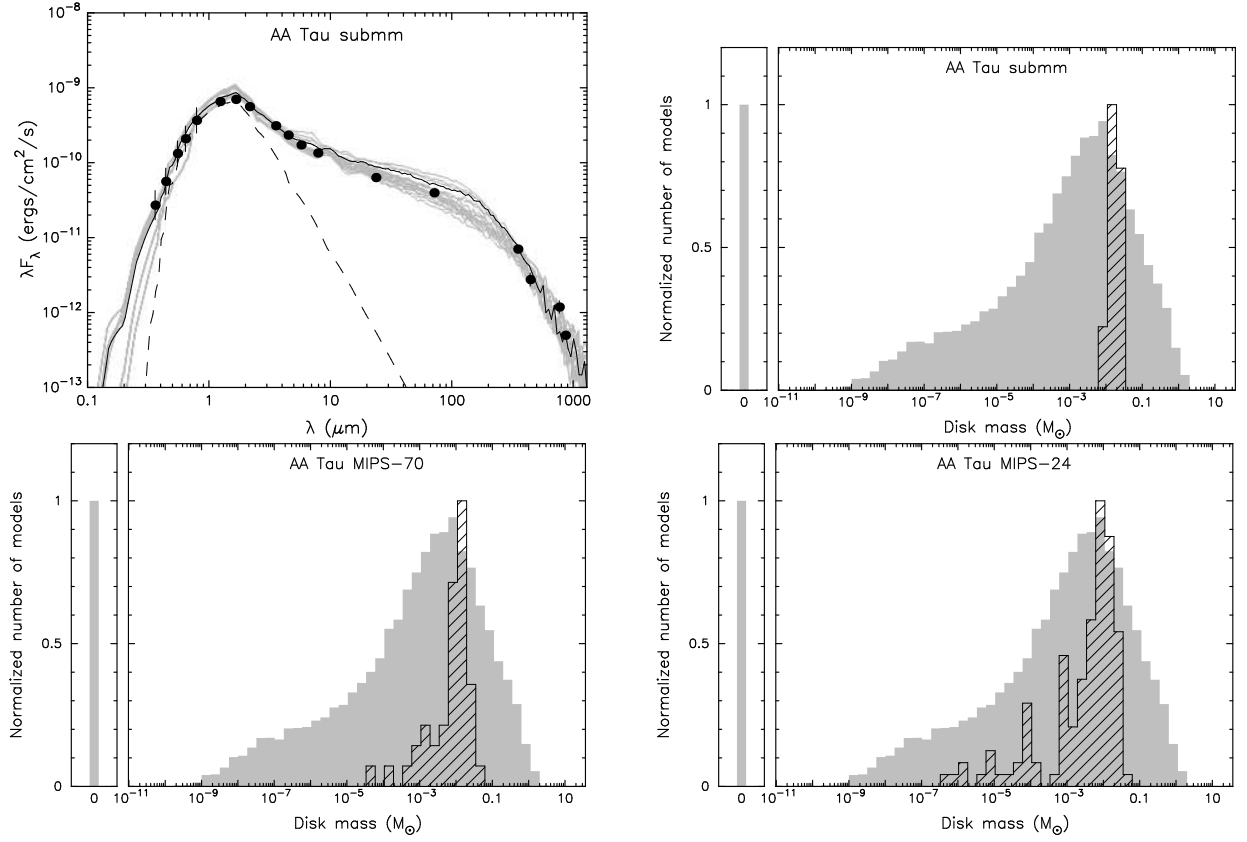


FIG. 20.— Analysis of AA Tau following Robitaille et al. (2007). The top-left panel shows the best-fit SED models to the AA Tau data from the optical through submillimeter; the top-right panel shows the histogram of disk masses from these best-fit models. The bottom two panels show the histogram of disk masses if we restricted our data to $70 \mu\text{m}$ or less (bottom-left panel) and $24 \mu\text{m}$ or less (bottom-right panel).

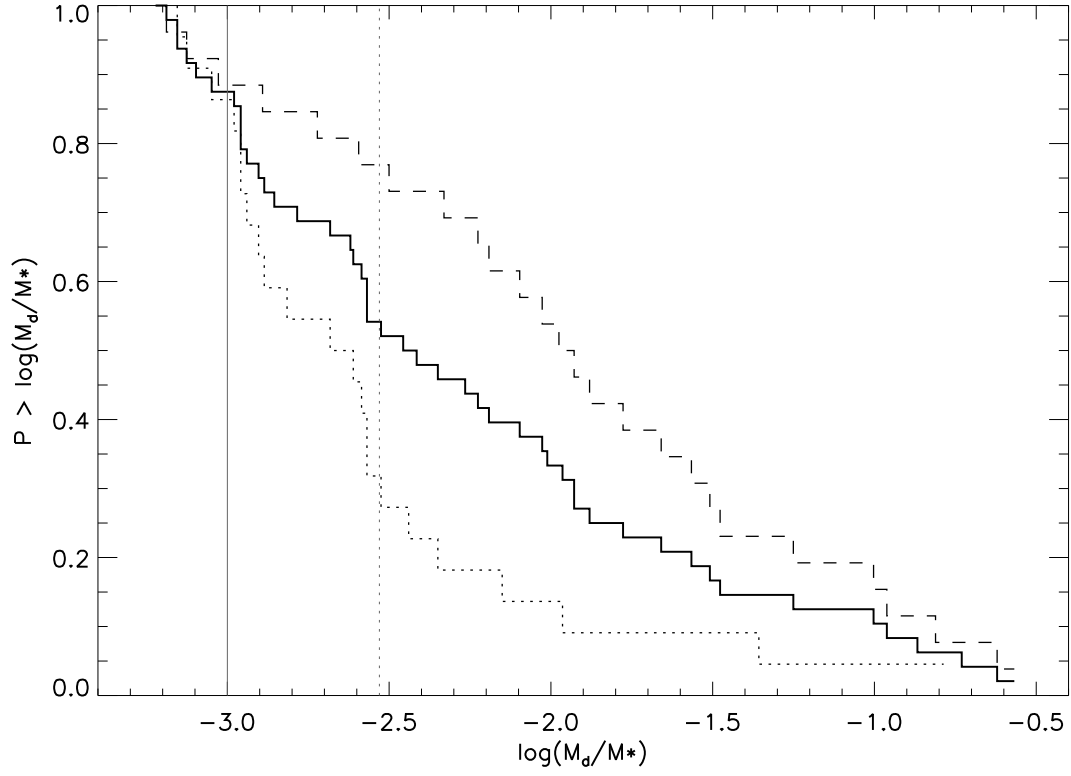


FIG. 21.— Cumulative distribution function of primordial disk masses for 48 K5–M6 Taurus members listed in Andrews and Williams (2005) based on Andrews and Williams’s disk mass estimates. Also shown are distribution functions for the ‘Table 1-only’ sample and ‘Table 2’ sample from Andrews and Williams (2005, see Appendix for definitions) identified by dotted and dashed distribution functions, respectively. For reference, our adopted limits for primordial disk masses $-0.001 M_\star$ and $0.003 M_\star$ – are shown as vertical solid and dotted grey lines, respectively.

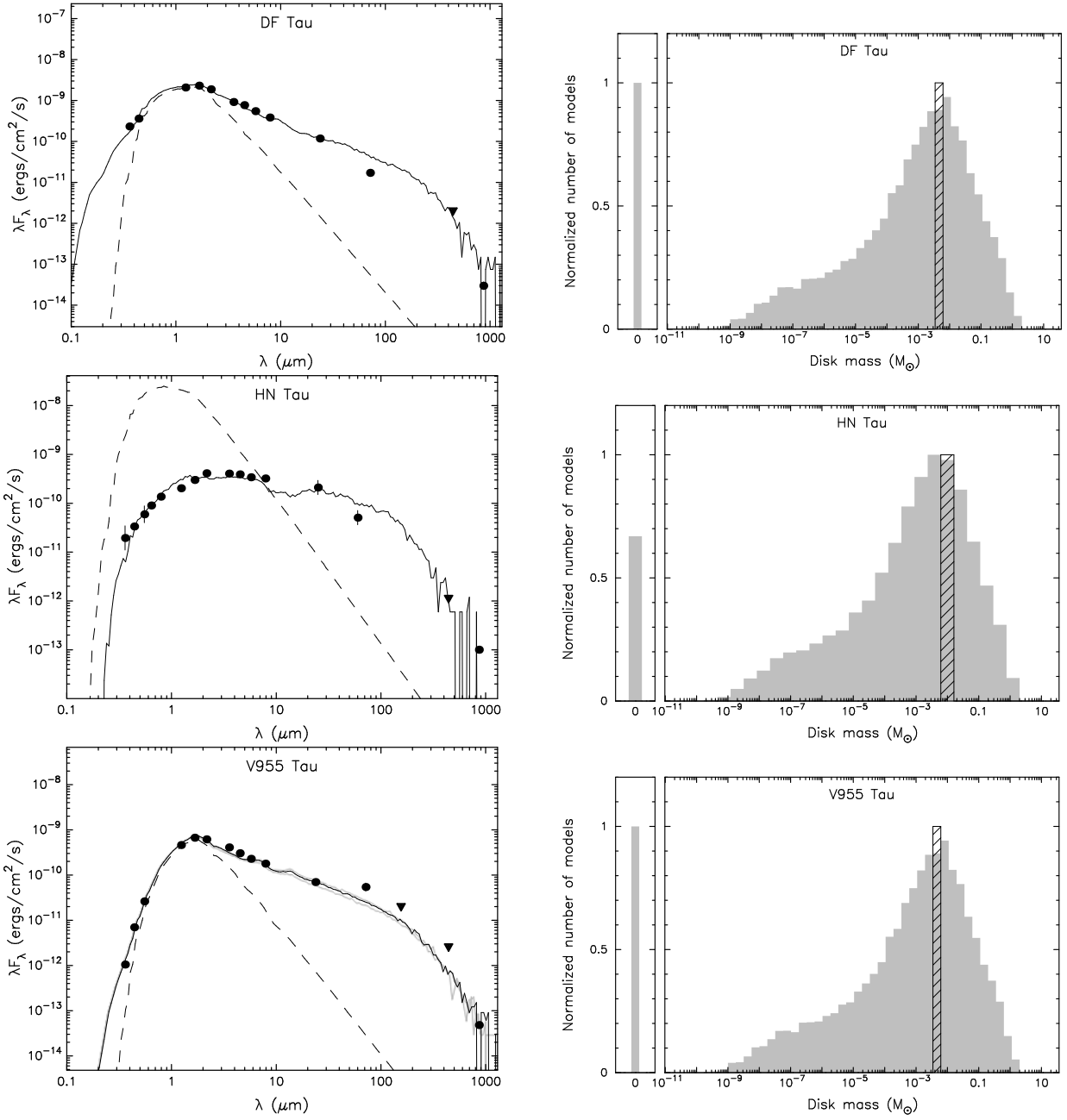


FIG. 22.— SED modeling results for Class II objects with optically-thick near-to-mid IR emission (primordial disks) in Taurus studied in Andrews and Williams (2005) that have $M_{disk} < 0.001 M_{\star}$ based on the Andrews and Williams (2005) SED modeling: DF Tau, HN Tau, and V955 Tau. The division corresponding to $M_{disk}/M_{\star} = 10^{-3}$ for DF Tau, HN Tau, V955 Tau occurs at $M_{disk} = 1 \times 10^{-3}$, 8.5×10^{-4} , and 5.5×10^{-4} , respectively. Using the Robitaille models, we find that all of these sources have disk masses larger than $0.001 M_{\star}$.

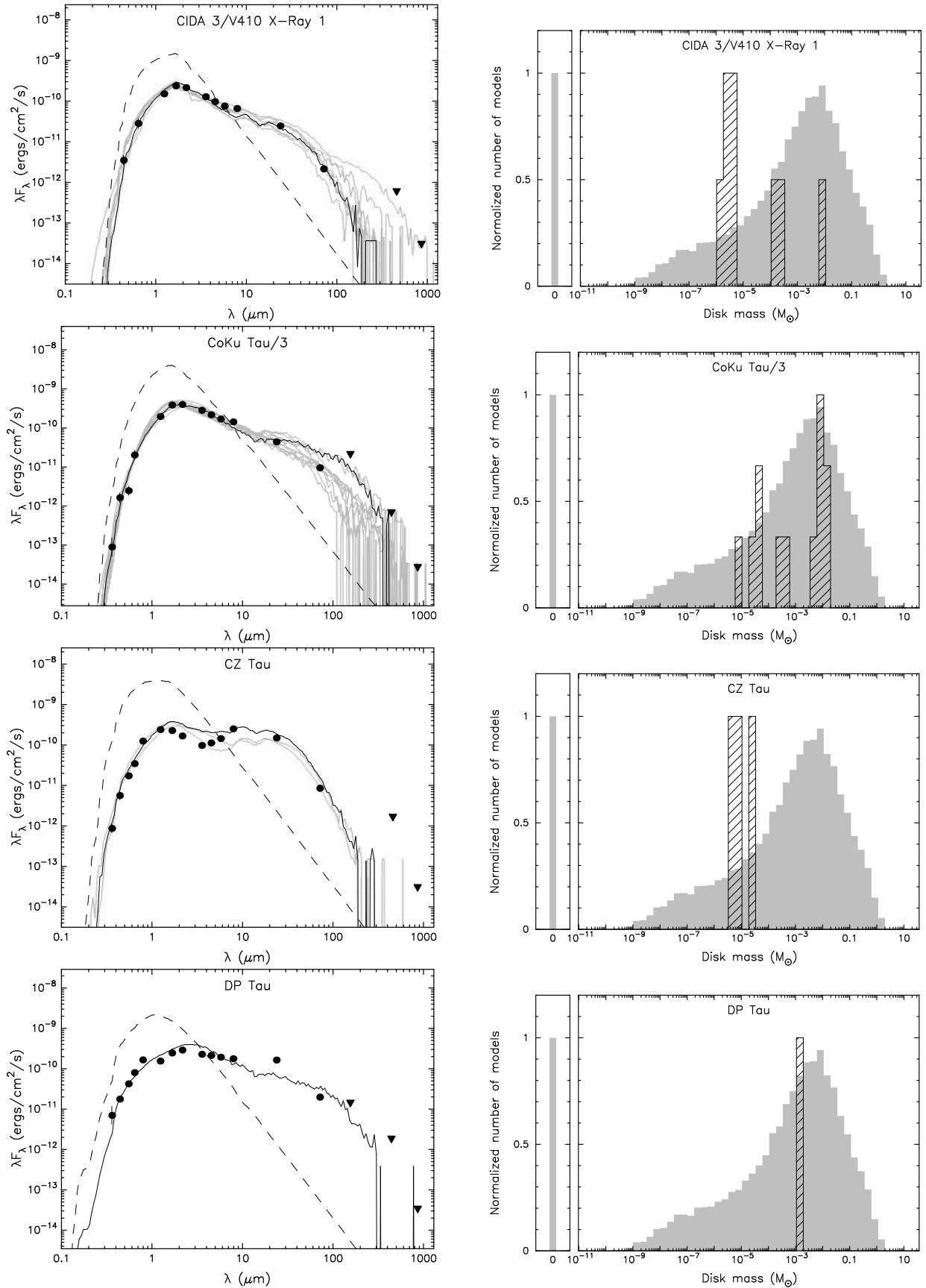


FIG. 23.— SED fits and distribution of masses from best-fitting models for other primordial disks in Taurus with data from Andrews and Williams (2005). The division corresponding to $M_{disk}/M_{\star} = 10^{(-3)}$ for CIDA 3/V410 X-Ray 1, CoKu Tau/3, CZ Tau, and DP Tau occurs at $M_{disk} = 6 \times 10^{-4}$, 6×10^{-4} , 5.5×10^{-4} , and 4×10^{-4} , respectively. Based on the Andrews and Williams (2005) submillimeter estimates, all of these have disk masses less than $0.001 M_{\star}$. Our analysis finds that only two of the four have such low masses.

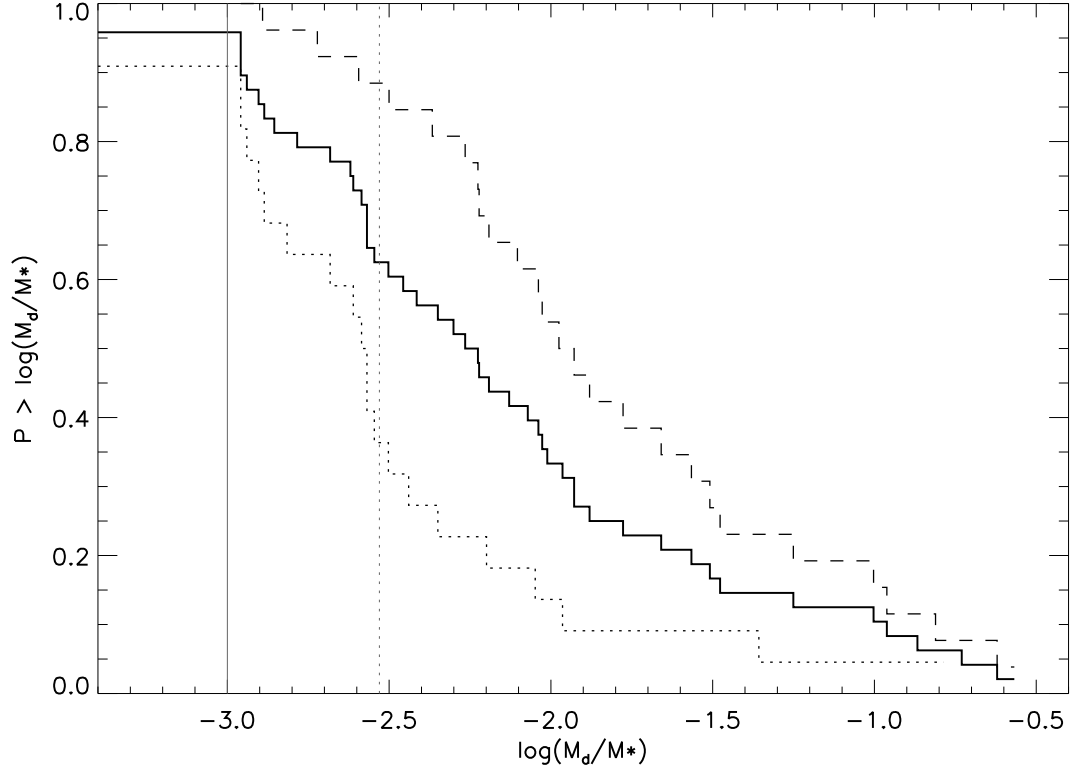


FIG. 24.— Cumulative distribution function of primordial disk masses for 48 K5–M6 Taurus members listed in Andrews and Williams (2005) taking into account revised mass estimates for Taurus members discussed in the Appendix. Our results show that the disk mass range of $0.001\text{--}0.003 M_\star$ defines a meaningful lower limit for the masses of optically-thick primordial disks.

